Developing a Multi-Lead Wireless ECG

A Major Qualifying Project submitted to the Faculty of WORCESTER POLYTECHNIC INSTITUTE in partial fulfillment of the requirements for the Degree of Bachelor of Science

Submitted by:
Nisha Goel

Other Contributors:
Emma Fountain
Ben Guerriero
Josh Reeder
Logan Young

Advised By:
Professor Edward A. Clancy
Professor Songbai Ji

December 2021

Acknowledgements

I would like to thank the following individuals for their contributions towards this project's success: Professor Edward Clancy, Professor Songbai Ji, Emma Fountain, Ben Guerriero, Josh Reeder, Logan Young.

I would like to thank Emma Fountain, Ben Guerriero, Josh Reeder, and Logan Young for being excellent teammates and supporting me in the project as I graduate early. It has been a pleasure to work with all of them!

I would also like to thank Professor Clancy, my MQP advisor, for supporting me with my decision to graduate early and guiding me to ensure I complete in time. His guidance, support, and feedback in all aspects of the project including components, technical explanations, understanding and improving the MATLAB functions, and providing resources that helped develop the project have been invaluable.

Abstract

This report focuses on the design of a multi-lead wireless electrocardiogram (ECG) monitor, the design of an atrial fibrillation detector, and the design and implementation of an R-wave detector in MATLAB. The circuit has leads that collect ECG signals from a subject and send the signals to a Nordic microcontroller (nRF52840) that uses Bluetooth to wirelessly transfer the data to a computer. Signal processing is done on the collected signal using an R-wave detector and atrial fibrillation detector. An ECG circuit using an instrumentation amplifier-based front end, linear filtering, and ADC conversion was designed on a protoboard, solderboard, and is now ready to be manufactured on a PCB. We also implemented an atrial fibrillation detector in MATLAB that classifies beat segments based on calculated values for Shannon entropy and the time varying coherence function. Finally, an R-wave detector was implemented in MATLAB by cascading a bandpass filter (fourth-order Butterworth, 5-15 Hz passband), squaring operation, lowpass filter (second-order, 5 Hz cutoff), and a peak detector. Our R-wave detection algorithm works well for both the arrhythmia and atrial fibrillation databases, producing a QRS sensitivity of 85% or higher for 64/71 of the records we tested from both the Physionet arrhythmia and atrial fibrillation databases, and a QRS positive predictivity of 91% or higher for 69/71 of the records from both databases.

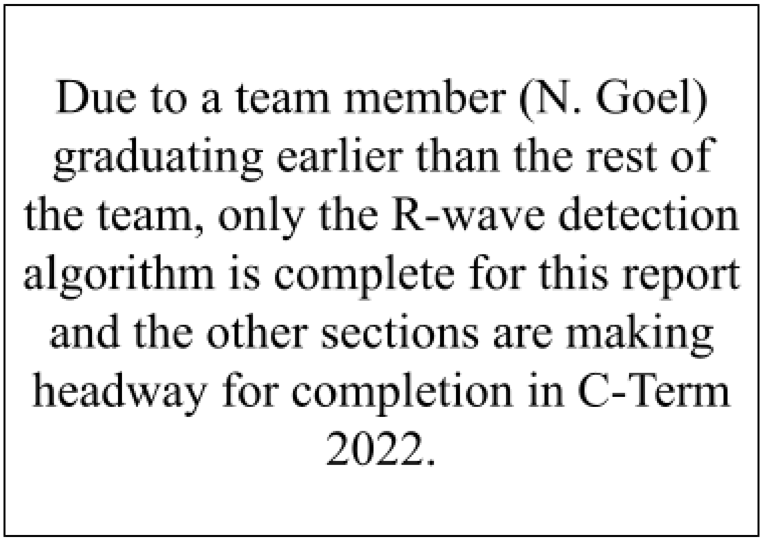

Due to a team member (N. Goel) graduating earlier than the rest of the team, only the R-wave detection algorithm is complete for this report and the other sections are making headway for completion in C-Term 2022.

Table of Contributions

Section	**Primary Author(s)**	**Primary Editor(s)**
Abstract	Nisha Goel	Joshua Reeder
1: Introduction	Nisha Goel	All
2.1 The Heart and ECG Signals	Emma Fountain	Nisha Goel
2.2.1: 12 Lead ECG	Logan Young	Joshua Reeder, Emma Fountain
2.2.2: 3 Lead ECG	Ben Guerriero	Logan Young
2.2.3: 2 Lead ECG	Ben Guerriero	Logan Young
2.2.4: Modern ECG Applications	Joshua Reeder	Ben Guerriero
2.3: Analog Front End and all subsections	Joshua Reeder	Ben Guerriero
2.4.1: Heart Rate	Emma Fountain	Nisha Goel
2.4.2: R-wave Detection Algorithm and all subsections	Nisha Goel	Emma Fountain, Joshua Reeder
2.4.3: Heart Rate Variability	Nisha Goel	Emma Fountain
2.4.4: Atrial Fibrillation and all subsections	Emma Fountain	Nisha Goel
2.5: Standards & Specifications Used	Logan Young	All
3.1: Original Client Statement	Provided by Project Advisor	N/A
3.2: Objectives and Constraints	Nisha Goel	Joshua Reeder
3.3: Project Approach	Nisha Goel	Joshua Reeder
3.3.1: Tools	Nisha Goel, Joshua Reeder	Joshua Reeder
4.1: Instrumentation Amplifier	Logan Young	Ben Guerriero
4.2: Operational Amplifier	Logan Young	Ben Guerriero
4.3: Analog to Digital Converter	Joshua Reeder	Ben Guerriero
4.4: Voltage Regulator	Ben Guerriero	Joshua Reeder
4.5: Microcontroller	Joshua Reeder	Ben Guerriero
4.6: Multi-Leads Selection	Nisha Goel	All

4.7.1: R-Wave Detection	Nisha Goel	Emma Fountain
4.7.2: Atrial Fibrillation Detection	Emma Fountain	Nisha Goel
5.1: Design Process	Logan Young	Nisha Goel
5.1.1: PCB Layout	Nisha Goel	Emma Fountain
5.2: Hardware Design Verification in Multisim	Ben Guerriero	Nisha Goel
5.3: Hardware Design Verification on a Protoboard	Joshua Reeder	Nisha Goel
5.4: Hardware Design Verification on a Solderboard	Logan Young	Nisha Goel
5.5: Discussion	Ben Guerriero	Nisha Goel
6: R-Wave Detection Algorithm and all subsections	Nisha Goel	All
7: Atrial Fibrillation Detection Algorithm and all subsections	Emma Fountain	Nisha Goel
8: Discussion	Nisha Goel	All
9. Summary	Nisha Goel	All

Executive Summary

The study of electrocardiogram (ECG) signals produced by the human heart has allowed technological and medicinal advancements over the last 100+ years. In more recent years, information that ECGs provide have been used to diagnose heart ailments such as atrial fibrillation (an irregular rapid heartbeat), heart attacks, and heart disease. Looking at an ECG trace provides information on the locations of where blood flow may be reduced or where there are sudden rapid heartbeats, and this allows for quick medical intervention when necessary.

Our Major Qualifying Project was to build a battery-powered, three-lead wireless ECG monitor that will be comfortably mounted on the human body for an extended period of time, collect the subject's ECG signals, and wirelessly transmit the signals for analysis using an R-wave detector and an atrial fibrillation detector. The project was split into three major sections: hardware, R-wave detection algorithm, and atrial fibrillation detection algorithm. The diagram below shows the overall flow of how our system is intended to function:

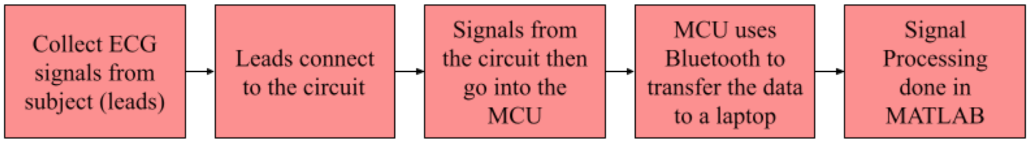
Collect ECG signals from subject (leads)
Leads connect to the circuit
Signals from the circuit then go into the MCU
MCU uses Bluetooth to transfer the data to a laptop
Signal Processing done in MATLAB

High Level Blackbox Diagram of System

The hardware portion consisted of building an ECG circuit, programming the Nordic (nRF52840) microcontroller units (MCU), and testing all components individually and when combined to produce satisfactory ECG signals. The signal processing portion of the project was to design and implement an R-wave detection algorithm and an atrial fibrillation detection algorithm. Once written, the detection algorithms were first tested on the MIT/BIH arrhythmia and atrial fibrillation databases (atrial fibrillation detection algorithm only used the atrial fibrillation database) and then they optimized for accuracy.

The ECG circuit was built using an LT1167 instrumentation amplifier, an LM324N quad operational amplifier, and a TPS73615MDBVREP voltage regulator. These components and a series of basic components (resistors and capacitors) comprised the entirety of the circuit design. The ECG signal is processed through an instrumentation amplifier stage to take the difference and amplify the signal between two leads. Then a series of highpass and lowpass stages are implemented to shape the waveform to the desired frequency range and remove external artifacts. Finally, the signal is level shifted upwards to properly adjust to a unipolar power supply for an Analog to Digital Converter (ADC). We simulated the circuit in NI Multisim and created a protoboard, solderboard, and PCB version of the circuit, as shown in the figures below.

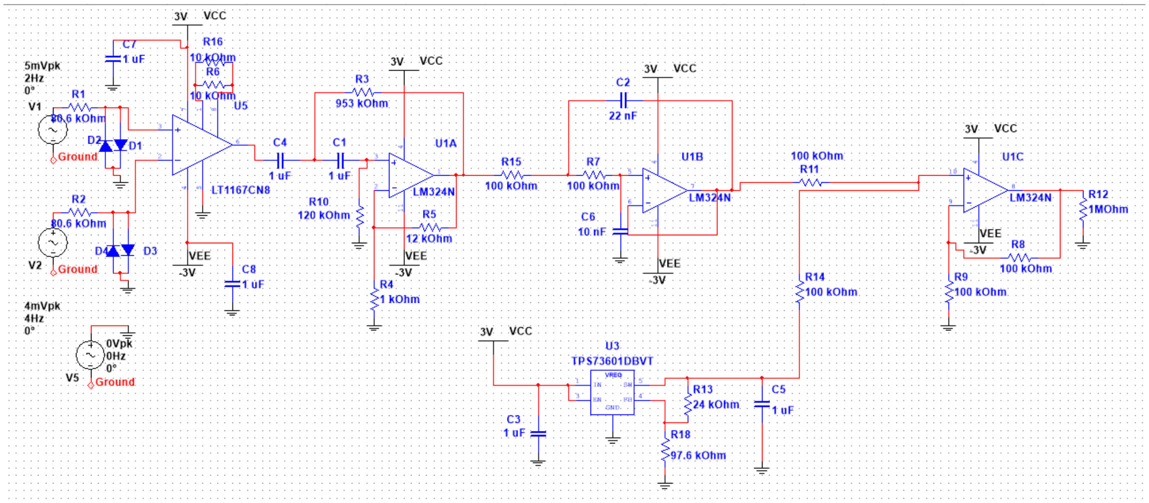

ECG Circuit Schematic

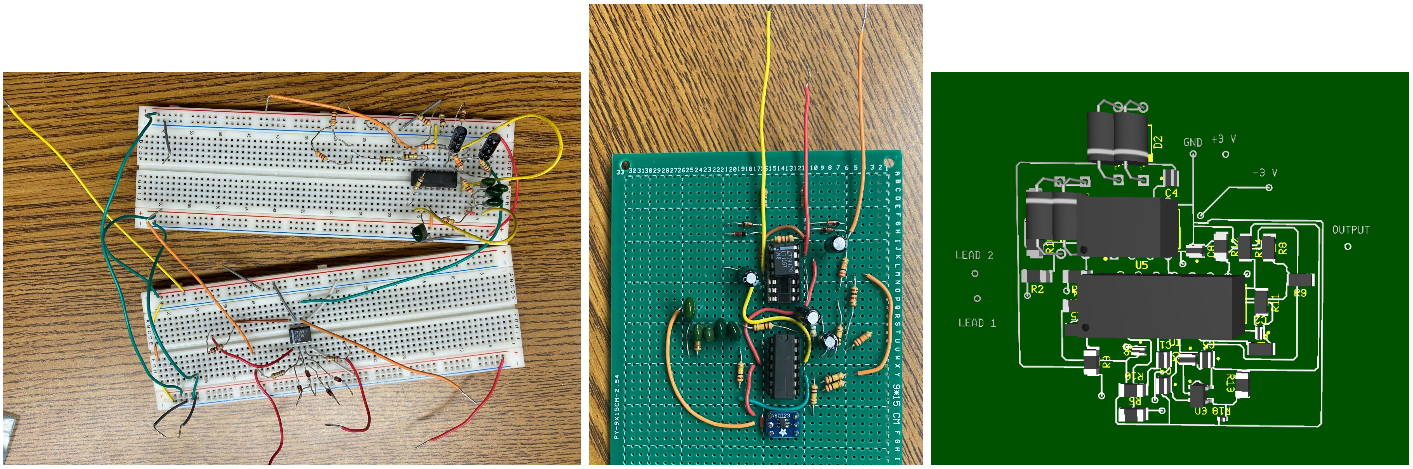

ECG circuit on a protoboard (left), solderboard (middle), and PCB mock-up (right)

The second part of our project was to write detection algorithms in MATLAB. The R-wave detection algorithm was implemented using Pan-Tompkins' methodology. We designed a fourth-order Butterworth bandpass filter with a passband of 5-15 Hz, a squaring function, and a second-order Butterworth lowpass filter with a cutoff frequency of 5 Hz using MATLAB filter design functions. After that, we implemented a peak detector using thresholds that automatically update with each new peak detected. The blackbox diagram below illustrates the flow of the signal being filtered and the R-waves being detected.

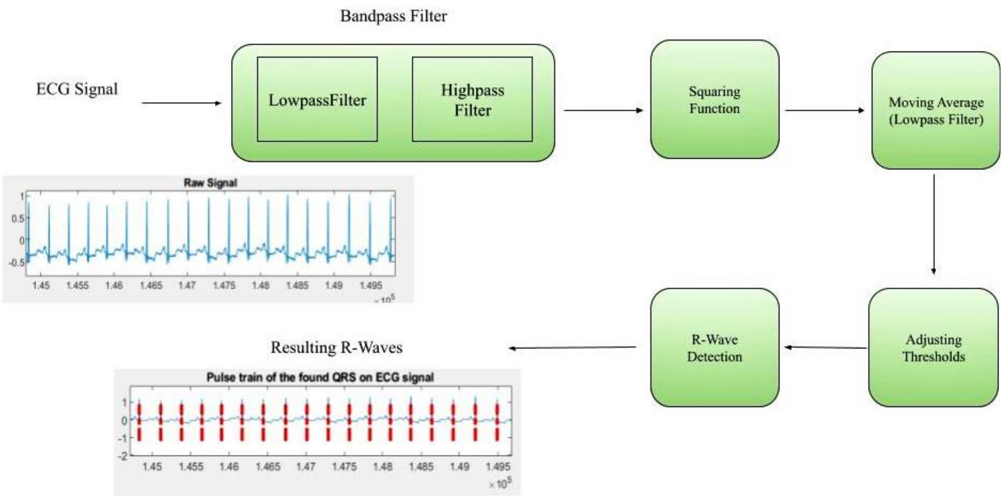

Blackbox diagram of the R-wave detection signal flow

Once the detection algorithm was complete, we tested it using the MIT/BIH arrhythmia and atrial fibrillation databases, which combined, had a total of 71 subjects, over 255 hours of recordings, and the recordings included normal sinus rhythm, arrhythmias (such as PVCs), and atrial fibrillation. We were able to produce graphs of whole recordings and overlay vertical red dashed lines where detections are found, as shown in the figure below:

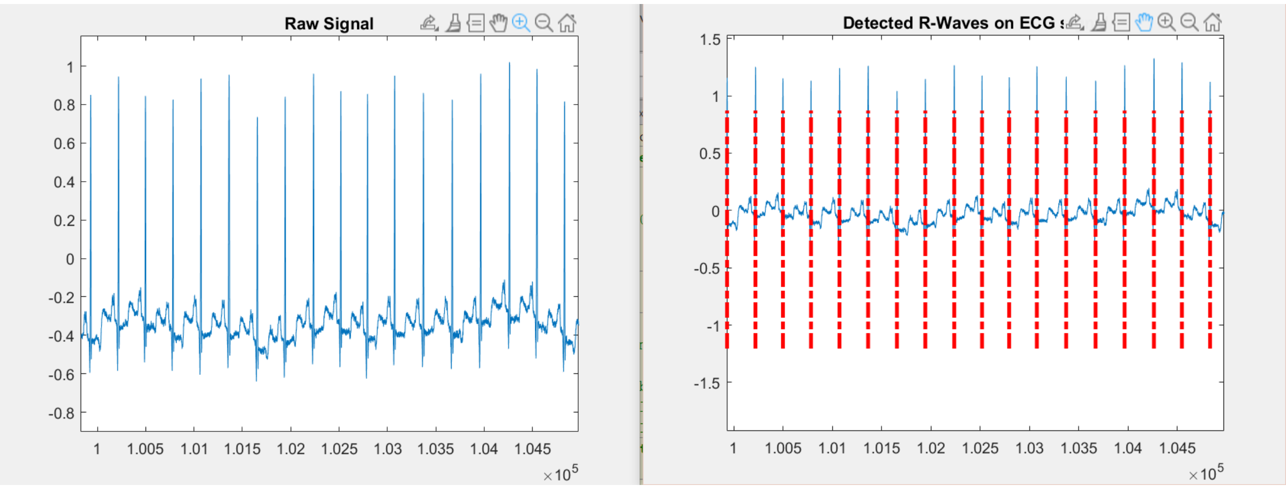

Left graph shows normal sinus rhythm for Lead I of subject 100, showing 4500 samples of data. Red dashed lines in the right graph mark each detected R-wave, using the same data.

Our initial algorithm produced a QRS sensitivity of 85% or higher for 64/71 of the records we tested from both the Physionet arrhythmia and atrial fibrillation databases, and a QRS positive predictivity of 91% or higher for 69/71 of the records from both databases when tested on the first channel of the ECG array. There were seven "outlier" datasets, which we later realized was because six out of the seven recordings had very low amplitudes. To fix this amplitude issue, we attempted to use the second channel in the ECG array for all the records. Six out of the seven outliers from our first test produced a QRS sensitivity of 98% or higher and positive predictivity of 97% or higher; however, some of the records that performed well using Channel 1 did not perform as well using Channel 2, producing QRS sensitivities of 50% or less. This makes sense, because generally one channel has lower amplitudes and poor SNR, and for those records, Channel 1 produced the optimal signal. There were also records that performed well using both channels, with minor changes in the QRS sensitivity and positive predictivity.

We also modified the bandpass and lowpass filter orders and cutoff frequency and tested all the records with the modifications to determine the best parameters with the highest QRS sensitivity and positive predictivity. Specifically we changed our second-order lowpass filter to a first-order lowpass filter and modified the bandpass filter cutoff frequency from 5-15 Hz to 5-12 Hz. With this modification, we produced a QRS sensitivity of 85% or higher for 61/71 of the traces we tested from both the Physionet arrhythmia and atrial fibrillation databases, and a QRS positive predictivity of 91% or higher for 70/71 traces from both databases. While we were able to remove one of the seven outliers that the first set of testing produced, our overall improvement was not significant.

Our initial hypothesis was that modifying the cutoff frequency and changing the order of our filters would fix all of our outlier datasets, however, simply changing the channel did a better job than that. Additionally, there is one record in the atrial fibrillation database (subject 07162) that has low values for every modification that we tried. To make this algorithm more accurate, more complex logic would need to be implemented to ensure better QRS sensitivity and QRS positive predictivity for noisier signals with very high amplitudes.

The atrial fibrillation detection algorithm created was based on the methods used by Lee et al. RR intervals were calculated using R wave locations found from an R wave detector. The time varying coherence function (TVCF) was applied to segments of 128 RR intervals and the results analysed. The window size used by Lee et al. in their TVCF calculations was changed for our algorithm because we used a nonparametric versus their parametric approach which resulted in noisier data as seen in the figure below. To smooth the data we decreased the window size.

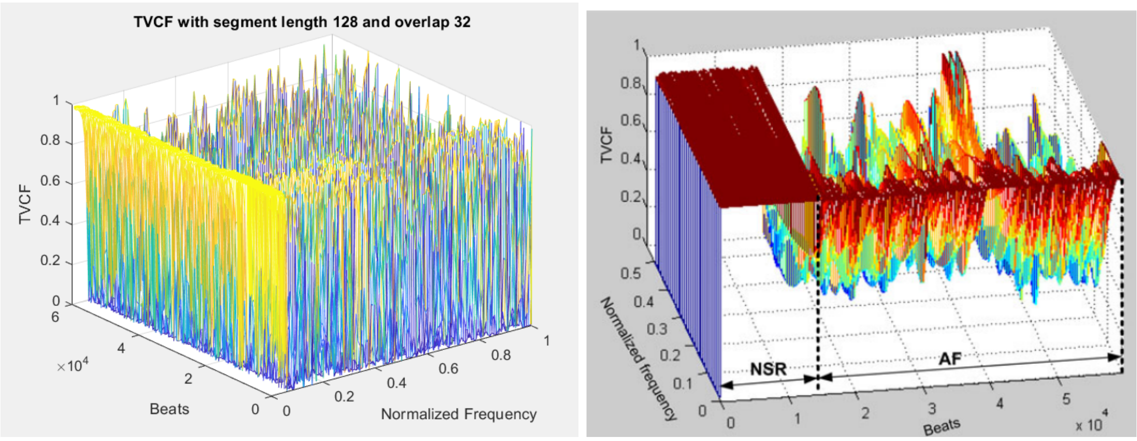

Plot of TVCF data for MIT/BIH Atrial Fibrillation subject 08455 with RR interval segment length of 128. Our data left and Lee et al. data right

Instead of calculating the frequency variation of the TVCF as done by Lee et al. a line was fit for each segment of the data. The y-intercept of the fitted line was found to be a good indicator of atrial fibrillation and was therefore used in our classification algorithm.

Another indicator that was used to classify atrial fibrillation was Shannon entropy. It measures the chance that patterns exhibiting regularity over some duration of data will also exhibit similar patterns over the next duration. Both the y-intercept and Shannon entropy values for subject 08455 are shown below. Segments are classified as atrial fibrillation if they have a Shannon entropy above 0.79 and a y-intercept below 0.71.

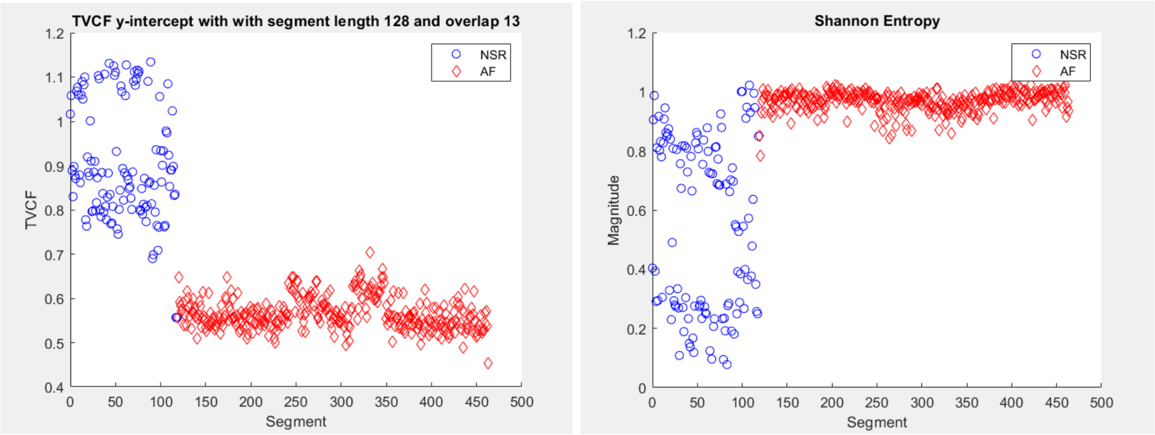

Y-intercept (left) and Shannon entropy (right) with classification from MIT/BIH Atrial Fibrillation annotations

Ultimately, the goals of this report were accomplished. We completed our ECG circuit schematic, implemented it on a protoboard and solderboard, and designed a PCB that will be ready for testing in the upcoming break. We were able to design and implement an R-wave detector in MATLAB, test on the MIT/BIH arrhythmia and atrial fibrillation databases, vary parameters such as filter orders and cutoff frequencies, and compare the differences between them, which resulted in us sharing our recommendations for how to further improve the algorithm. The atrial fibrillation algorithm is able to calculate the TVCF, the y-intercept of the frequency spectra, and the Shannon entropy for RR interval segments. The algorithm uses this information to classify segments as atrial fibrillation or normal sinus rhythm. These deliverables were made possible through extensive research and design done early in the project.

Table of Contents

1: Introduction

The human body creates electrical signals mediated by neural impulses, often initially triggered by stimuli. Stimuli can include a sound or pressure, but chemical release by other neurons can also trigger nerve impulses. Some electrical signals that can be measured from the body emanate from the heart, eye muscles, stomach muscles, and the brain, just to name a few. The primary focus of our research was on the heart and how to measure and analyze the electrical signals, electrocardiograms (ECG), it produces. Additionally, our research was focused on how to detect issues in the heart using ECG signals in order to diagnose illnesses. Finally, we focused on the hardware side, primarily how to build an ECG circuit and all the component specs that we looked into to determine the best option for our circuit, since our objective was to build a multi-lead wireless ECG monitor.

ECG has historically been measured using tethered wired measurement systems, but the newest generation of devices, such as exercise ECG monitors and the Apple Watch, are both wireless and untethered. These systems allow people to see their heart signals in a non-clinical setting, get their heart rate (as opposed to their pulse rate that most devices such as Fitbit provide), and also record the traces so that they can be reviewed at a later time. Our ECG monitor also follows the new generation of devices, being wireless and untethered, and is used to record ECG signals for a long period of time. It is intended to be small so that it can be mounted on the body for an extended period of time and collect ECG signals, which can be wirelessly sent to a computer for signal processing. For the signal processing, an R-wave detector and atrial fibrillation detector are used so that if the subject has atrial fibrillation, an episode can be detected. The ideal wireless system will be low power and use small components for efficiency and convenience and the ideal signal processing algorithms will be high accuracy and efficient.

2: Background

This chapter focuses on ECGs and ECG signals, the different types of algorithms that exist to analyze raw ECG signals, and the technical research that we did to understand the components needed to build our ECG circuit. We used literature written by experts in the fields to understand and later determine how we want to create our multi-lead wireless ECG monitor, R-wave detection algorithm, and atrial fibrillation detection algorithm.

2.1 The Heart and ECG Signals

The heart is the organ responsible for pumping blood throughout the body. Through the contraction of the cardiac muscles of the heart, blood moves between four chambers and circulates throughout the body and lungs. The four chambers of the heart consist of the right and left atria, and right and left ventricles. These chambers are separated by valves that only permit the flow of blood in one direction. The location of the chambers and valves can be seen in Figure 2.1. Deoxygenated blood moves into the right atrium (RA) then into the right ventricle (RV) where it is then pumped to the lungs and becomes oxygenated. The oxygenated blood moves to the left atria (LA) and finally into the left ventricle (LV). The LV is responsible for pumping oxygenated blood to the rest of the body. This whole process is part of the cardiac cycle. [1]

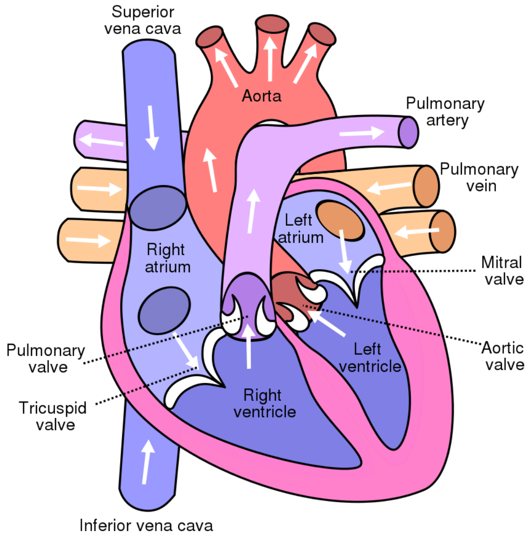

Figure 2.1: Basic heart anatomy [2]

The cardiac cycle is triggered by the sinoatrial node. This group of cells, located in the right atria, acts as the "heart's natural pacemaker" and sends a signal to the RA to contract. The signal is then passed to the atrioventricular node where there is a delay of about 0.1 seconds providing adequate time for the ventricles to fill with blood. The signal is then passed to the Bundle of His and then Purkinje fibers which are located in the inferior aspect of the heart and in the lateral aspects of the right and left ventricles**.** This signal causes the two ventricles to contract at the same time. The conduction system is depicted in Figure 2.2. The impulses in the heart create an electric potential that can be measured and used to calculate heart rate and diagnose many heart conditions. [3]

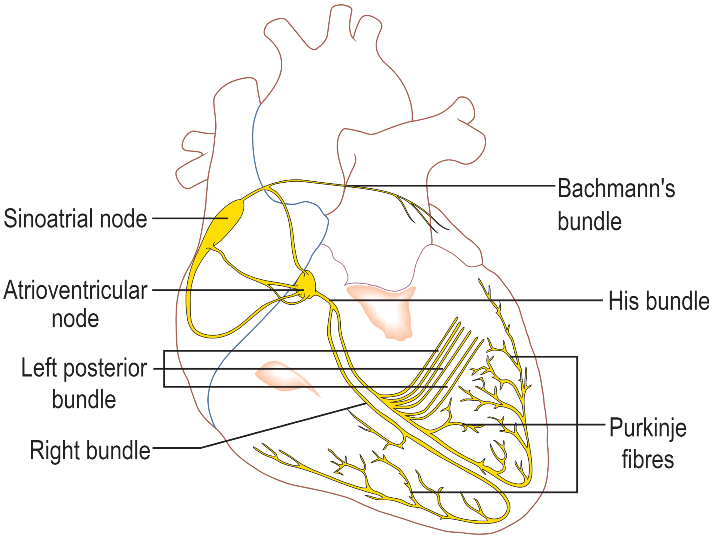

Figure 2.2: Electrical nodes of the heart [4]

An electrocardiogram (ECG, used interchangeably with EKG) is used to record electrical signals from the heart. There are both non-invasive and invasive tests available which use electrodes and leads attached onto specific sites of the body. Figure 2.3 shows the lead connections for non-invasive tests. The electrodes are then connected to electronics that transduce the signals from the body. LA corresponds to the left arm, RA corresponds to the right arm, LL corresponds to the left leg, and RL corresponds to the right leg.

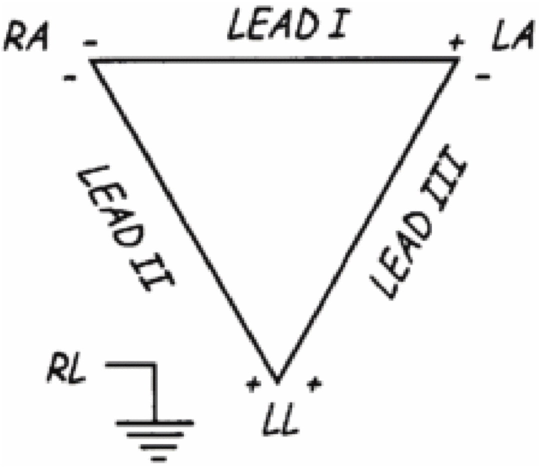

Figure 2.3: ECG Electrode Placement [5]

A normal ECG during one heartbeat resembles the signal in Figure 2.4. Figure 2.4 also identifies the five waves in an ECG: the P-wave, QRS complex, and T-wave. The P-wave corresponds to atrial depolarization, which is the contraction of the atria. The QRS wave is the ventricular depolarization and atrial repolarization, which means that the ventricles contract and the atria relaxes. Finally, the T-wave is the ventricular repolarization, where the ventricles relax thereafter then the next P-wave begins [6]**.**

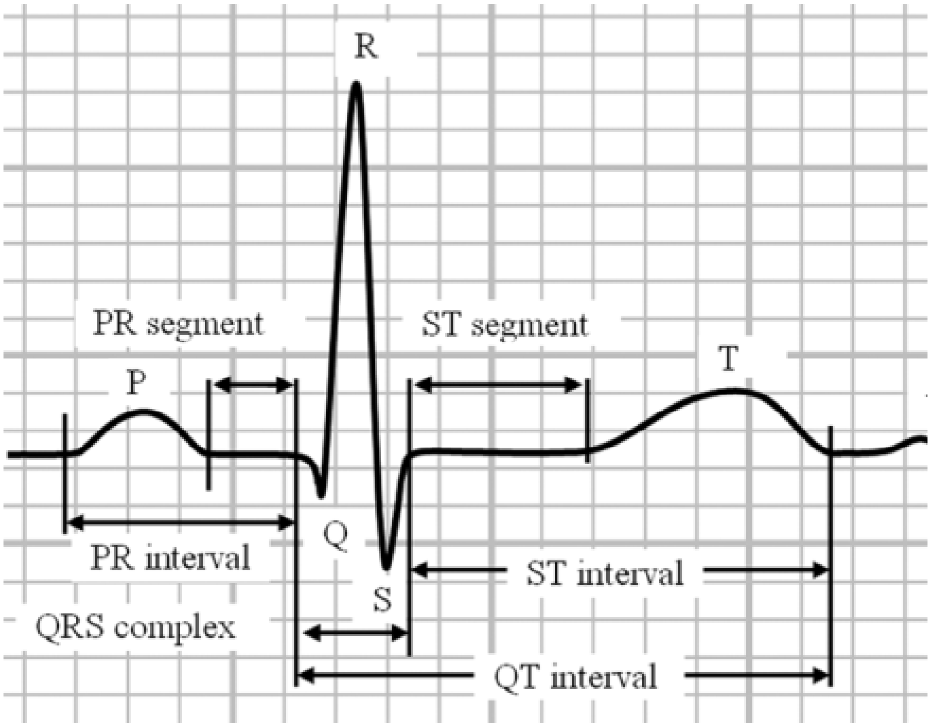

Figure 2.4: An ECG Signal with Labels [7]

It's important to note the QRS complex labeled in Figure 2.4 because later we will discuss a QRS detection algorithm, which can be used for extracting information on how the heart signal looks and for determining if the patient has any medical conditions. All information from the ECG signal is important, including the duration between each wave, in determining abnormalities.

Types of ECG abnormalities include beat and rhythm abnormalities. Beat abnormalities that originate in a location other than the SA node are called ectopic beats, the most common are premature ventricular contractions and premature atrial contractions [8]. These are characterized by their short long R wave-like impulse between normal beats [9]. Rhythm abnormalities are indicated by the heart beating too fast (tachycardia), too slow (bradycardia), or irregularly. The most common irregular heart rhythm is atrial fibrillation which will be discussed in a later section [10].

2.2: ECGs Today

ECG recordings are used in clinical environments to make sure that the heart is functioning as intended. These recording devices are built to be monitored by professionals, specifically 12-lead ECGs. In addition to the 12-lead ECGs used in professional environments such as hospitals, there are modern innovations in technology that have made electrocardiogram recordings more accessible and practical for average consumer use. Devices such as the Apple Watch (series 4 and onwards) and the Fitbit (Sense or Charge 5) have revolutionized the ECG field by creating a means of analyzing your heart from your wrist.

2.2.1: 12 Lead ECG

ECG recordings are extremely common procedures in doctors' offices, clinics, and hospitals. They are noninvasive procedures that pose essentially no risk of electrical shock and allow the monitoring of electrical signals going through the heart [11].

Higher end systems found in hospitals tend to record twelve leads in order to best observe the pattern of the heart. The system is referred to as a twelve lead system, but it is actually commonly composed of ten electrodes on the body. There are six precordial electrodes placed on the chest in a semi-circular pattern above the heart. These unipolar electrodes around the heart are identified as V1, V2, V3, V4, V5, and V6. These electrodes are all measuring data with respect to the common voltage reference which, in this 12 lead case, is the electrode on the right leg. V1 and V2 measure the right ventricle while V3 and V4 measure activity in the left ventricle and the front of the heart. Lastly, V5 and V6 cover the side of the heart. This formation is so that the leads can generate more amplitude from the signals in the heart with alternative “views" of the heart’s electrical activity as well as less noise when compared to the remaining electrodes on the extremities [12].

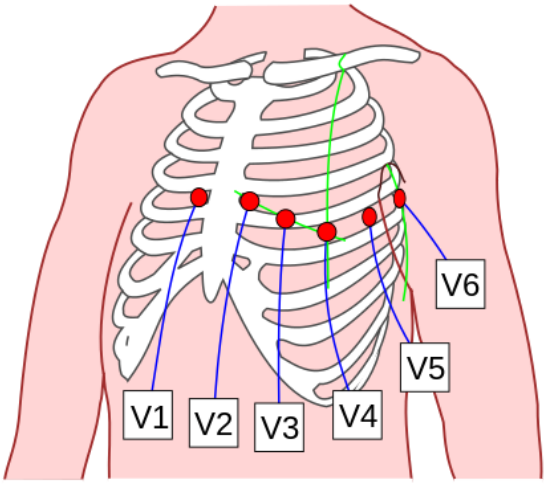

Figure 2.5: Placement of six unipolar electrodes [13]

With each heart contraction, blood is pumped through the body propagating the heart beat’s signal. As the heart contracts and pumps blood it moves around slightly in the chest. This movement causes the cleanest signal produced by the heart to move as well. Hence, this is the reason that there are 6 electrodes placed on the chest. The heart’s movement can make the signal hard to read and with the electrodes placed around the heart the ECG is able to use the different electrodes to create a more accurate signal [11]**.**

The remaining four limb electrodes are put in the four corners of the body with one on the left arm (LA), one on the right arm (RA), one on the left leg (LL), and one on the right leg (RL). In a twelve lead ECG, the right leg electrode acts as the ground for the system, with the benefit of minimizing ECG artifact [14].

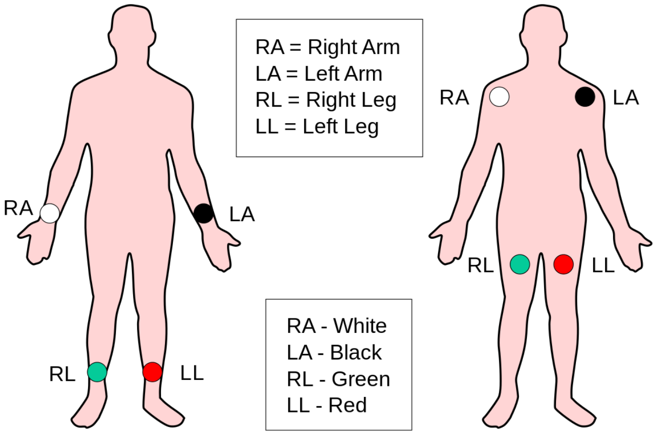

Figure 2.6: Placement of four dipole electrodes [15]

With four limb electrodes it is possible to receive 6 leads worth of data in a system known as Einthoven's Triangle. The principle behind Einthoven's Triangle is that the electrodes record not only relative to themselves which produce unipolar leads aVR, aVL and aVF but also relative to each other resulting in bipolar leads I, II, and III. This forms an equilateral triangle that we refer to as Einthoven's Triangle (Figure 2.7) [11].

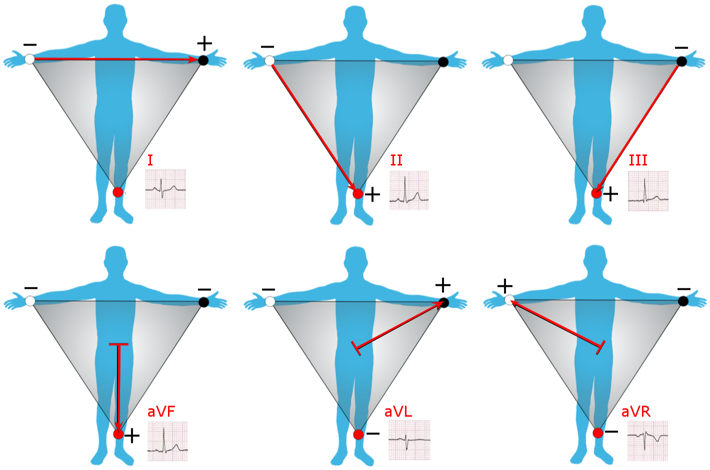

Figure 2.7: Einthoven's Triangle [16]

2.2.2: 3 Electrode ECG

A 12 lead ECG system is standard for use in hospitals, as it provides the most information and reliability. A 12 lead ECG requires 10 electrodes, which are not practical for a system that would be worn on the body outside of the hospital. For a system designed to be worn for long periods of time without restricting a person's normal daily activity, an ECG device with fewer electrodes is desired. As mentioned above, ECG measurements can also be taken using only 3 electrodes. Using Einthoven's Triangle, voltage differences between the electrodes are measured with electrodes placed at the shoulders and left leg [37]. Lead I is defined between the right and left shoulders, lead II is between the right shoulder and left leg, and III is between the left shoulder and left leg. This configuration allows an equilateral triangle to be formed with each lead equidistant from the heart. Since the triangle forms a closed loop, the sum of the voltages must be zero according to Kirchoff's laws. In Einthoven's triangle, the polarity of lead II is reversed. Therefore, the voltage at lead II is subtracted from the sum of I and III to equal a total voltage of zero.

In addition to placing electrodes around the body, a circuit must be constructed to view the ECG measurements taken from the electrodes. The voltage difference between leads I and III will be amplified using an instrumentation amplifier. The electrode placed on the leg acts as a reference node to ground to help reduce noise in the system. The resulting wave after the difference is amplified must be filtered to block out interference at unwanted frequencies outside of the ECG signal range. Additional amplification may also be required. The ECG circuit operation and relevant components are discussed in later sections.

2.2.3: 2 Electrode ECG

The purpose of using a 3 electrode ECG device is to make a system that is more comfortable for the user. Reducing the number of necessary electrodes for ECG measurement from 3 to 2 would create an even more convenient system. In Einthoven's Triangle, the ECG measurements are taken using the difference between leads I and III, and an additional electrode is placed at the right leg as a ground reference. Removing this ground node and creating a virtual ground between the other two electrodes still allows for ECG measurements to be taken [38]. However, the resulting signal would likely have additional noise that would not be seen with 3 electrodes. It is possible to see clear measurements with only 2 electrodes, but additional filtering is usually required.

2.2.4: Modern ECG Applications

Two modern practices include the placement of electrodes on your chest or the use of a single chest strap. The first method, requiring the placement of electrodes across your body, is the Holter Monitor. Holter Monitors are often requested by healthcare providers when symptoms such as dizziness, fatigue, low blood pressure, fainting, and palpitations are prevalent and the resting ECG measurements are inconclusive. Holter Monitors, shown in the image below, include the placement of five electrodes across the chest. The electrodes are wired to the ECG reading device (the Holter Monitor) and readings are recorded across a 24 hour period.

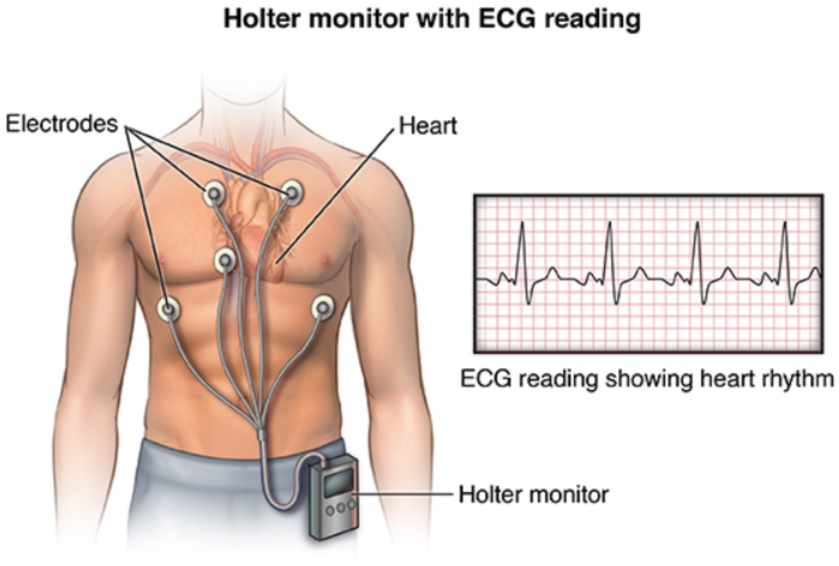
Holter monitor with ECG reading
Electrodes
Heart
ECG reading showing heart rhythm
Holter monitor

Figure 2.8: Holter Monitor Demonstration [17]

The second method of chest worn ECG recording devices is the use of a single compact chest strap. The Polar H7 Heart Rate Sensor and Fitness Tracker is a compact, Bluetooth-capable fitness device that provides features such as measuring heart rate, recognizing heart rate variability, and counting calories. The device is also waterproof and has 200 hours of battery life, making the device practical for endurance athletes. A validation study for the device, consisting of a variety of male subjects (age, body composition, and fitness level), was conducted and the results demonstrated that the H7 produces interchangeable results with lab based ECG readings at rest, excellent agreement during exercise, and reasonable agreement during intense exercise.

Apple Watches perform pulse rate and electrocardiogram measurements through the use of two features within the watch. By utilizing the pulse rate monitor on the underside of the Apple Watch, along with placing an individual's finger on the digital crown to the side of the watch, the watch can collectively record and present valuable and relatively reliable data on your heart. The pulse rate monitor on the underside of the Apple Watch uses a process known as photoplethysmography (PPG). The PPG sensor emits green LED light paired with photodiodes to detect how frequently an individual's blood is pushed through the veins in their wrist. By flashing the LED light hundreds of times per second the watch can recognize the variation in light absorbed, thus, creating a proper pulse rate measurement (this sensor is capable of recording between 30 and 210 beats per minute). The digital crown has built-in electrodes that, when a fingertip from your contralateral hand is placed on top, create a closed circuit between your heart and both arms. Apple advertises the watch as capable of recording recognition of sinus rhythm (depolarization of the heart beginning in the sinus node characterized by correctly oriented P-waves), atrial fibrillation (heart beating irregularly, the most common form of serious arrhythmia), a low or high heart rate, and an inconclusive result. As of the most current application software, the Apple Watch is capable of measuring heart rate readings within the range of 50 to 150 beats per minute.

The Fitbit Sense and Charge 5 operate similarly to the Apple Watch. Both the Sense and Charge 5 utilize sensors within the frame of the watch along with their biosensor core to record ECG measurements when an individual places their fingers to the sides or corners of the watch frame. Possible results from Fitbit measurements as advertised include sinus rhythm, atrial fibrillation, and inconclusive.

Without the addition of the digital crown in the Apple Watch or the sensors within the Fitbit frames to close the circuit across an individual's arms and chest, the watches would only be capable of measuring pulse rate (a significant distinction). Heart rate, measured with ECG devices, reads the quantity of times that the heart contracts per minute. Pulse rate, on the other hand, reads the pulse of blood flow through the arteries (caused by the contraction of the ventricles). Apple Watch and Fitbit both utilize green LED lights to calculate the blood flow through the capillaries, thus, without the additional sensors, would only be measuring pulse.

An emerging substitute for the Apple Watch or Fitbit is a wearable PPG recording device that can be worn on the finger. The Oura Ring is a multisensory wellness device that weighs roughly 4 grams and can survive for one week on a single battery charge. Through studies within a relatively small sample group (60 participants) it was determined that the PPG sensors within the Oura Ring are capable of producing nearly identical measurements to the ECG recording devices provided to the group. These measurements, however, are limited to the ring's capability of reading only pulse rate or pulse rate variability. While the Oura Ring is less capable than an Apple Watch or Fitbit, the small size and comfortability provides the unique opportunity to collect nightly readings across an extended period of time when compared to its competitors.

Finally, further revolutions within the field are bringing ECG measurements to headphones. In 2019, Heart.Zone released headphones with continuous ECG reading capability. The technology uses electrical contacts within the ears and on the skin, and its performance is advertised as unaffected by sweat, hair, or wobbling due to motion. The Application Programing Interface (API) within the headphones enables communication with cellular applications and provides real time visualization of the ECG measurements as well as the capability to store the data measurements on a phone or in the cloud. In late 2020, Apple announced their commitment to create a miniature version of their PPG sensor for use within Beats headphones.

2.3: Analog Front End

The upper limit of ECG voltage readings on the skin while the heart is beating in regular sinus rhythm is 2.5 - 3.0 mV and the typical frequency range for ECG readings is 0.5 to 100 Hz [18]. ECG readings can be measured utilizing two different methods, bipolar or unipolar. Bipolar leads register the voltage difference between two electrodes on the skin while unipolar leads compare the difference between the heart's activity and what is known as an indifferent or Wilson electrode. The indifferent electrode acts as a virtual reference (negligible voltage activity). Given the voltage and frequency ranges, and in understanding the functionality of unipolar and bipolar ECG readings, to properly analyze the electrical signals generated from an individual's heart the circuitry must be capable of taking the difference, amplifying, and filtering the signal to a reasonable viewing standard. The following section will discuss the methodology in doing so along with relevant explanations of the chosen circuit components.

2.3.1: Differential and Instrumentation Amplifiers

As mentioned previously, bipolar ECG readings measure the electrical potential difference between corresponding electrodes attached to the skin and unipolar readings compare the heart's activity with a virtual reference. Therefore, circuitry that can take the difference between the two electrical potentials and output that difference is required. Furthermore, typical voltage readings within sinus rhythm are in the range of millivolts. The circuit must also be capable of amplifying the resulting difference for proper viewing. Figure 2.9 shows an example of circuitry capable of this functionality.

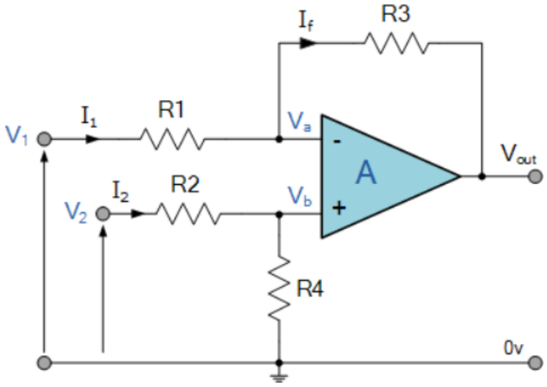

Figure 2.9: Differential Amplifier Circuit

Differential amplifier circuits utilize both inverting and non-inverting amplifier configurations. If the input voltage V_2 is 0, the circuit assumes the role of an inverting amplifier with input-output expression:

$$V_{OUT} = (-R3/R1)V_1 \tag{2.1}$$

If the input voltage V_1 is 0, the circuit assumes the role of a non-inverting amplifier with input-output expression:

$$V_{OUT} = (R3/R2)V_2 \tag{2.2}$$

Through applying the superposition principle to the two previous equations, and equating R2 to R1 as R, an input-output expression for the entire differential amplifier is:

$$V_{OUT} = (V_2 - V_1)(R3/R) \tag{2.3}$$

The gain of a difference amplifier is reliant on the resistance values within the expression above. Namely, for there to be significant gain, the value of R must be smaller than R3. The differential amplifier functions properly while inputs to the circuit have a low output impedance.

However, when input impedances are similar to resistance R, -as is the case for ECG- the measurement becomes faulty. To resolve this issue, the following circuit maintains the amplification functionality of the difference amplifier with the necessary additional high input impedance. This elaborated circuit, shown in Figure 2.10, is referred to as an instrumentation amplifier.

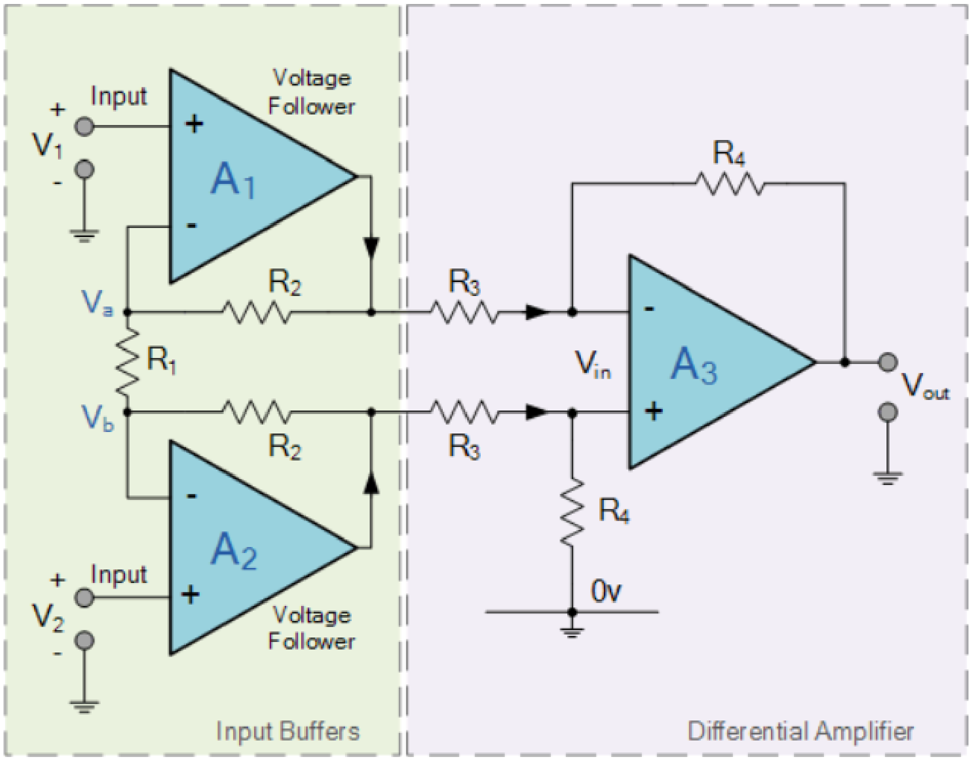

Figure 2.10: Instrumentation Amplifier Conceptual Design

The instrumentation amplifier introduces two non-inverting amplifiers to the input of the difference amplifier. The output of each non-inverting “buffer” amplifiers serve as the input to the differential amplifier and can be modeled with input-output expression:

$$V_{OUT} = (1+ 2R2/R1)V_{IN} \tag{2.4}$$

By combining the expression for the non-inverting amplifiers with the previous input-output expression for the differential amplifier, the entire input-output expression for the instrumentation amplifier is obtained as (Konar et al. 2019):

$$V_{OUT} = (V_2 - V_1)(1+ 2R2/R1)(R4/R3) \tag{2.5}$$

The instrumentation amplifier circuit forces the output impedance of the non-inverting amplifiers to serve as the input impedance of the difference amplifier. Therefore, the impedance can be selected to prevent interference with the differencing. Ultimately, the final circuit produces high input impedance to the instrumentation amplifier and low output impedance from the instrumentation amplifier. Analog Devices's AD620 instrumentation amplifier is one of the two models used in preliminary ECG circuit testing for the group. The AD620 is capable of producing gains of up to 10,000 while drawing a maximum current supply of 1.3 mA. The low power capabilities of the AD620 make it ideal for battery powered operation, thus making the amplifier advantageous for future design implementations. Finally, the AD620's gain is set by an external programmable R1 resistor and the unit has eight pins. Analog Devices' AD624 on the other hand, has gain set by programmable pins, with the chip providing gains of 1, 100, 200, 500, and 1000 by pin selection. There is also the capability to set gains between 1 and 10,000 with a programmable resistor. The AD624, unlike the AD620, has sixteen external pins including input and output null pins.

2.3.2: Filtering

Typical ECG measurement produces frequencies between 0.05 and 100 Hz (for non-infants) in the passband. The QRS complex, the most significant portion of the ECG wave for the group's measurements, falls within 8-50 Hz. Furthermore, a collection of other unwanted artifacts, including baseline wander, powerline interference, EMG noise, and electrode motion artifacts amongst others also prevent a clean ECG signal reading. Therefore, it is necessary to use a variety of filtering techniques to eliminate the unwanted artifacts.

As aforementioned, the pin layout on the AD624 differs significantly from the AD620. Input pins 4 and 5 on the AD624 are the designated input null pins. These pins have the capability of nullifying the potential 300 mV offset voltage within the differentiator. DC offset measures the voltage across a gel-to-gel electrode pair due to the difference in their electrode half-cell potentials. In an ideal situation the potentials would be identical, however, impurities within the metal electrode or variations within the gels produce a maximum allowable DC offset of 300 mV [19].

Utilizing the AD620 instrumentation amplifier removes the built-in input nulling functionality that the AD624 provides, however, the filtering techniques used after each amplifying stage will be identical. Active highpass and lowpass filters would be connected across the output of both amplifiers to form a bandpass filter. Sallen-Key filters are commonly used highpass and lowpass circuit topologies given the easily cascadable lowpass and highpass stages. Figures 1.12 and 1.13 are the topologies of the second order highpass and lowpass Sallen-Key filters respectively:

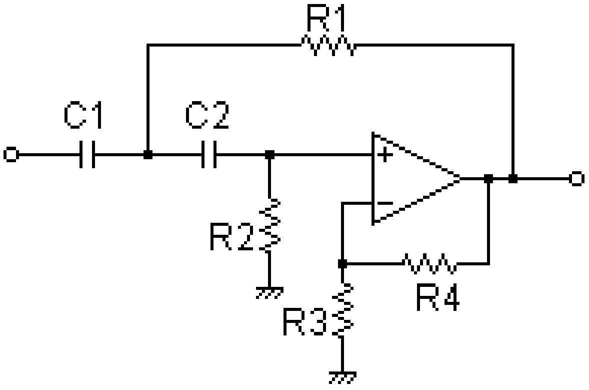

*Figure 2.12: Second order Sallen-Key highpass filte*r

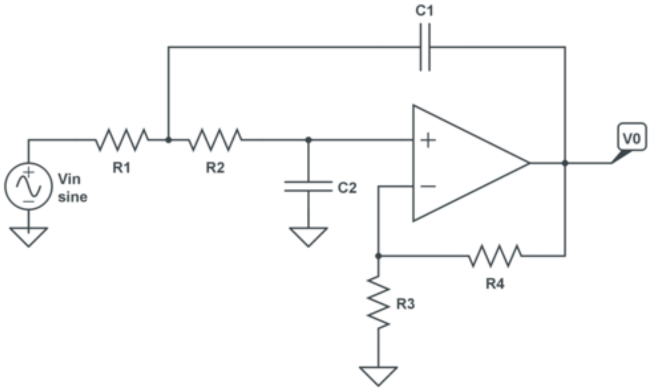

Figure 2.13 : Second order Sallen-Key lowpass filter

The transfer functions of the Sallen-Key second order highpass filter and second order lowpass filter respectively are [20]:

$$H(s) \ = \frac{\frac{R_3-R_4}{R_3} s^2 R_1 R_2 C_1 C_2}{s^2(R_1 R_2 C_1 C_2) + s(R_2(C_1+C_2) + R_1 C_2(1-\frac{R_3+R_4}{R_3})) + 1} \tag{2.6}$$

$$L(s) \ = \frac{\frac{R_3+R_4}{R_3}}{s^2(R_1 R_2 C_1 C_2) + s(C_1(R_1 +R_2) + R_1 C_2(1-\frac{R_3+R_4}{R_3})) + 1} \tag{2.7}$$

With the ideal bandpass filter, a flat magnitude response is desired in the pass band. Butterworth filters are often referred to as “maximally flat filters” due to their flattest pass band magnitude response (when compared with other filter designs such as Chebyshev or Elliptic). Seen below is the ideal magnitude response for a Butterworth lowpass filter:

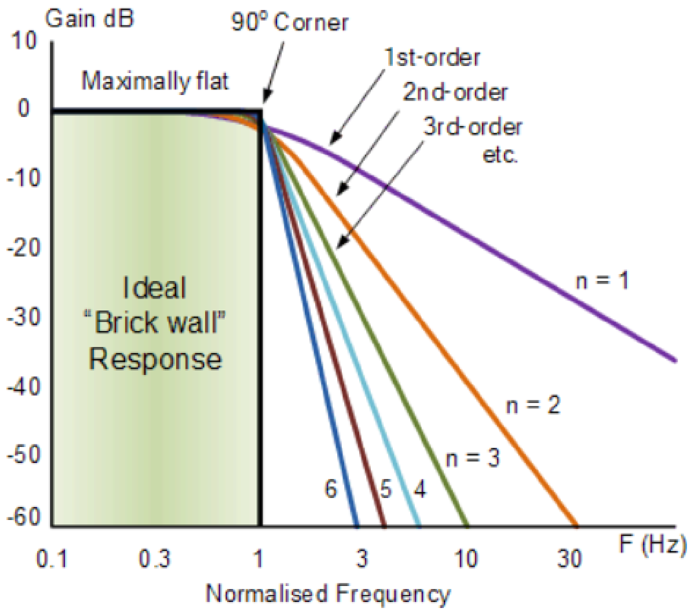

Figure 2.14: Ideal Frequency Response for a Butterworth Lowpass Filter

Butterworth filters can be constructed by cascading Sallen-Key active filters. As can be seen from Figure 2.14, the higher order the filter the steeper the roll off. Therefore, higher order filters are desirable to attenuate the various artifacts. However, this comes at the cost of a greater number of circuit components and power consumption. To construct the necessary bandpass filter, the output of the instrumentation amplifier is passed through an n^{th} order highpass filter then through an n^{th} order lowpass filter. The active highpass filter occurs before the lowpass filter to implement the gain with the least noise possible. As the signal is passed through various circuit components it will accrue noise. By introducing gain in an earlier stage of the circuit design the inevitable noise from later stages in design will not be amplified.

2.3.3: Summing Amplifier Level Shift

Following the filtering stage of the ECG circuit is a necessary level shifting phase. This stage is necessary due to the input voltage readings to the circuit swinging both positive and negative, with the negative parts being amplified throughout the circuit. The entirety of the circuit prior to the level shifting stage operates off a bipolar power supply. The Analog to Digital Converter (ADC) on the Microcontroller, however, operates off unipolar power. Given the switch from bipolar to unipolar power supply, an upward shift of the voltage is necessary. This level shift is accomplished with a summing amplifier stage. An example of a summing amplifier is shown below in Figure 2.15.

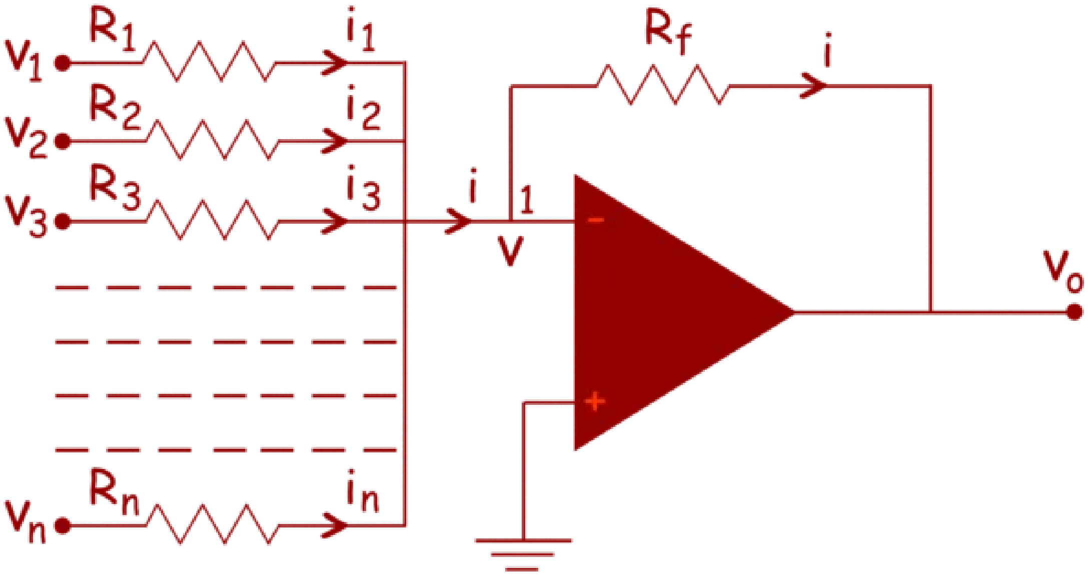

Figure 2.15: Summing Amplifier Level Shift Example [21]

Given the fundamental functionality of no voltage differential between input terminals in op amps (exhibiting stable negative feedback), the voltage into the amplifier can be determined utilizing Kirchoff's Current Law as follows. By treating the negative input node to the amplifier as V:

$$(V1 - V)/R1 + (V2 - V)/R2 + \dots + (VN - V)/RN = 0 \qquad (2.8)$$

If each of the resistance values are identical they cancel out within the equation, leaving only:

$$V1 + V2 + \dots + VN = NV \qquad (2.9)$$

The final voltage of the circuit can then be expressed as:

$$V = (V1 + V2 + \dots + VN)\,/\,N \qquad (2.10)$$

This results in a simple voltage added, while simultaneously reducing the amplitude of each signal by the quantity of signals being summated. Implementing a non-inverting feedback stage can reverse the decrease in amplitude of each signal and effectively create the desired summated signal.

2.3.4: Analog to Digital Converter

Regardless of the instrumentation amplifier chosen for the design, both designs would require the connection of an analog to digital converter across the output of the filtering stage. An analog to digital converter (ADC) converts the analog output of the instrumentation amplifier into digital data, which is necessary for processing and storing the information with a data logging format. Traditional 12 lead ECG systems were hardware intensive. Minimizing both the cost and power consumption of the ADC component is crucial for this project's final application.

There are a variety of stand-alone ADCs available including but not limited to flash, folding, half-flash, pipelined, SAR, and integrating (unknown) ADCs. Furthermore, Microncontrollers exist in the current market with ADCs implemented within the system. When discussing ADCs there are three universal performance parameters to compare; sampling rate, resolution, and power dissipation. For the application within this MQP, the performance characteristics are weighed against the cost of the component. Figures 2.16 and 2.17 demonstrate the stated (as advertised) and effective (as measured) number of bits per sampling rate for each of the ADC types.

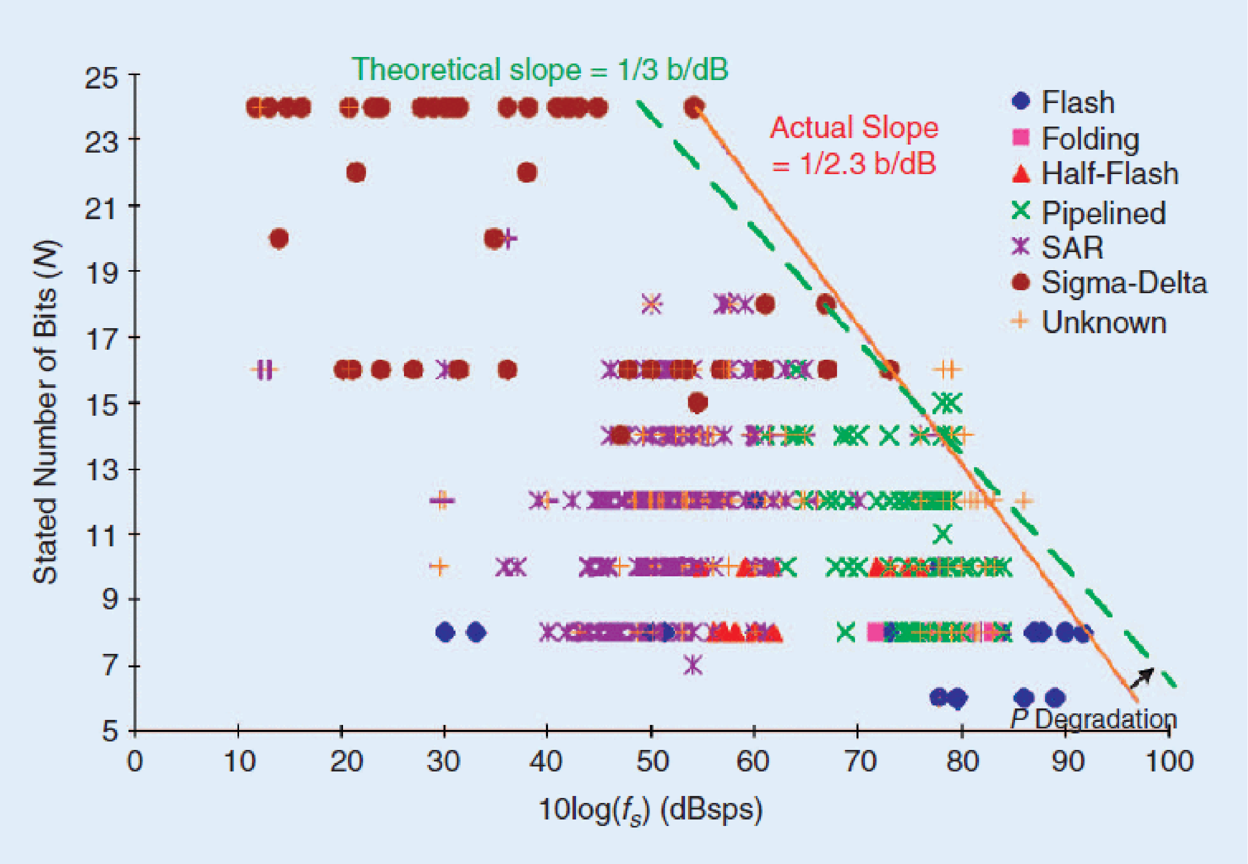

Figure 2.16: ADC Stated Number of Bits vs. Sampling Rate (sps = samples per second) [22]

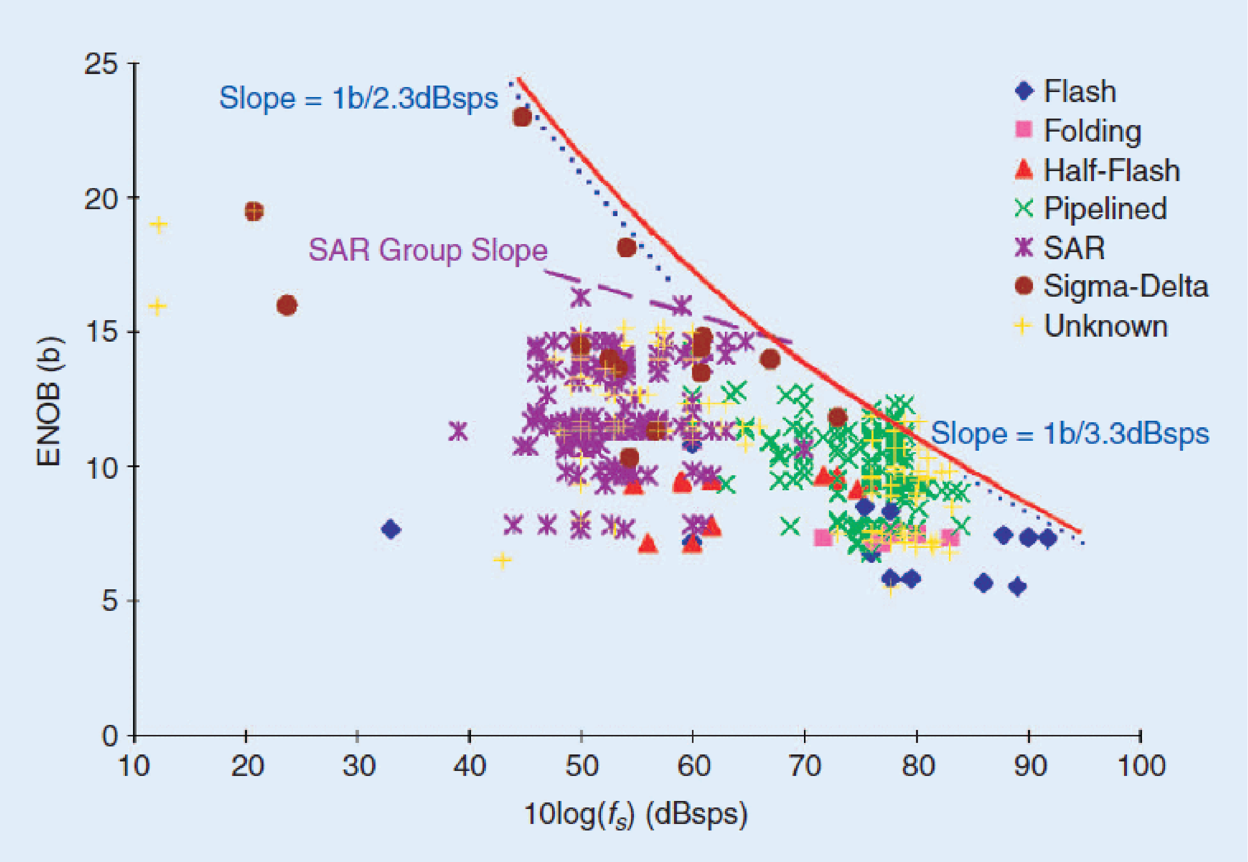

Figure 2.17: ADC Effective Number of Bits vs. Sampling Rate [22]

The pipelined and unknown structures have the best overall performance and are frequently used in military applications. SAR ADCs provide a wide range of speeds and resolutions at a relatively low cost and power dissipation rate. Sigma-Delta ADCs have the highest resolution with low sampling rates while Flash ADCs have the highest sampling rates. Figure 2.18 demonstrates the power dissipation per sampling rate for each of the ADCs.

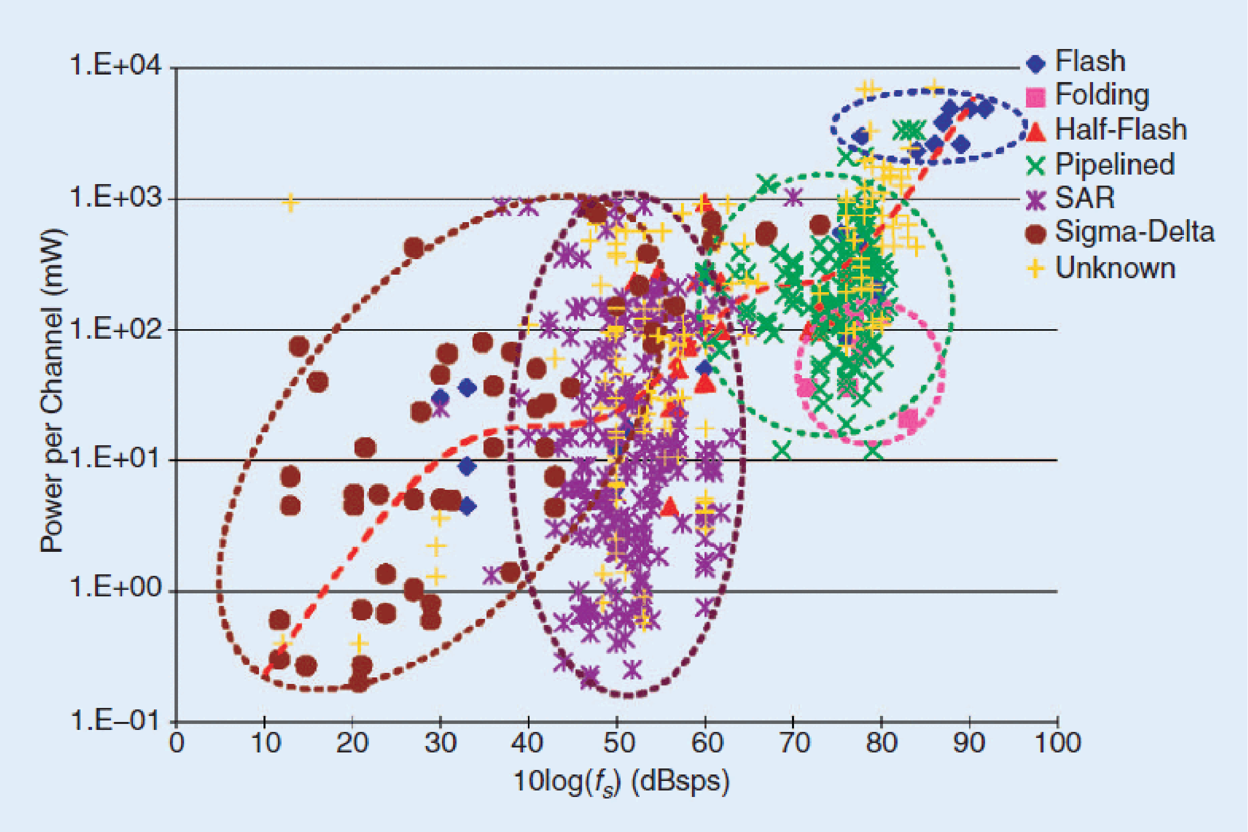

Figure 2.18: ADC Power Dissipation vs Sampling Rate [22]

After evaluating the power dissipation and bit rates of the various ADCs, two figures-of-merit can be determined. These figures-of-merit, P and F, are widely used and are modeled in their respective equations below. In these equations, B stands for the effective number of bits (ENOB), f_S is the sampling rate, and P_{diss} is the power dissipation. Figure-of-merit P evaluates the combined resolution and speed performance of the ADC while F factors in power efficiency against performance [22].

$$P = 2^B * fs \qquad (2.11)$$

$$F = (2^B * fs) / P_{diss} \qquad (2.12)$$

2.3.5: Additional Components

The final component necessary within the nodes of the ECG system are the wireless microcontroller units (MCUs). Both Texas Instruments and Nordic Semiconductor offer wireless microcontrollers, among others. TI and Nordic MCUs offer similar performance characteristics/prices and include ADCs within the board. The wireless MCUs are necessary to transfer the signal data via Bluetooth to our data logging device (a phone or laptop). Notable MCU choices are the TI CC2642R and the Nordic nRF52840. Table 2-1 offers relevant features for both microcontroller options.

Table 2-1: MCU Features

Feature	TI CC2642R	Nordic nRF52840
Price	$1-2 MCU alone Observed development kits ranging from $40-50	$3-6 MCU alone Observed development kits ranging from $40-70
Processor	Arm Cortex-M4F	Arm Cortex-M4F
Clock Speed	48 MHz	64 MHz
Memory	352 KB flash + 256 KB ROM + 8 KB SRAM + 80 KB ultra-low leakage SRAM	1 MB flash + 256 KB RAM
ADC	12 bit, 200 KS/s, 8 channels	12 bit, 200 KS/s, 8 channels
Receiver Sensitivity	-105 dBm	-103 dBm

The ADS1291 ECG system on a chip (SoC) presents an entirely different alternative to the previous analog designs discussed. The ADS1291, manufactured by Texas Instruments, features a 24 bit delta-sigma ADC along with built-in ECG analog front end with programmable gain control, internal reference, and an on-board oscillator. Furthermore, the SoC requires low power (335 µW/ channel) and can function properly with a unipolar or bipolar power supply.

Regardless of whether the AD620, AD624, or ADS1291 is utilized for the peripheral nodes, the intent is to power the unit with a bipolar source. In other words, two batteries will be the power source for each of the nodes attached to the individual’s body. This, while occupying more physical space, will assist in making our low power circuit design.

2.4: ECG Information Analysis

After a raw signal is collected, it is important to analyze the signal to find any anomalies. Often, the raw signal is noisy and needs to be filtered to make the signal cleaner and then use the information provided by that signal to determine measurements such as heart rate. This can be accomplished by running the signal through algorithms that will, for example, detect the R-waves and determine data such as the time interval between each heartbeat and subsequently the heart rate. An algorithm for atrial fibrillation will detect any irregular beats in the signal through calculations and using the R-waves that are detected.

2.4.1: Heart Rate

One simple use for ECG is to calculate heart rate. Heart rate is usually expressed in units of beats per minute. If the time between successive R waves is known, the heart rate can be found. The heart rate for a healthy adult should be around 60 to 100 beats per minute [23]. One method of finding heart rate is to find the average of the instantaneous heart rate within a certain period of time. The instantaneous heart rate is calculated based on the time between successive beats. Another method is to manually count the number of beats in a minute, or count the number of beats in 15 seconds and multiply that by 4 to convert to the beats per minute. [24]

2.4.2: Pan and Tompkins R-wave Detection Algorithm

There have been various R-wave detection algorithms designed in the past years, but the first was done in 1985 by Jiapu Pan and Willis J. Tompkins. The Pan-Tompkins R-wave detection algorithm, also known as QRS detection algorithm, was originally designed in assembly language to operate on a Z80 or NSC800 microprocessor. It utilizes a dual threshold technique, which means that thresholds are determined from the filtered signal at two different filtering stages. The only disadvantage with this technique is that it works well mostly for regular heart rates and arrhythmias, but not so well with abnormalities such as bigeminy or trigeminy, since the time interval would change. Pan-Tompkins tested their algorithm using data from the Physionet Arrhythmia database. The algorithm is designed so that the ECG signal goes through an analog filter that bandlimits the signal to 50 Hz. This is the same as the dataset used in the

Pan-Tompkins tests, and it utilizes an analog-digital converter (ADC) to sample the signal at 200 samples/s. [25]

2.4.2.1: Algorithm Design Overview

The algorithm designed by Pan and Tompkins passes a raw ECG signal through three digital filters: the first is a linear integer coefficient bandpass filter which is composed of cascaded lowpass and highpass filters to reject noise. The second filter approximates a derivative, and the third filter squares the amplitude and then sends the signal through a moving-window averager. After filtering, the decision portion of the algorithm is initiated, and is divided into three distinct phases: two learning phases and detection.

The first learning phase requires two seconds of data to initialize and set threshold values for peaks from the ECG signals and noise. The second learning phase utilizes two full heartbeats to initialize the RR-interval average and RR-interval limit values. The detection phase creates two sets of thresholds, one set of signal and noise thresholds after the bandpass filter, and the other set of signal and noise thresholds after the moving average. They are used to make the algorithm as accurate as possible and to detect any missed beats, as the SNR improves after bandpass filtering. Every peak detected as an R-wave is represented by a vertical red dashed line on the signal. For every QRS complex that is detected, there is a 200 ms refractory period, which matches the physiological function of the heart [25].

2.4.2.1.1: Filter 1- Bandpass Filter

The first filter, a bandpass filter, is used to reduce any muscle noise and outside frequency interference. However, to ensure the desired passband frequency of 5-15 Hz that is used to maximize the QRS energy, Pan-Tompkins cascaded lowpass and highpass filters. In doing so, they achieved a 3 dB passband frequency of 5-11 Hz, which is close to their design requirements [25].

A lowpass filter is used with the following system function H(z) and amplitude response |H(ωT)||, where T = sampling period:

$$H(z) \; = \; \frac{(1-z^{-32})}{(1-z^{-1})} \tag{2.13}$$

$$|H(\omega T)| = \frac{\sin^{2}(3\omega T)}{\sin^{2}(\frac{\omega T}{2})} \qquad (2.14)$$

This results in the following difference equation that has a lowpass cutoff frequency of 11 Hz, a gain of 36, and has a filter processing delay of six samples:

$$y[n] - 2y[n-1] + y[n-2] = x[n] - 2x[n-6] + x[n-12] \qquad (2.15)$$

A highpass filter is used after the lowpass filter. It has the following system function H(z) and amplitude response |H(ωT)||, T = sampling period:

$$H(z) = \frac{(\frac{-1}{32} + z^{-16} - z^{-17} + \frac{1}{32}z^{-32})}{(1-z^{-1})} \qquad (2.16)$$

$$|H(\omega T)| = \frac{[256+\sin^{2}(16\omega T)]^{\frac{1}{2}}}{\cos^{2}(\frac{\omega T}{2})} \qquad (2.17)$$

This results in the following difference equation with a low cutoff frequency at 5 Hz, a gain of 32, and has a delay of 16 samples:

$$y[n] - y[n-1] = \frac{-x[n]}{32} + x[n-16] - x[n-17] + \frac{x[n-32]}{32} \qquad (2.18)$$

With the removal of all the noise and extra points from the raw signal, this filtered signal is used for learning phase one to determine the thresholds [25].

2.4.2.1.2: Filter 2 - Derivative

To obtain the QRS-complex slope, the signal is differentiated using a five-point derivative with the following system function H(z) and amplitude response |H(ωt)||, T = sampling period:

$$H(z) = 0.1T(-2z^{-2} - z^{-1} + z + 2z^{2}) \qquad (2.19)$$

$$|H(\omega T)| = \frac{1}{4}T[\sin(2\omega T) + 2\sin(\omega T)] \qquad (2.20)$$

This results in the following difference equation with essentially a linear frequency response between DC and 30 Hz:

$$y[n] = \frac{1}{8}[2x[n] + x[n-1] - x[n-3] - 2x[n-4]] \qquad (2.21)$$

The derivative filter mostly adjusts the slope to make the signal more visible but it does not have much of an impact on the overall algorithm performance [25].

2.4.2.1.3: Filter 3 - Squaring Function and Moving-Window Averager

Once the derivative signal is created, every single point is squared to make the data points non-negative and to provide non-linear amplification. The equation for this is:

$$y[n] = x[n]^2 \tag{2.22}$$

It then goes into moving-window averaging to merge the Q, R, and S waves into one large wave that can be detected as the largest peak by the algorithm. The number of samples, denoted by N in the equation, is important in the displaying of the waveform. We want the width of the window to hold the widest QRS complex, because if it is too narrow then there will be extra peaks in the averaged waveform and make it a challenge for QRS detection, and if it's too wide then the averaged waveform would merge the QRS and T waves. The equation to calculate the moving-window integration is:

$$y[n] = (\frac{1}{N})[x[n - (N - 1)] + x[n - (N - 2)] +\ldots+ x[n] \tag{2.23}$$

With this signal now filtered and modified to be more visible, the R-wave can soon be detected once parameters are set [25].

2.4.2.1.4: Setting Thresholds & R-Wave Detection

To determine the thresholds, a fiducial mark, which is the location of a potential R-wave, is first set to determine when to expect an R-wave. Since the time duration of the rising edge corresponds to how wide a single QRS complex is expected to be, the fiducial mark can be determined either from where the maximum slope of one QRS complex is located, or from the peak of the R-wave.

At the start of signal analysis, the first and second learning phases are initialized. The first learning phase requires two seconds of data to set threshold values for peaks from the ECG after the moving average and the bandpass filter for the signals ($SigPk_{est}$, $SigPkFilt_{est}$) and noise ($NoisePk_{est}$, $NoisePkFilt_{est}$). These values are the running estimates of the noise and signal thresholds that are automatically updated after each peak is detected and classified as a signal peak or a noise peak. The second learning phase utilizes two full heartbeats to initialize the RR-interval average ($RRAvg$) and RR-interval limit values ($RR\ Low\ Limit,$ $RR\ High\ Limit,\ RR\ Missed\ Limit$).

Next, for the detection phase, there are four thresholds created in total: a signal threshold after the ECG signal is filtered through the digital bandpass filter ($SigPkFilt$), a noise threshold after the ECG signal is filtered through the digital bandpass filter ($NoisePkFilt$), a signal threshold after the ECG signal goes through the moving average ($SigPk_{final}$), and a noise threshold after the ECG signal goes through the moving average ($NoisePk_{final}$). The higher threshold for both sets, generally the signal threshold, is used for the initial analysis of the signal. The lower threshold for both sets, usually the noise threshold, is used only in searchback and only if there is no peak caught by the higher threshold in the expected time interval (which was determined by the fiducial mark). Searchback is a technique that looks back once the whole signal is analyzed to detect any peaks that may have been missed the first time around. Equations 2.24-2.27 calculate what the estimated signal peak and noise peak thresholds would be for the final signal after all filtering:

$$SigPk_{est} = 0.125SigPk_{final} + 0.875SigPk_{est} \tag{2.24}$$

$$NoisePk_{est} = 0.125NoisePk_{final} + 0.875NoisePk_{est} \tag{2.25}$$

$$Thresh1 = NoisePk_{est} + 0.25(Sigpk_{est} - NoisePk_{est}) \tag{2.26}$$

$$Thresh2 = 0.5 * Thresh1 \tag{2.27}$$

Thresholds are applied to the bandpass filtered signal in the same way as above in Equations 2.28-2.31:

$$SigPkFilt_{est} = 0.125SigPkFilt + 0.875SigPkFilt_{est} \tag{2.28}$$

$$NoisePkFilt_{est} = 0.125NoisePkFilt + 0.875NoisePkFilt_{est} \tag{2.29}$$

$$ThreshFilt1 = NoisePkFilt_{est} + 0.25(SigpkFilt_{est} - NoisePkFilt_{est}) \tag{2.30}$$

$$ThreshFilt2 = 0.5 * ThreshFilt1 \tag{2.31}$$

During searchback, the signal peak is recalculated since the threshold is at a lower amplitude. Equations 2.32 and 2.33 present the new calculation:

$$SigPk_{est} = 0.25SigPk_{final} + 0.75SigPk_{est} \tag{2.32}$$

$$SigPkFilt_{est} = 0.25SigPkFilt + 0.75SigPkFilt_{est} \tag{2.33}$$

Additionally, if irregular heart rate is present, then both thresholds are reduced by 50% to accommodate lower amplitudes and make the algorithm more sensitive.

After this, the average RR-interval and rate limits are determined. There are normally two RR-intervals that are maintained: the first being the average of the eight most-recent beats ($RRAvg2$), and the other based on the average eight most-recent beats that fall within certain limits ($RRAvg2$). These limits are located at the threshold or very close to it:

$$RR\ Low\ Limit\ =\ 92\%\ *\ RRAvg2 \tag{2.34}$$

$$RR\ High\ Limit\ =\ 116\%\ *\ RRAvg2 \tag{2.35}$$

$$RR\ Missed\ Limit\ =\ 166\%\ *\ RRAvg2 \tag{2.36}$$

Finally the T-waves are identified when an RR interval is less than 360 ms. This identification is based on the maximal slope of the waveform, and if a maximum slope of a peak is determined to be less than half of the maximum slope of the preceding peak, then it is a T-wave. Otherwise, it is a QRS-complex. This can be tested using a database that has ECG signals; specifically, Pan and Thompkins used the MIT/BIH arrhythmia database to test their algorithm. [25]

2.4.3: Heart Rate Variability

Heart rate variability (HRV) is the measure of the time variation between instantaneous heartbeats and RR intervals. A healthy heart should vary in heart rate, and these variations are caused by changes, such as exercise, emotions, temperature, etc. Since there are variations in the heartbeats, the R-wave time locations that are detected are generally non-periodic; to make it periodic, the time series is resampled by interpolation so that the new periodic series can then be analyzed using power spectrum analysis. These time differences are normally on the order of hundreds of milliseconds [26].

HRV is important because it can be used to find anomalies in patients. An example of this is atrial fibrillation, where HRV is used to calculate the root mean square of successive differences (RMSSD), which is the difference between the size of adjacent RR-intervals. In the RMSSD formula below, “a” represents RR intervals in a sequence of length *l* and a(j) represents the RR-interval in “a”. [27]

$$RMSSD\ =\ \sqrt{\frac{1}{(l-1)}\sum_{j=1}^{l-1}\left(a(j\ +\ 1)\ -\ a(j)\right)^{2}} \tag{2.37}$$

There are algorithms that have been designed to calculate HRV, using time domain, statistical, and geometric methods. Time domain uses the detection of the QRS complex to determine the instantaneous heart rate or cycle length. The intervals between QRS-intervals are called normal-to-normal (N-N) intervals. Statistical methods are great for long ECG traces, such as ones that are 24+ hours long. HRV can then be determined in one of two ways: either from the direct measurements of the instantaneous heart rate or derived from the differences between N-N intervals. Using the standard deviation of the occurrences of N-N intervals, variability can be determined (among other measures). RMSSD is a measure that is derived from these interval differences. Geometric methods create a sample density distribution using N-N intervals. This method needs longer traces such as a minimum of a 20 minute trace, but 24 hours is preferred [26].

2.4.4: Atrial Fibrillation

Atrial fibrillation (AF) is a heart condition where the atria of the heart contracts irregularly [28]. Kannel et. al. [29] found that the incidence of AF increases every decade after 50 years of age and by the age of 80 about 10% of people are likely to develop this condition [29]. Men are 50% more likely to develop AF than women. The nonuniform electrical impulses occurring in the atria cause irregularly timed heart beats because of the unpredictability of impulses across the atrioventricular node [28]. The atrioventricular node sends signals to the ventricles telling them to contract, and when the node sends abnormal signals from the atria, the ventricles will contract irregularly [28].

Some possible causes of atrial fibrillation include surgical procedures, lung disease, hypertension, and coronary artery disease [28]. Those diagnosed with atrial fibrillation often report experiencing fatigue, dyspnea, dizziness, chest pain, and palpitations [28]. Atrial fibrillation increases the risk of thromboembolism and stroke which is why it is important to diagnose it as early as possible [28].

Electrocardiograms are used to help diagnose atrial fibrillation [28]. One aspect of the ECG wave that is associated with atrial fibrillation is the absence of a P wave [28]. This property of atrial fibrillation is hard to detect with computer algorithms, so most algorithms use the irregularity of R waves as the primary indicator. These two characteristics can be seen in Figure 2.19.

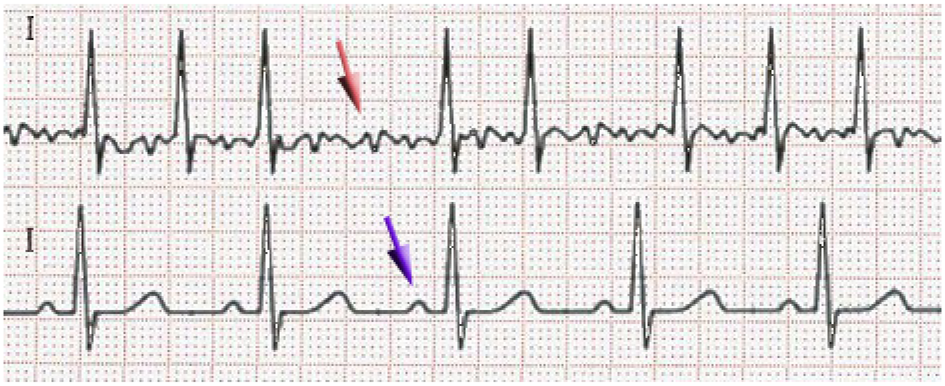

Figure 2.19: Bottom arrow points to a normal ECG P wave. Top arrow points to an ECG with atrial fibrillation

2.4.4.1: Atrial Fibrillation Detection Algorithms

We describe three methods in the literature that outline how to detect atrial fibrillation, with only one indicating that it could run in real-time.

2.4.4.1.1: Algorithm 1: Tateno and Glass, 2001

Tateno and Glass [30] used the coefficient of variation of RR intervals and probability density histograms. The coefficient of variation (CV) represents the relative variability in a data set [23, Ch. 4, pp. 169]. It is calculated by dividing the standard deviation by the mean and multiplying by 100% [23, Ch. 4, pp. 169].

$$CV = \frac{\sigma}{\mu} * 100\% \qquad (2.38)$$

$$\sigma = \sqrt{\frac{\Sigma(x_i - \mu)^2}{N}} \qquad (2.39)$$

In the above equations μ is the mean, N is the size of the data set, and x_i is each value in the data set. The higher the CV, the greater variability is present [23, Ch. 4, pp.169]. For atrial fibrillation, because of its inherent variability, the coefficient of variation is a good indicator of its presence in an ECG signal.

From the MIT/BIH ECG atrial fibrillation database, standard density histograms were created by categorizing beats into bins based on their RR and ΔRR intervals, where the ΔRR interval is the difference between successive RR intervals. After the histograms are constructed, the standard CV of the RR intervals and the standard CV of ΔRR intervals are calculated. When calculating the CV of the ΔRR interval, ΔRR is divided by the RR interval mean. This is done because the ΔRR mean from the histogram is approximately zero. Next, both the CV of RR and ΔRR intervals were calculated from a test data set. If the test coefficients of variation are within ±35% of the standard coefficients of variation, calculated from the histogram data, it is labeled as atrial fibrillation [30].

The data from the test recording is placed into a density histogram, and with the Kolmogorov-Smirnov test, compared to the standard density histogram created from the atrial fibrillation database. The Kolmgorov-Smirnov test is used to measure the difference between two distributions [30]. The equation for this test is

$$p = Q(\lambda) = 2 \sum_{j=1}^{\infty} (-\ 1)^{j-1} * e^{-2j^2\lambda^2} \tag{2.40}$$

where

$$\lambda = \frac{N_1 N_2}{(N_1 + N_2)}, \tag{2.41}$$

where N_1 is the number of points in the standard distribution and N_2 is the number of points in the test distribution. If the value of p is greater than parameter P_c=0.01 it is an indication of atrial fibrillation. The sensitivity and specificity of the Tateno-Glass model were 94.4% and 97.2%, respectively [30].

2.4.4.1.2: Algorithm 2: Dash et al., 2009

The model of atrial fibrillation detection developed by Dash, Chon, Lu, and Reader [27] finds the turning points ratio, the root mean square of successive RR differences, and Shannon entropy of an ECG in order classify a heart rhythm as being in atrial fibrillation. This model was published in 2009 and can run in real time [27].

The turning point ratio (TPR) is a nonparametric statistical test used to determine if the data set is random. For atrial fibrillation detection it is used to determine if the time between RR intervals is random by comparing them to their neighbors. The expected turning point ratio of an independent random set with Gaussian distribution is

$$\frac{2l-4}{3} \pm \sqrt{\frac{16l-29}{90}}, \tag{2.42}$$

where *l* is the length of the series. The TPR is calculated using the following equations,

$$\overline{p} = \frac{2l-4}{3}, \tag{2.43}$$

$$var(\overline{p}) = \frac{16l-29}{90}, \text{ and} \tag{2.44}$$

$$z = \frac{|p-\overline{p}|}{\sqrt{var(\overline{p})}} \tag{2.45}$$

where $\overline{p}$ is the number of turning points in a random set, $var(\overline{p})$ is the variance of the random set, p is the number of turning points in the set of RR intervals, and z is the TPR. If the series has a turning point ratio outside of the 95% confidence interval, it is considered to be in regular sinus rhythm [27].

The root mean square of successive RR difference (RMSSD) is an atrial fibrillation because of its high variability. It helps compensate for outliers that can cause false detection of atrial fibrillation. The RMSSD is used to find the value for RmsTHresh, one of the classification parameters. RmsThresh is the ratio of the RMSSD and the mean RR interval [27].

Shannon entropy measures the chance that patterns exhibiting regularity over some duration of data will also exhibit similar patterns over the next duration. White Gaussian noise has a Shannon entropy, SE, of 1, which is the maximum value because it is entirely random, whereas a sinusoidal wave has a SE of 0. For this application, the first segment of RR intervals is used to create a histogram. The eight highest and lowest values are removed and considered outliers. The remaining values are sorted into equally spaced bins. Once the values are sorted, the probability distribution is calculated for the ith bin by dividing the number of beats in the bin by the total beats in the segment, i.e.:

$$p(i) = \frac{N_{bin(i)}}{l-N_{outliers}} \tag{2.46}$$

where N_{bin} is the number of beats in the bin, *l* is the length of the segment, and $N_{outliers}$ is 16. Once all p(i) are found, SE can be calculated using the following equation,

$$SE = -\sum_{i=1}^{16} p(i)\frac{log(p(i))}{log(1/16)} \text{ [27]} \tag{2.47}$$

For the Dash et al. method, the presence of ectopic beats tends to result in the false classification of atrial fibrillation. In order to fix this issue, they propose filtering these beats out before applying the classification algorithms. The Dash et al. method has a sensitivity of 94.4% and a specificity of 95.1% [27].

2.4.4.1.3: Algorithm 3: Lee et al., 2013

The method of atrial fibrillation that had the highest sensitivity and specificity is that of Lee, McManus, and Chon [9]. It uses time varying coherence functions and Shannon entropy to classify ECG signals as having atrial fibrillation. The time-varying coherence function (TVCF) can be used to detect atrial fibrillation because the values for the function will significantly decrease if all or part of the segment contains atrial fibrillation [9].

Before the TVCF and Shannon entropy can be calculated ectopic beats are removed to reduce detection error. The RR interval ratio is calculated using the equation,

$$RR(i)/RR(i-1) \qquad (2.48)$$

where RR is the RR interval vector and i is the index value. The ratio is calculated for every value in the vector. The 1st, 25th, and 99th percentile were calculated for the ratio data. The conditions for a beat to be considered ectopic are

$$RR(i)/RR(i–1) < percentile\,1, \qquad (2.49)$$

$$RR(i+1)/RR(i) > percentile\,99, \qquad (2.50)$$

$$\text{and } RR(i+1)/RR(i+2) > percentile\,25 \qquad (2.51)$$

This method assumes that the surrounding beats are normal and therefore will not remove all the ectopic beats present but will remove enough to reduce overall error.

The TVCF can be found by calculating the nonparametric time-frequency spectra of the RR interval time series. The equation for the time-frequency spectra is:

$$|\gamma(t,f)|^4 = \frac{\left|S_{xy}(t,f)\right|^2}{S_{xx}(t,f)S_{yy}(t,f)}\frac{\left|S_{yx}(t,f)\right|^2}{S_{yy}(t,f)S_{xx}(t,f)} \qquad (2.52)$$

where $S_{xy}(t,f)$ and $S_{yx}(t,f)$ are the time-frequency cross spectrum of two signals, x and y. $S_{xx}(t,f)$ and $S_{yy}(t,f)$ represent the auto spectra of the two signals. The result of the above equation is a vector in the frequency domain. This equation is applied to two adjacent segments consisting of

RR interval data from an ECG. The first segment is signal x and the next segment is signal y. AF is indicated when the magnitude of the TVCF in the frequency domain decreases below a threshold as the frequency increases [9].

Once the TVCF is found the Shannon entropy is calculated to aid in accurate detection of atrial fibrillation. If the Shannon entropy value is above a threshold value of 0.79 and the TVCF frequency variation threshold value of 0.019, then the beats indicate atrial fibrillation. This method has a sensitivity of 97.41% and a specificity of 97.54% [32]. In Table 2-2, direct comparison of the three detection algorithms can be seen.

Table 2-2: Comparison of different atrial fibrillation detection algorithms

Comparison of Atrial Fibrillation Detection Algorithms			
Methods	MIT/BIH atrial Fibrillation database		MIT/BIH Normal Sinus Rhythm database
	Sensitivity (%)	Specificity(%)	Specificity (%)
Lee et al [32]	97.41	97.54	100
Dash et al [27]	94.4	95.1	99.7
Tateno and Glass [30]	94.4	97.2	N/A

2.5: Standards & Specifications Used

- To prevent any possible risk of shock to the person, we will be using high value resistors to keep the current at the worst case scenario of the full 4 V to the person with a current of under 10µV.
- IEC 60601-2-25:2011 applies to the basic safety and essential performance of electrocardiographs intended by themselves or as a part of a medical electrical system, for the production of electrocardiogram reports for diagnostic purposes. [33]
- IEEE 802.15.1-2002 This IEEE Standards product is part of the 802 family on LAN/MAN. Abstract: The lower transport layers [(Logical Link Control and Adaptation

Protocol (L2CAP), Link Manager Protocol (LMP), baseband, and radio] of the Bluetooth™ wireless technology are defined. Bluetooth is an industry specification for short-range radio frequency (RF)-based connectivity for portable personal devices. [34]

- ANSI/AAMI EC38:1998, the American National Standard for Ambulatory ECGs, and ANSI/AAMI EC57:1998, the American National Standard for Testing and Reporting Performance Results of Cardiac Rhythm and ST Segment Measurement Algorithms: These are the standards that are used to create beat-by-beat (bxb) comparison reports.

3: Project Strategy

In this section, we will share our deliverables, how we completed a portion of this project, and future directions we plan to take with the remainder of the project.

3.1: Original Client Statement

In this project, you will design a wireless, wearable ECG system comprised of multiple independent peripheral nodes and one central node. Each peripheral node will record one ECG lead with all electrodes in close proximity, such that no wires need to extend from the node (and, of course, there will also be no wires between the multiple nodes). All of the peripheral nodes will simultaneously transmit to a common central node. An ability to record multiple ECG leads simultaneously and unobtrusively will advance the information available from these wearable devices—just as most clinical ECG recordings are collected from multiple wired leads simultaneously.

3.2: Objectives and Constraints

The end goal of this project is the prototype production of a small, battery-powered, three electrode wireless ECG system that logs data in real time and processes the signal afterwards. Specifically, the signal processing portion will include detecting R-waves and atrial fibrillation. The system will consist of a central node to house most of the electronics in addition to peripheral ECG nodes placed around the body. These lead nodes will wirelessly communicate with the central node so that data can be collected and analyzed. The data will then be sent to a computer for the signal processing (the central node can be wired to a computer). Our system will preferably be small enough that it can be concealed on a person’s body and capable of monitoring continuously. Due to a team member graduating earlier than the others, a large portion of this report is the design and testing of a functional R-wave detection algorithm in MATLAB.

Future plans in the project include testing our circuit on human subjects with healthy sinus rhythms and atrial fibrillation. An IRB application has been submitted and is awaiting approval, and once approved, we will be able to test and collect our own data. In the meantime, we will conduct clinical bench testing on the circuit to ensure that it is safe and make our microcontrollers compatible with our circuit. On the algorithms side, we will complete our atrial fibrillation detection algorithm and test it. Time permitting, we hope to size down the system by designing a two lead system and making the device more power efficient.

3.3: Project Approach

Figure 3.1 shows the overall flow of how our system is intended to function.

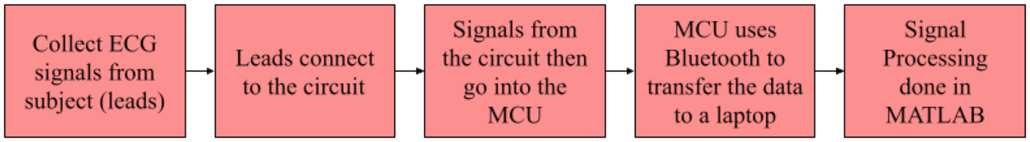
Collect ECG signals from subject (leads)
Leads connect to the circuit
Signals from the circuit then go into the MCU
MCU uses Bluetooth to transfer the data to a laptop
Signal Processing done in MATLAB

Figure 3.1: High Level Blackbox Diagram of System

We split the project into three major deliverables: hardware, R-wave detection algorithm, and atrial fibrillation detection algorithm. The hardware portion consisted of building an ECG circuit, programming the Nordic microcontroller units (MCU), and testing all components individually as well as when combined to produce satisfactory ECG signals. Additionally, the battery and ECG electrodes need to be packaged well. The R-wave detection algorithm portion consisted of writing the detection algorithm in MATLAB, testing on the MIT/BIH Arrhythmia and Atrial Fibrillation databases, and optimizing the algorithm to produce satisfactory results. The atrial fibrillation detection algorithm portion consisted of writing the detection algorithm in MATLAB, testing on the MIT/BIH Atrial Fibrillation database, and optimizing the algorithm to produce satisfactory results.

3.3.1 Tools

To accomplish this project, we used various software and hardware tools to create, modify, and test all the different portions of our design. To build our ECG circuit, we used NI Multisim (National Instruments), an online circuit simulator and schematic tool, to design and test all of the different circuits we were considering. This also gave us an idea on how the circuit might operate prior to us purchasing any hardware components. Once we finalized our circuit design, we were able to transport the schematic into NI Ultiboard, which is a Printed Circuit Board (PCB) layout program. Ultiboard allowed us to place components where we wanted them, route our signals, and then verified our design.

To write code, we used MATLAB and Segger. We used MATLAB to design our R-wave detection and atrial fibrillation algorithms, and used the MIT/BIH Arrhythmia and Atrial Fibrillation databases on Physionet to test both algorithms. PhysioNet has the ECG recordings that have been reviewed by cardiologists who have indicated the time locations of R waves and different types of arrhythmias. This information is used to determine the accuracy of our algorithms.

Segger is the IDE that is compatible with the Nordic microcontroller units (MCU) that we are using for this project, and it will be programmed in C/C++. Once the device has been constructed and programmed, the data it collects will be analyzed and conclusions can be formed. Data will be sent wirelessly from the system to MATLAB for processing, and the results will be displayed for the user.

Tools used throughout the hardware design included a digital multimeter, an oscilloscope, and a series of basic components. Those components included jumper wires, resistors, capacitors, and a protoboard. Throughout the design process, prototypes were constructed on the protoboard using the basic components along with a collection of instrumentation amplifiers and operational amplifiers utilized by previous MQP applications (namely the AD620 instrumentation amplifier and LM348 operational amplifier). As prototypes were constructed, the digital multimeter and oscilloscope verified proper voltage, current, resistance, and signal shape. Finally, as the protoboard design became mature, a solderboard and soldering iron were utilized to create the final effective prototype of the circuit.

4: Design Options

The construction of a wireless ECG signal reader necessitates analog front end signal conditioning along with Bluetooth communication via a microcontroller to deliver data to the receiver (laptop) for heart rate analysis. Figure 4.1 describes the topology of that wireless system.

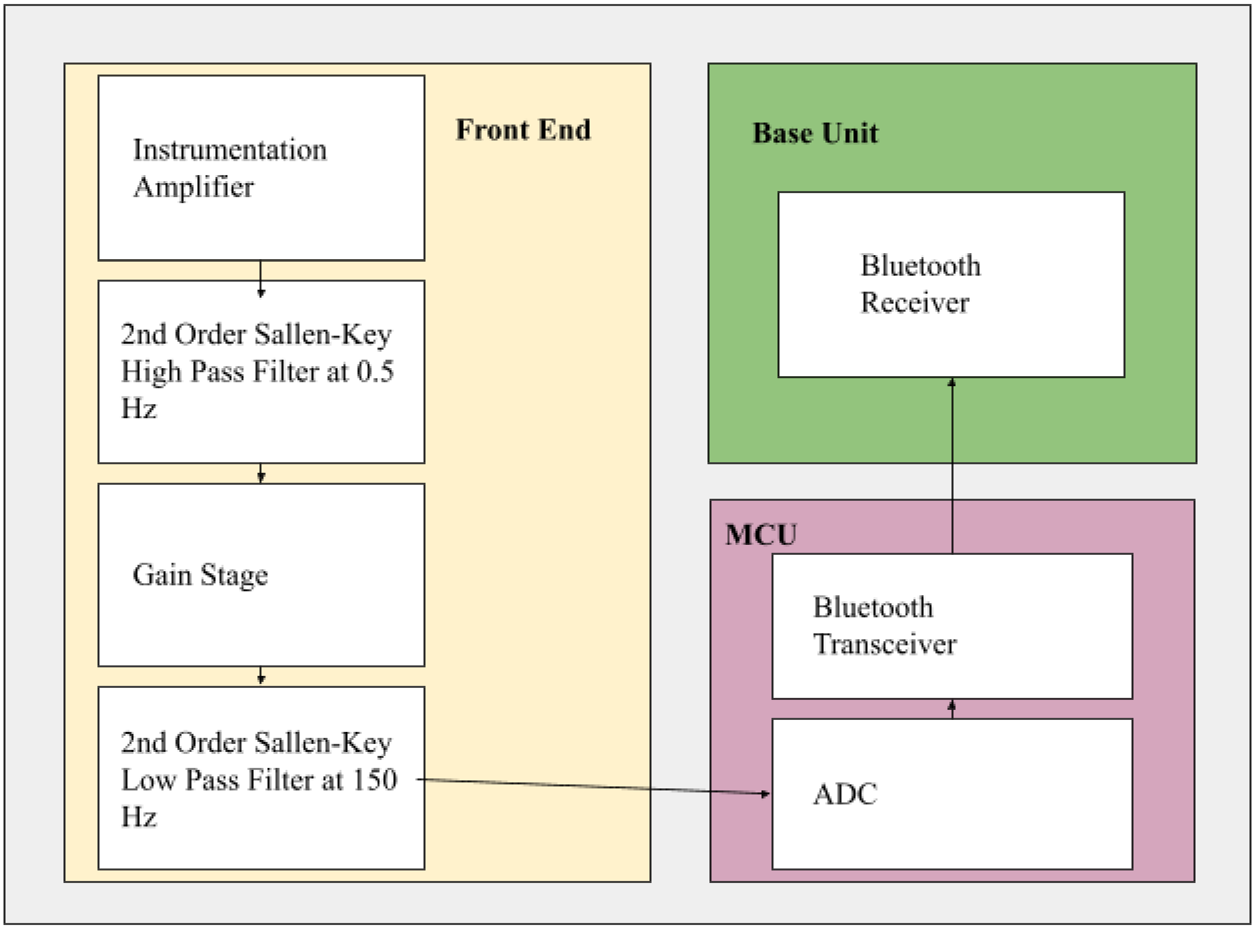
Front End
Instrumentation Amplifier
2nd Order Sallen-Key High Pass Filter at 0.5 Hz
Gain Stage
2nd Order Sallen-Key Low Pass Filter at 150 Hz
Base Unit
Bluetooth Receiver
MCU
Bluetooth Transceiver
ADC

Figure 4.1: Block Diagram of Wireless ECG Topology

The steps outlined in the topology consist of an instrumentation amplifier stage, two second order Sallen-Key filters, selectable gain, an ADC, and Bluetooth transceivers/receivers. The following sections will discuss the design options for each component necessary for the wireless ECG circuit along with design options for heart rate analysis algorithms.

4.1: Instrumentation Amplifier

For the purposes of this project an instrumentation amplifier will need to be used to amplify the signal coming from the leads on the body. The three amplifiers that were looked at were the INA118, the LN1167, and the AD 624. All of these components work for our applications and have different benefits but in our final design only one will be used.

The first one that was looked at was the AD624, a 16 pin DIP (Dual in Line Package) that met our requirements for our early prototyping design. The AD624 requires a minimum supply voltage of ± 6 V. One of the major benefits of this IC is that it has the gain already built into the package. If a gain of 100, 200, 500, or 1000 is needed, all that needs to be done is short the corresponding pins. One of the drawbacks of this system, however, is that it only comes in a DIP form and it is fairly hard to get a hold of due to it being somewhat outdated. In the scenario where the circuit needs to be shrunk to a smaller overall package this IC would not allow the freedom of using a SOIC (small outline integrated circuit) package. The primary issue with this IC is that it needs more voltage than our current system is able to supply.[35, p. 624]

The next instrumentation amplifier that was looked at was the AD8227, an eight pin IC that is available in both SOIC and DIP. This IC also has a high enough maximum supply voltage of ± 18 V as well as a minimum input voltage of ± 1.5 V which works far better for a lower power system using ± 3 V. The issue with this IC is its availability, it is unrealistic that we would be able to have it delivered in time. The AD8227 also has a price tag of between $3 to $10 for the SOIC and DIP systems.[36]

The last of the instrumentation amplifiers looked at was the LT1167, another eight pin IC that is available in both SOIC and DIP. This amplifier has a slightly higher maximum supply voltage of ± 20 V and a minimum of ±2.3 V which also works for the intended supply voltage of ± 3 V. The LT1167 has plenty of availability as of this writing and should pose no issue in getting the components needed. A benefit that the LT1167 has over the other two amplifiers is that it is slightly cheaper with prices ranging from $8 to $15 on the SOIC and DIP systems.[37]

For the sake of this project the instrumentation amplifier that will be used is the LT1167 due to its availability, its price, and its specifications meeting all the requirements that are needed. It is likely that any of these different amplifiers would work for the job that is needed but for this project the LT1167 will be used. For more information see Table 4-1.

Table 4-1: Comparison of Instrumentation Amplifiers

Amp	Min Vin	Input Noise	Maximum Single Resistor Gain
AD624	±6 V	10 nV/√Hz	1000
AD8227	±1.5 V	24 nV/√Hz	1000
LT1167	±2.3 V	7.5 nV/√Hz	10000

4.2: Operational Amplifier

For this project there is a need to use multiple operational amplifiers in the highpass and lowpass filters. There are a lot of choices when it comes to op-amps and the one that the group ended up selecting was the LM324. This rail-to-rail amplifier is a 16 pin DIP that has four amplifiers in the package which is enough in the package for us to only need one chip. The LM324 also has a minimum supply voltage that is low enough for our intended use of ± 3 V. One of the major benefits of this op-amp is that it can be bought in either a SOIC or DIP version and each of the styles is less than a dollar per package. Lastly the main benefit of this amplifier is the availability of the ICs as there were some available to us now as well as many available online [38].

4.3: Analog to Digital Converter

The design choices for the ADC has the most flexibility, and also the widest range in price variation among all the components being selected. The options available for this decision are the ADS1291 (discussed earlier in Section 1.3.4), a TI sigma-delta ADC, or a USB-1608G series ADC module from Measurement Computing. The ADS1291, designed specifically for ECG circuitry, is a low power device with one input channel, low noise programmable gain amplifiers, two high resolution amplifiers, and a built in oscillator. A sigma delta ADC uses a sigma modulator and digital filtering. Filtering of an ADC involves oversampling of the signal, noise shaping, digital filtering, and decimation. Finally, the USB-1608G series can connect to a

PC through the USB port and has 16 bit resolution. Furthermore, the USB-1608G also has a measurement of 250 kS/s.

There is also a significant distinction in the price of each of the ADCs. The ADS1291 is roughly $7 per unit, making it extremely cost effective for our design. It will, however, require a degree of software installation and configuration to the microcontroller and PC. The USB-1608G ranges between $400 and $800 USD. While the PC based models are significantly more expensive, they are being considered based on their capabilities for configuration with PCs and MATLAB.

4.4: Voltage Regulator

In order to use the summer amplifier to level shift the voltage within the range of the ADC, 1.5 V must be added to the signal. As the voltage from the battery decreases over time, a voltage regulator is required to maintain a constant voltage at the input of the summing amplifier. One of the components considered was the TPS73615MDBVREP, a 1.5 V voltage regulator made by Texas Instruments. It had an input voltage range of 1.7-5.5 V, which is ideal for an expected input of 3 V. It also has a 400 μA operating supply current and within 0.5% voltage output accuracy. The TPS73615MDBVREP is a surface mount component, which is not as convenient for protoboarding and soldering as a through-hole component [39].

The LP38841T-1.5/NOPB is a throughole voltage regulator similar to the TPS73615MDBVREP but with slightly different performance characteristics. The LP38841T-1.5/NOPB also has a constant output voltage of 1.5 V and has an input voltage range of 1.575-5.5 V. Its operating supply current is 32 mA and its output voltage accuracy is within 1.5% [40].

With its better accuracy and lower supply current, the surface mount TPS73615MDBVREP was chosen over the through hole LP38841T-1.5/NOPB. In addition to the voltage regulators, surface mount to through hole adapter sockets will be purchased to allow for the convenience of a through hole component.

4.5: Microcontroller

Design options for the MCU were narrowed down to the TI CC2642R and the Nordic nRF52840. As discussed in Section 1.3.4: Additional Components, the two microcontrollers have similar performance characteristics. Both models have identical processors and 12-bit ADC sampling at 200 kS/s. Furthermore, the Nordic model has more memory and faster clock speeds than the CC2642R. Finally, the difference in receiver sensitivity between the two MCUs is negligible; the nRF52840 having a sensitivity of -103 dBm and the CC2642R having a sensitivity of -105 dBm. The Nordic MCU is more expensive, but only in the range of a few dollars, so that factor is not important for the decision making process. A primary advantage in favor of the Nordic MCU, outside of performance characteristics, is its recommendation of use by graduate students assisting our project group. These recommendations come from prior MQP experience. In previous projects, the TI units produced transmission collisions. To accommodate that problem, the project groups had to insert a third inactive device to prevent the missing packets and introduced delays. Nordic models allow the packets to be more spread out, and thus, don't require the third additional device. Outside of graduate student recommendations, and factoring in their relatively similar performance capabilities, it can be generally noted that there is no substantial difference between the two MCUs for our application.

4.6: Multi-Leads Selection

For the multi-lead portion of the device, we can build either a two or three electrode ECG peripheral node. A two-electrode device is grounded using the signal path rather than an electrode, which makes it noisier compared to having an electrode that is meant to serve as the ground. However, an advantage of it is that the hardware is not very complex so it works excellent for a wireless ECG monitor [39]. Another advantage of a two-lead ECG is that since there are less leads, it is a much more comfortable fit on the body compared to a three-lead system. However, we are choosing to build a three-electrode device because the signals are more accurate and less noisy, but it is at the expense of being large for a system that is wireless and is mounted on the body for a long period of time.

4.7: Algorithm Selection

One of our major deliverables was to write algorithms that will successfully process the signal and produce an ECG waveform. Additionally, the algorithms needed to detect R-waves and atrial fibrillation. There are various algorithms and methods designed by experts that can accomplish both of these, but in this section we elaborate on the specific algorithms we implemented and our reasoning for choosing it.

4.7.1: R-Wave Detection

For R-wave detection, we implemented a detector using Pan and Tompkins' QRS detection algorithm methodology. We accomplished this by using a MATLAB implementation of this algorithm found online as a reference and eliminated unnecessary steps, such as the derivative filter, which did not have much of an effect on the final output of the signal. The success of our algorithm was tested by using the MIT/BIH ECG Arrhythmia Test Database and the MIT/BIH ECG Atrial Fibrillation Database and comparing the results to Pan and Thompkins' results.

4.7.2: Atrial Fibrillation Detection

For the detection of atrial fibrillation, algorithm three was implemented. The characteristics of AF were used to identify its presence in an ECG signal. By finding the TVCF and Shannon entropy, segments of the ECG signal were tested for the presence of AF. This algorithm consists of two primary steps and is nonparametric. Algorithms one and two involve more computation, a greater number of tests, and are less accurate than algorithm three as seen in Table 2-2. This is why algorithm three was chosen for this application. The success of our algorithm will be tested by comparing it to the results of Lee et al.'s paper and the MIT/BIH Atrial Fibrillation database.

5: Hardware

Our final circuit design is constituted by an LT1167 instrumentation amplifier, an LM324N quad operational amplifier, the TPS73615MDBVREP voltage regulator and a series of basic components (resistors and capacitors). Each of these components were selected to satisfy a low power circuit condition (± 3 V rail-to-rail design). The selection was limited to availability of components in the market due to the electronic components shortage, along with an understanding of the trade-off between power consumption and noise. Originally, the instrumentation amplifier of choice was Analog Device's AD8227. However, the AD8227 was unavailable when we were constructing the prototypes and had a lead time of approximately one year. The LM324N and the TPS73615MDBVREP were both selected as they satisfied the low power requirement of the circuit along with the design requirements, which we will elaborate on in Section 5.1. The hardware construction process, outlined in greater detail in the following sections, began with virtual simulation in Multisim, followed by prototype construction of the circuit on a protoboard, succeeded by constructing the circuit on a solderboard, and finalized with implementing the circuit on a PCB.

5.1: Design Process

The analog front end design corresponds to the set of design requirements for circuit performance listed in Table 5-1:

Table 5-1: Requirements for Analog Front End Design

System	Wireless ECG
Input Signal Amplitude	± 2-4mV
Input Signal Frequency	0.05 Hz - 150 Hz
Selectable Gain	600
CMRR	≥ 80 dB at 60 Hz
Noise	≤ 1 μV RMS RTI for full frequency band
Size/Weight	Relatively small, within the size of two fists
Power	3 V
ADC	12 bit resolution
Isolation	Medically isolated
Current Consumption	≤ 20 mA @ 3 V

Our analog front end design is fairly conventional and consists of six sections: the input, the instrumentation amplifier, the highpass filter, the lowpass filter, and the level shifter (Figure 5.1).

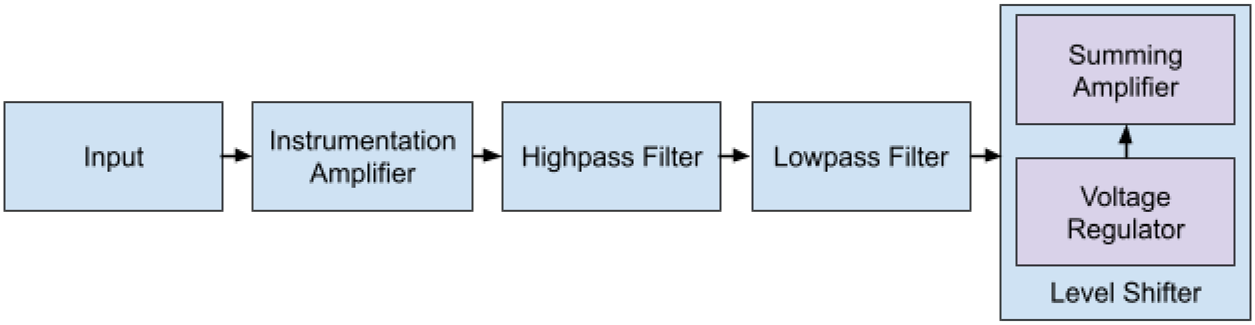

Figure 5.1: Abstract Circuit Diagram

Starting at the input there are three electrodes that will be used, one will be tied to ground to act as a reference for the other two. The other two will pass through an 80 kΩ resistor separately that limits the highest possible current going to the body at 50 μA. This value was found by taking the maximum possible voltage in the circuit which, if the batteries are fully charged, can be as high as ± 4 V and dividing it by the current of 50 μA. After this resistor on each electrode, there are two diodes going to and from ground that will protect the circuit in the unlikely scenario where the body outputs enough voltage to pass through the diodes in either direction. This works as the diodes require a minimum voltage in order to trigger which, under normal operation, the human body will not reach. If for some reason the body exceeds this voltage threshold of 400mV, then it will be shorted to ground. After this,both electrodes go into the next stage which is the instrumentation amplifier.

For this project, we will be using the LT1167 instrumentation amplifier, which currently has its gain set to 10 using a 5 kΩ resistor across pins one and eight. The relatively low gain of this stage is to keep the noise as low as possible when going into the amplifier stages, where it can be filtered out before amplifying. The instrumentation amplifier uses the full range of the two batteries with the amplifier tied to both the positive and negative rail.

The combined signal from the instrumentation amplifier is then sent through a second-order Sallen key high pass filter with a gain of 21 and a cut-off frequency of 46 Hz to filter out as much of the low frequency noise as possible and increase the strength of the signal. Then the highpass filter goes into the second-order Sallen key lowpass filter with no gain which also attempts to get rid of noise in the signal. Both of these filters are using the LM324 operational amplifier in the same four amplifier package. The gain of these stages is as it is to make sure that noise does not get amplified as much. The gain of 210 brings the overall amplitude of the signal to around 1.5 V depending on the input amplitude, which is perfect for the 3 V range of the ADC.

The last two stages go together as a level shifter in order to use the ADC on the nRF52840. The ADC is unipolar, however the signal coming out of the lowpass filter is bipolar. In order to make this work, a 1.5 V DC offset needs to be added to the signal. This is done by using a summing amplifier that combines the signal out of the low pass with a 1.5 V DC coming from the voltage regulator. The voltage regulator is used so that as the voltage of the batteries varies slightly, the 1.5 V offset will remain constant. Once the summing amplifier combines these and adds a final stage of amplification to the original signal, it can be sent to the nRF52840 MCU and have the signal converted to digital. The overall circuit diagram can be seen in Figure 5.2 with each major stage labeled.

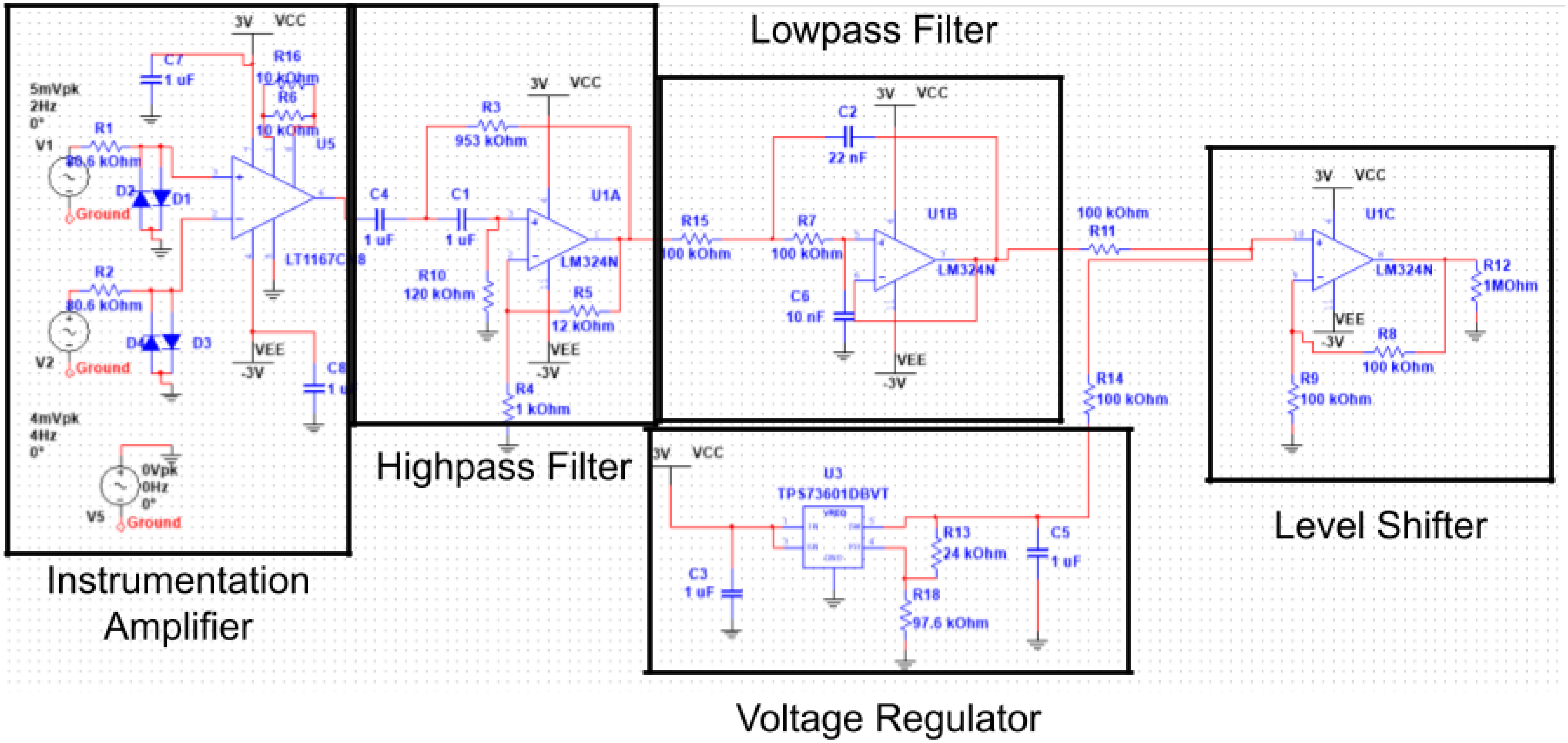

Figure 5.2: Overall Circuit Diagram

5.1.1 PCB Layout

Once the circuit was finalized in Multisim, we transported our design onto NI Ultiboard, where we prepared the layout for the PCB. Our PCB is built using the components in the circuit diagram (Figure 5.2), specifically, a LT1167 instrumentation amplifier, an LM324N quad operational amplifier, a TPS73615MDBVREP voltage regulator, resistors of various values that help us achieve a gain of 300, and capacitors of various values that serve as decoupling capacitors to maintain voltage levels. Figure 5.3 shows our final PCB layout.

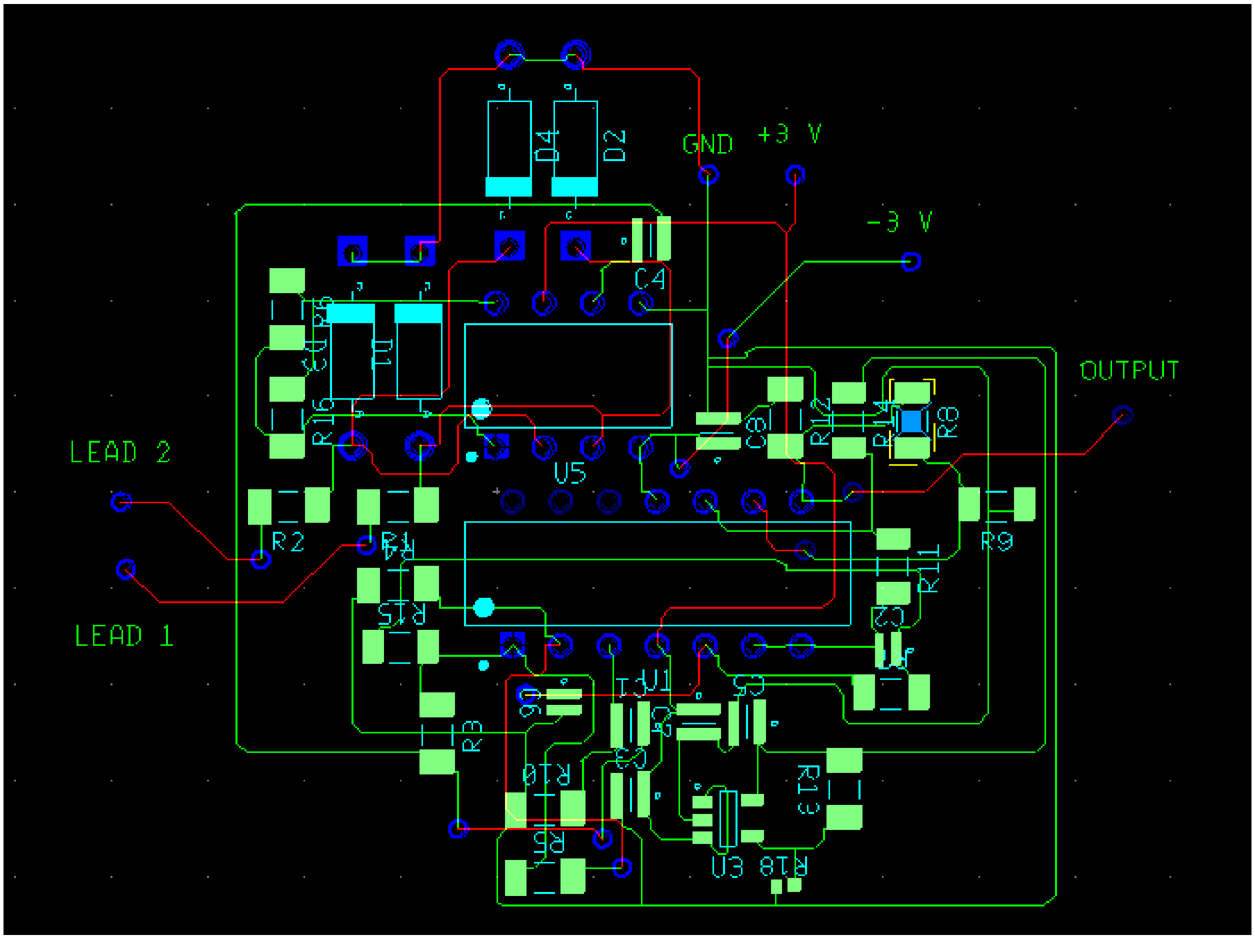

Figure 5.3: Final PCB Layout

Our PCB board will be two-layers: one copper top layer and one copper bottom layer. As part of the layout process, we ensured that signals did not cross each other and all decoupling capacitors were placed next to the component that they were connected to. All of our components are through-hole components except our resistors, capacitors, and voltage regulator which are surface-mounted. Since we have a lot of resistors, we chose to make them surface-mounted since they are smaller than through-hole components, which will make our overall PCB smaller. Additionally, all of our grounds are connected to each other and that common ground will be connected to the center tap of the battery. We also have signals coming out for Leads I and II, which are close to the grounded lead, and our leads can be manually soldered on. Finally, we have our VCC and VEE, which are +3 V and -3 V respectively, also coming out to be connected to the battery. We plan to leave some extra board space next to the connections where two batteries, for +3 V and another battery for -3 V, can be mounted. At this point, our PCB is ready to be sent to a manufacturer, and once we receive the board back, we will be able to manually solder our leads and batteries and test our circuit. Figure 5.4 shows what we expect our final PCB board to look like.

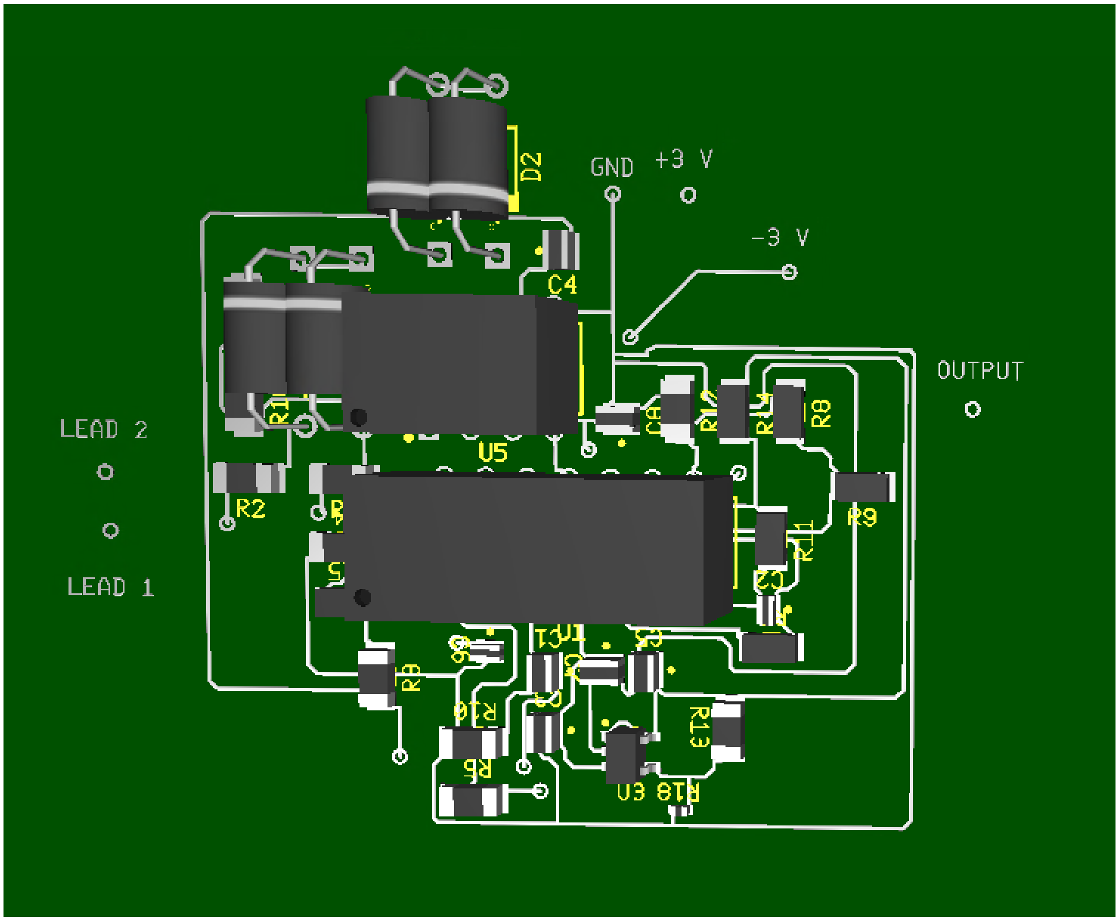

Figure 5.4: Expected Final PCB

5.2: Hardware Design Verification in Multisim

With all of the components chosen and the final circuit designed, the hardware was verified through simulation in Multisim. Figure 5.5 is a plot of the output of the circuit with sine waves applied at the input. A 5 mVpk 2 Hz sine wave and a 4 mVpk 4 Hz sine wave with no phase difference were used as the two ECG inputs in the simulation shown below.

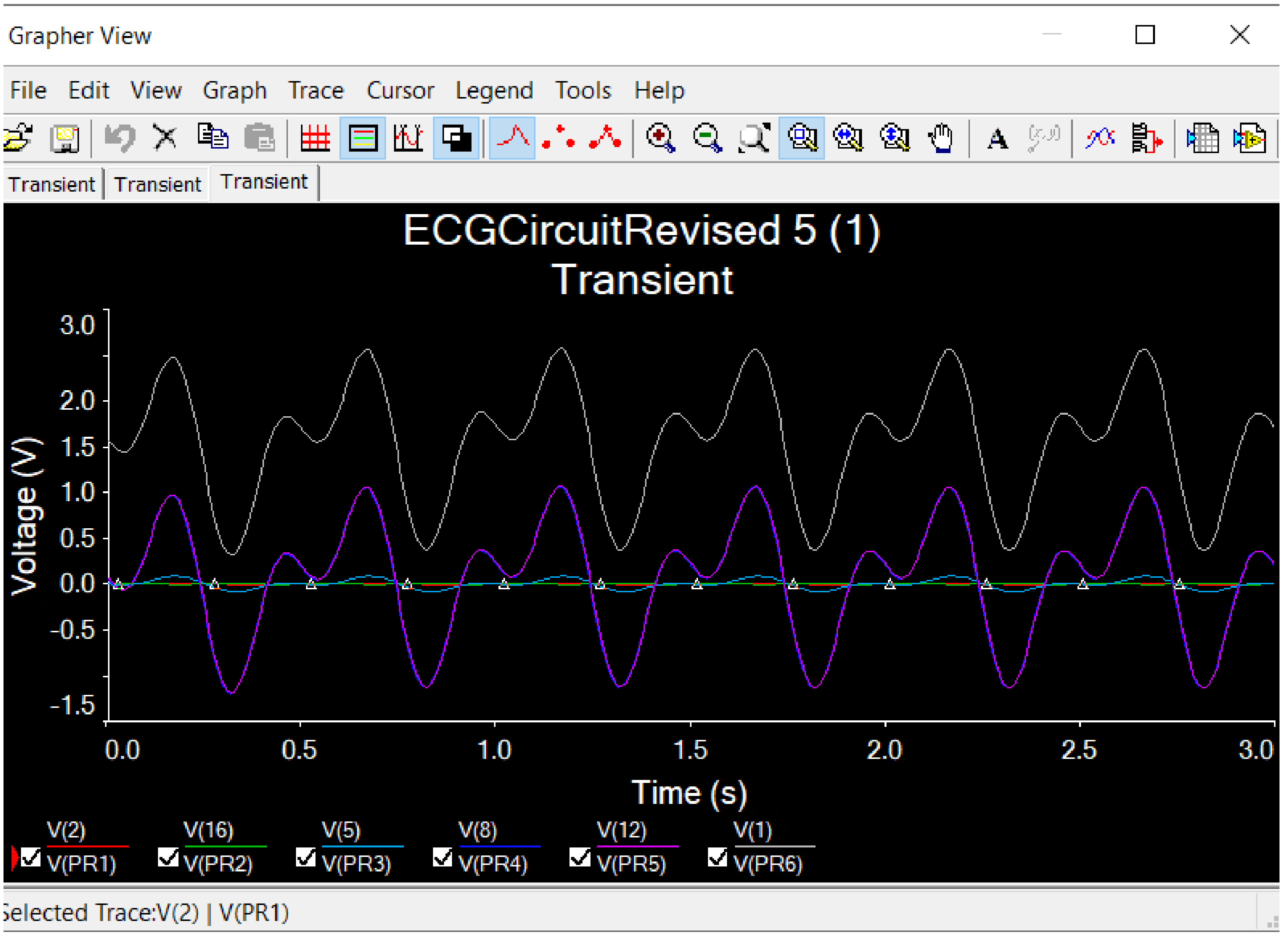

Figure 5.5: Multisim Output

The two small input waves shown as voltage probes 1 and 2 in Figure 5.5 are centered at 0 V and are slightly amplified at the output of the instrumentation amplifier, shown at probe 3. The resulting signal is then highpass and lowpass filtered with additional gain at the highpass stage. Probe 4 shows the result after highpass filtering, which appears the same as the output of the instrumentation amplifier due to the lack of noise and the unity gain of the filter. The lowpass filter stage further amplifies the signal, resulting in the wave labeled as probe 5. Finally, the signal is level shifted to center the wave at 1.5 V and allow it to be passed into the ADC, shown as probe 6 on the plot. The output signal ranges from 0 and 3 V and is centered at 1.5 V as desired. At every stage of the circuit, the simulated design performed as expected. With the correct circuit operation verified in Multisim, the hardware section of the project could then be further developed.

5.3: Hardware Design Verification on a Protoboard

Utilizing available components, the team verified the proper functionality of the circuit on a protoboard. The chosen components for the instrumentation amplifier and operational amplifiers are the LT1167 and the LM324N respectively. Due to significant shipping delays due to the ongoing COVID-19 pandemic, a prototype was created on a protoboard utilizing the AD620 instrumentation amplifier and the LM348 quad operational amplifier. The voltage regulator (TPS73615MDBVREP) for the summing amplifier stage was modeled with a separate 1.5 V DC power supply. Finally, the input voltage to the circuit utilized an ECG signal generating device. This device produces a realistic ECG signal (proper amplitude, waveform, and can model realistic artifacts within the body). With all the components listed, the circuit properly offset the input voltage by 1.5 V and introduced the desired gain. Switching the components used in the prototype to the components for the final design should constitute almost no changes in performance, since the LT1167 and LM324N are low power components. While there may be slightly more noise introduced due to that fact, the general performance of the circuit is expected to be identical. An image of the finalized circuit on the protoboard can be seen in Figure 5.6 with the resulting waveform in Figure 5.7.

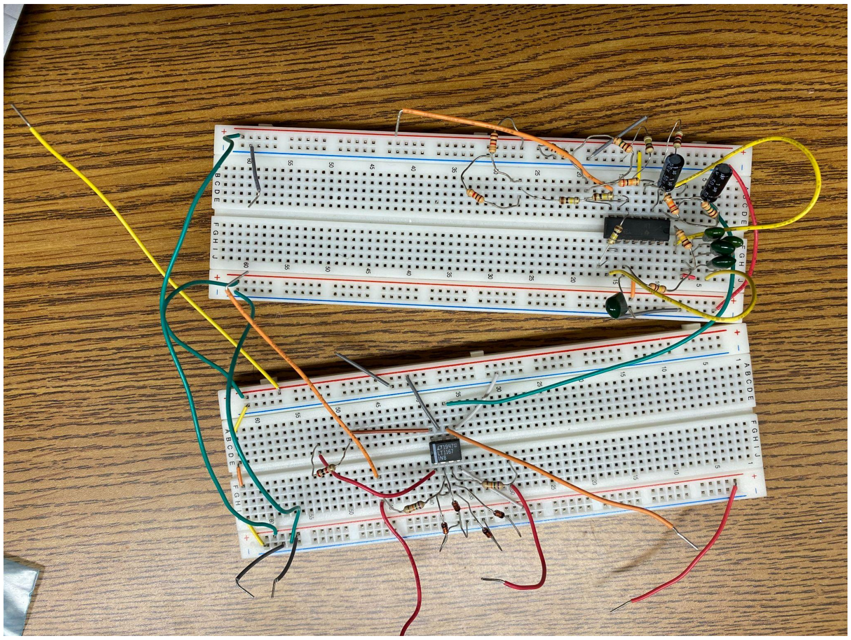

Figure 5.6: Finalized protoboard ECG circuit

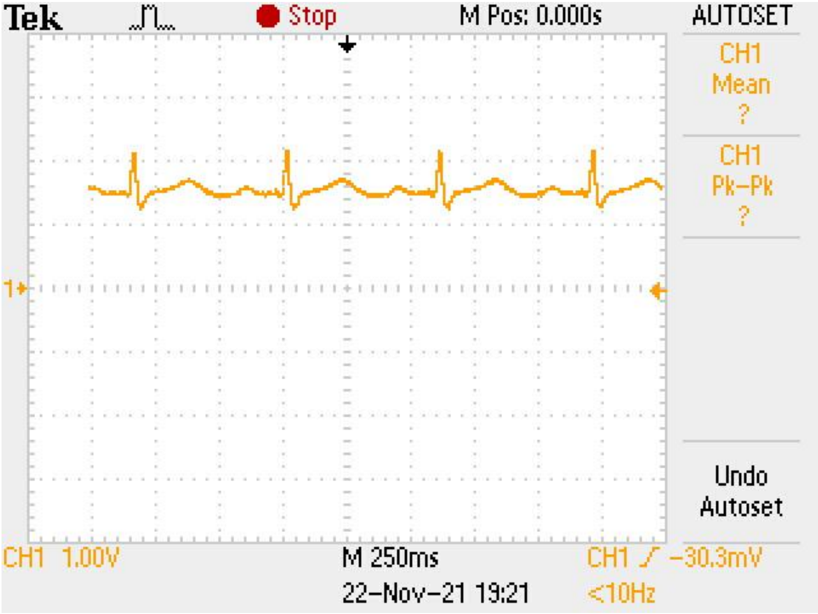

Figure 5.7: Output of ECG protoboard circuit utilizing ECG signal device

5.4: Hardware Design Verification on a Solderboard

Once the design was validated on the protoboard, that same design was replicated on a solderboard to test and attempt to gather data from it. The board was made using the same components as the previous designs. In the iteration shown in Figure 5.8, the only difference between the protoboard version and this version of the circuit is that it has been condensed and put in an easier to use format that will allow for testing to occur. You can see the final output wave of the circuit in Figure 5.9.

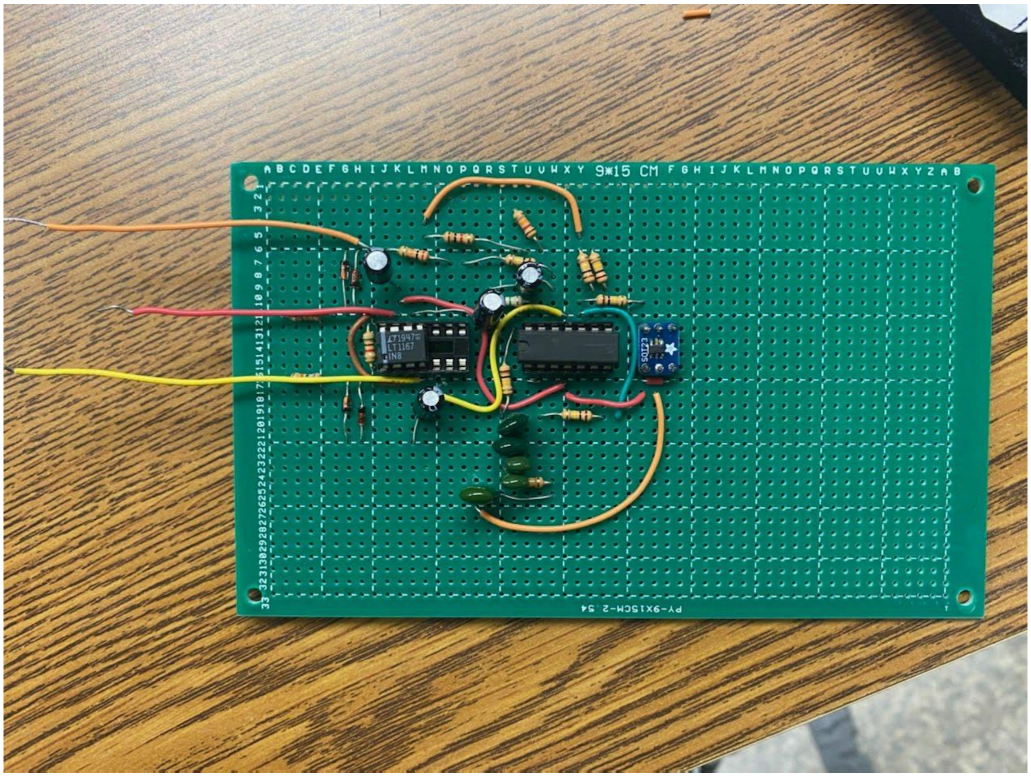

Figure 5.8: ECG Solderboard Circuit

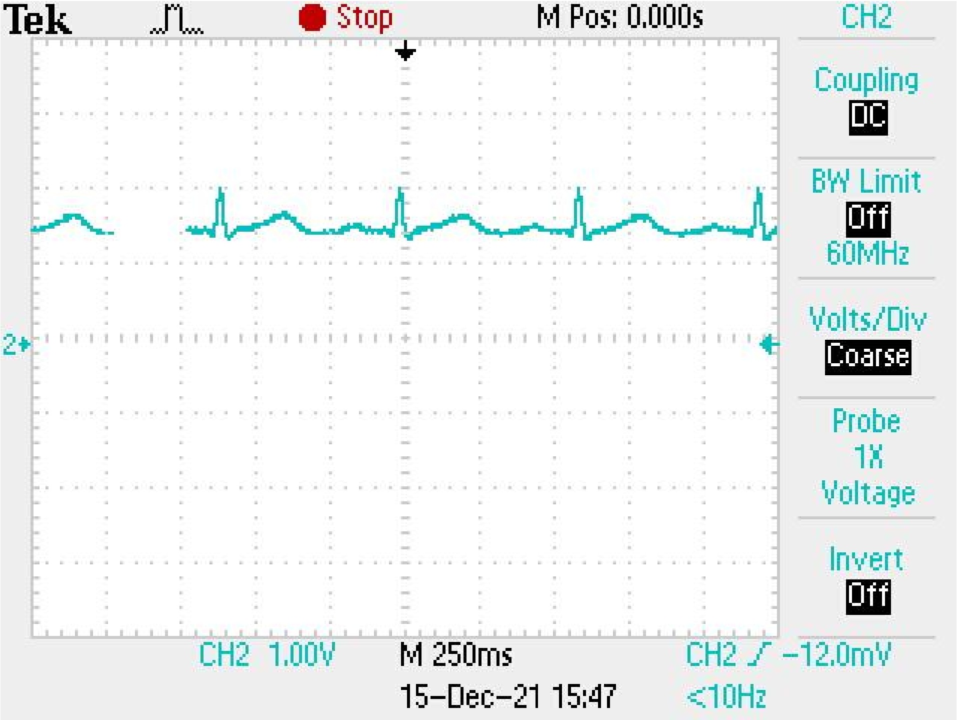

M Pos: 0.000s

CH2

Coupling DC

BW Limit Off 60MHz

Volts/Div Coarse

Probe 1X Voltage

Invert Off

CH2 1.00V M 250ms CH2 ⟋ −12.0mV

15-Dec-21 15:47 <10Hz

Figure 5.9: Output of ECG Solderboard Circuit Utilizing ECG Signal Device

5.5: Discussion

The analog ECG circuit was designed in Multisim and constructed on a protoboard. Once all components were chosen and ordered and the protoboard circuit was thoroughly tested, the circuit was soldered onto a solderboard. The soldered circuit functioned as intended, but more noise was observed at the output than expected. Figure 5.8 shows the output of the soldered circuit with significant noise present. A PCB of the circuit was designed and is ready to be ordered for future testing.

Future work will first involve testing the PCB circuit to confirm functionality. Physical housing for the components will be designed and 3D printed. With a complete prototype built, testing with human patients can begin. The real data collected will be transmitted wirelessly for processing and can be used to test the R-wave detection and atrial fibrillation detection algorithms described below. Reducing the amount of noise added to the signal and creating smaller prototypes are additional steps to further improve the hardware.

6: R-Wave Detection Algorithm

Our final R-wave detection algorithm was designed in MATLAB and inspired by Pan and Tompkins' QRS Detection Algorithm. The algorithm was tested using MIT/BIH databases, available on Physionet, where we had access to annotation files that allowed us to compare the expected R-wave locations with what our algorithm produced. Once our ECG circuit is complete, we will collect signals through the circuit, have it wirelessly transmit the data via Bluetooth to a computer, where we will run the algorithm to detect R-waves. We will also create our own annotation files just like Physionet does to check how accurate the detector is when we collect our own data. The goal of this detector is to be as optimized as possible so that we can detect R-waves in different scenarios, especially in noisy data, and then use the output R-waves as the input of the atrial fibrillation detector so that atrial fibrillation can be detected. Our implementation of the R-wave detector can be found in Appendix E.

6.1: Design Process

The R-wave detection algorithm was implemented using Pan-Tompkins' QRS detection algorithm as a reference. Guided by a MATLAB implementation available online [40], we wrote our own version of the algorithm by creating a new bandpass filter, removing the derivative filter, and modifying the moving average from convolution to a Butterworth lowpass filter. The algorithm was also optimized to read in the sampling frequency so that it could be used with any sampling frequency, and not just a 200 Hz sampling rate, which is what Pan-Tompkins designed their algorithm for. Figure 6.1 outlines the steps in the R-wave detector that lead to a resulting index of R waves.

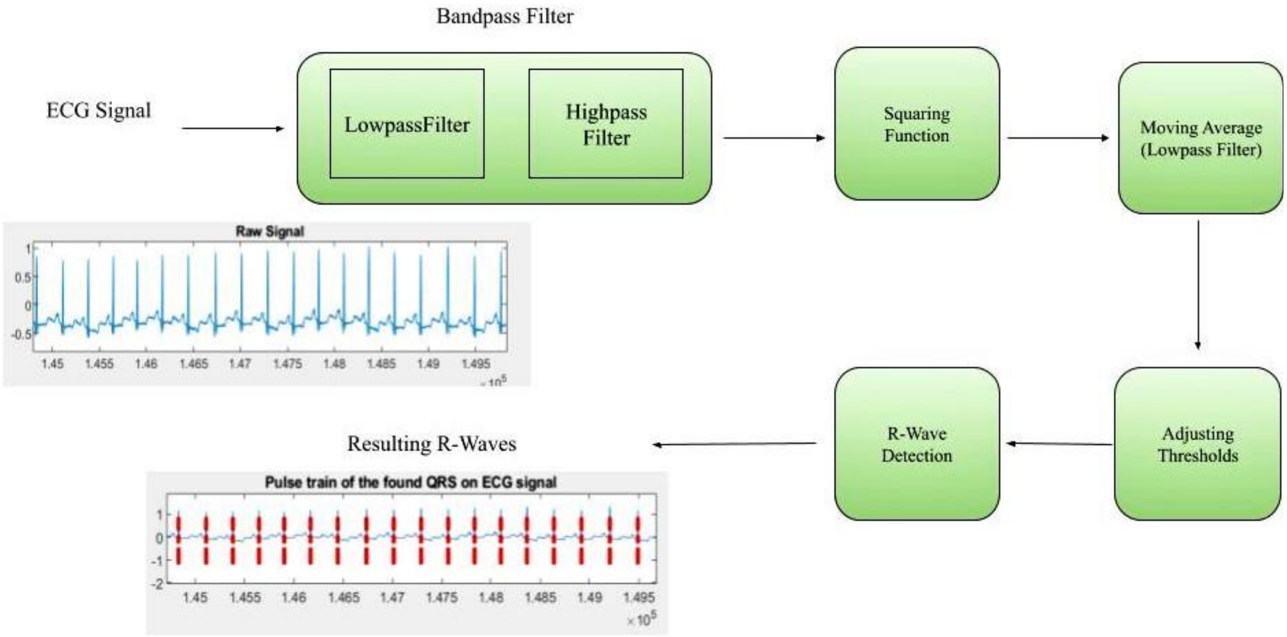

Figure 6.1: Black-box Diagram outlining the steps of the R-wave Detection Algorithm

Since the Pan-Tompkins R-wave detection algorithm was designed over 30 years ago, it was crucial to take into account the extra parameters that they included to run the algorithm over significantly slower systems. Since modern day systems run more efficiently and there are functions in MATLAB available to allow us to design filters, we decided to modify the algorithm to use those. Specifically, the bandpass filter that Pan-Tompkins designed was implemented by cascaded lowpass and highpass filters . In MATLAB, however, we were able to directly create a digital Butterworth bandpass filter using the butter() function. A Butterworth filter has a frequency response that is as flat as possible in the passband and has a monotonic roll-off in the stopband (as compared to other major filter types), which is what we needed for our bandpass filter. We chose to build a fourth-order bandpass filter with a passband between 5-15 Hz since that is the general range of where R-waves are located [25]. Varying this high cutoff frequency will allow all signals below 15 Hz to pass through. If we change it to, for example 12 Hz, then signals above 12 Hz will not pass through, which can be better if there is a record with a lot of high amplitude noise, but generally lower amplitude signals.

In Pan-Tompkins' algorithm, they had created a derivative filter after the bandpass to calculate a slope. However, in early testing, we realized that the derivative filter did not have an effect on our results, so we decided to remove it.

We also designed a lowpass filter when performing the moving average after squaring. Initially, Pan-Tompkins used convolution for moving average since that was more efficient on their hardware systems; however, moving average is a poor lowpass filter with slow roll-off and poor stopband attenuation, so we created a filter with similar characteristics to replace convolution. Once again, using the butter() function, we created a second-order lowpass filter with a cutoff frequency of 5 Hz.

Once the filters were created, we needed to set the thresholds for the detection phase. We decided to keep most of this section of the MATLAB implementation because it matched with what Pan-Tompkins' did for their algorithm.

First, we set the fiducial marks that serve as a reference for the locations of potential R-waves. Since the heart has a refractory period of about 200 ms, we ensured that all peaks that are located will be at least 200 ms apart. Next, we initialized the learning phases; the first learning phase is to use the first two seconds of data to set the running estimates of the signal and noise thresholds for both the bandpass filtered and the moving averaged signal. For the second learning phase, we used the first two heartbeats to initialize the RR-interval average and calculate RR-interval limit values. After that, we initialized the two sets of thresholds using the bandpass filtered signal noise peaks and signal peaks and the moving averaged signal noise peaks and signal peaks using equations 2.24-2.31. The higher threshold, for both the bandpass and moving average, is usually the signal height threshold, which is what the detector determines where most of the peaks lie, and the lower threshold, for both the bandpass and moving average, is usually the noise height threshold, which is what the detector determines where most of the noisier peaks lie. The lower one is only used during searchback if there is no peak caught by the higher threshold in the 200 ms time interval.

Additionally, just like Pan-Tompkins, we take the average of the eight most-recent beats and the average of the eight most-recent beats that fall within certain limits, set by equations 2.34-2.36. We determine if any peaks are T-waves, and skip a peak if there is more than one peak detected in less than a 200 ms time interval. Finally, we take the SNR into account and adjust the thresholds when the signal and noise thresholds are not zero, before plotting our final signal with the R-wave detections overlaying on the plot with a red dashed vertical line.

6.2: Design Verification

To verify that the R-wave detection algorithm works as intended, we compared graphical results to the MATLAB implementation of the Pan-Tompkins algorithm and compared the detected locations of the R-waves to the “truth”locations.

For the graphical results, we plotted the original ECG signal and the resulting R-wave detections determined from our algorithm implementation and the MATLAB implementation of Pan-Tompkins algorithm. Figures 6.2 and 6.3 demonstrate that for normal sinus rhythm, the outputs from the Pan-Tompkins and our algorithm match.

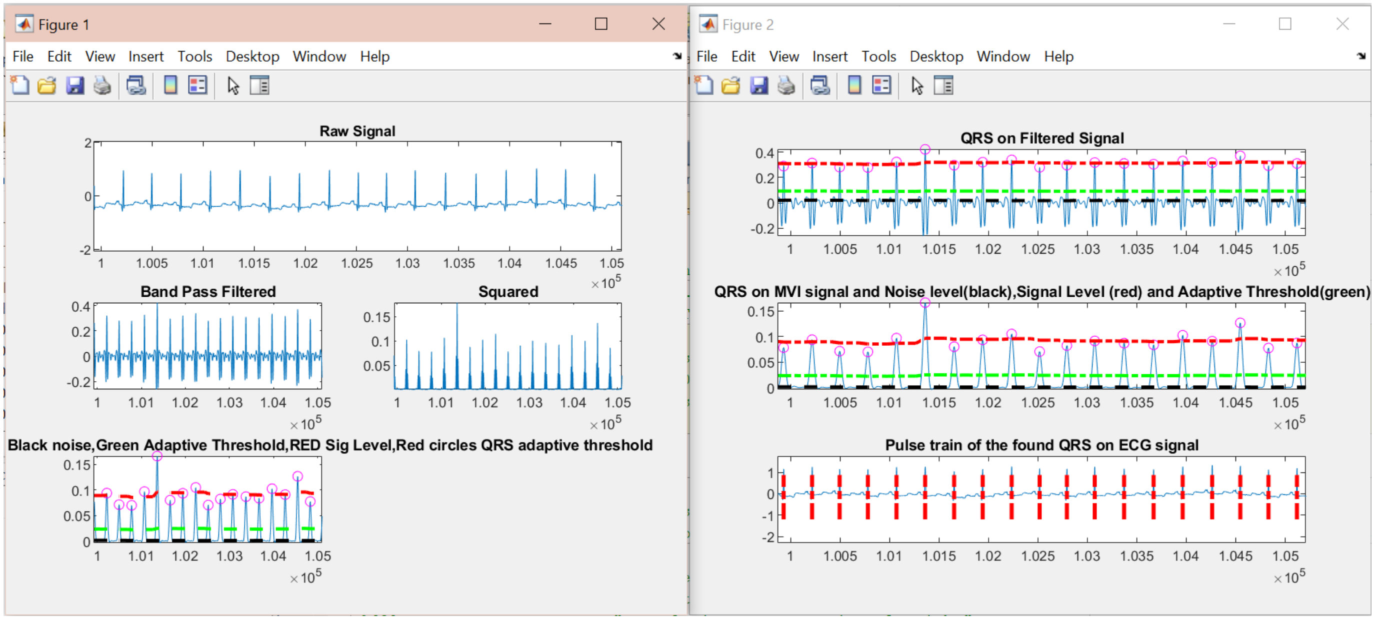

Figure 6.2: Pan-Tompkins Algorithm Implementation reacting to normal sinus rhythm for Lead I of subject 100

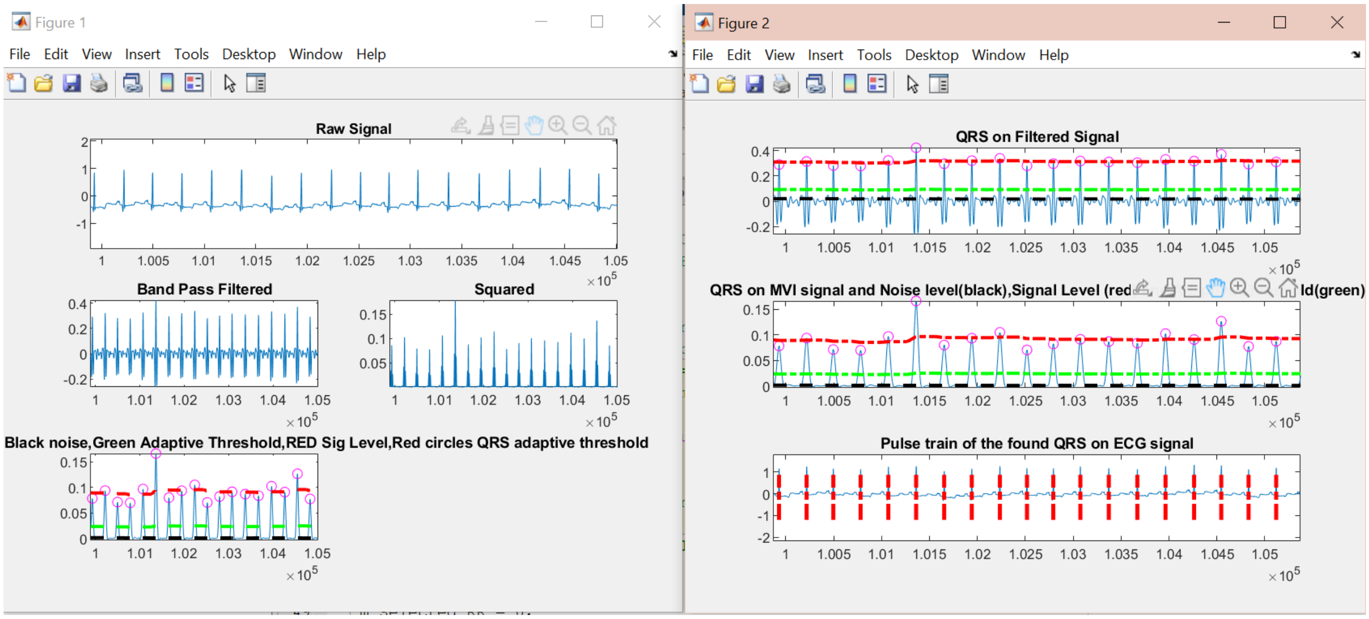
Figure 1
File Edit View Insert Tools Desktop Window Help
Figure 2
File Edit View Insert Tools Desktop Window Help
×10^5

Raw Signal

Band Pass Filtered

Squared

Black noise,Green Adaptive Threshold,RED Sig Level,Red circles QRS adaptive threshold

QRS on Filtered Signal

QRS on MVI signal and Noise level(black),Signal Level (red ... ld(green)

Pulse train of the found QRS on ECG signal

Figure 6.3: Our R-Wave Detection Algorithm reacting to normal sinus rhythm for Lead I of subject 100

As part of testing, we manually reviewed portions of the plotted signal that have artifacts to see how the algorithm performs. Specifically, instances of premature ventricular contractions (PVC) and possible muscle noise have some differing QRS trains when comparing the Pan-Tompkins MATLAB implementation and our algorithm. Figures 6.4 and 6.5 compare the different outputs from Pan-Tompkins and our algorithm.

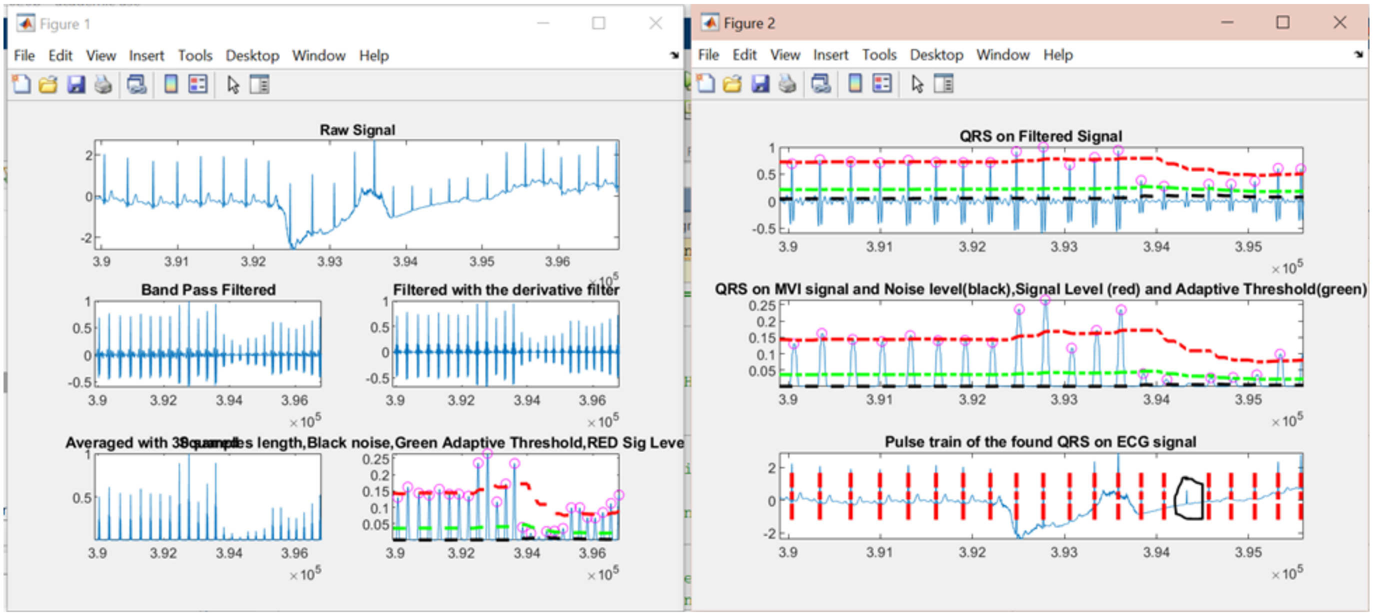
Figure 1
File Edit View Insert Tools Desktop Window Help
Raw Signal
2
0
-2
3.9 3.91 3.92 3.93 3.94 3.95 3.96
×10^5
Band Pass Filtered
Filtered with the derivative filter
1
0.5
0
-0.5
3.9 3.92 3.94 3.96
×10^5
Averaged with 30 samples length,Black noise,Green Adaptive Threshold,RED Sig Leve
Squared
0.25
0.2
0.15
0.1
0.05
Figure 2
File Edit View Insert Tools Desktop Window Help
QRS on Filtered Signal
1
0.5
0
-0.5
3.9 3.91 3.92 3.93 3.94 3.95
×10^5
QRS on MVI signal and Noise level(black),Signal Level (red) and Adaptive Threshold(green)
0.25
0.2
0.15
0.1
0.05
Pulse train of the found QRS on ECG signal
2
0
-2

Figure 6.4: Pan-Tompkins Algorithm Implementation reacting to a PVC for Lead I of subject 103

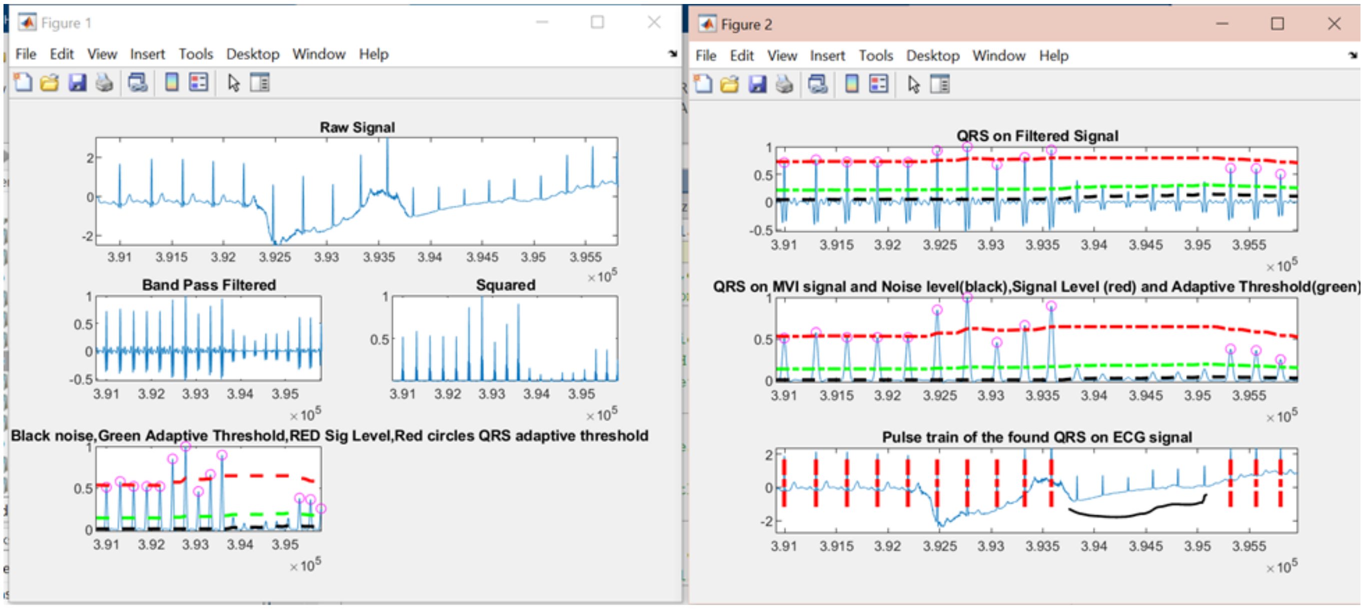
Figure 1
File Edit View Insert Tools Desktop Window Help
Raw Signal
2
0
-2
3.91 3.915 3.92 3.925 3.93 3.935 3.94 3.945 3.95 3.955
×10^5
Band Pass Filtered
1
0.5
0
-0.5
3.91 3.92 3.93 3.94 3.95
×10^5
Squared
Black noise,Green Adaptive Threshold,RED Sig Level,Red circles QRS adaptive threshold
Figure 2
File Edit View Insert Tools Desktop Window Help
QRS on Filtered Signal
QRS on MVI signal and Noise level(black),Signal Level (red) and Adaptive Threshold(green)
Pulse train of the found QRS on ECG signal

Figure 6.5: Our R-Wave Detection Algorithm reacting to a PVC for Lead I of subject 103

Specifically in Figures 6.4 and 6.5, there are R-waves that were detected in Pan-Tompkins' algorithm implementation between 3.94x10^5 and 3.95x10^5 samples that are not identified in our detection algorithm. This is likely due to the trend where large amplitudes in the dataset increase the threshold, making smaller R-wave peaks negligible.

To verify that the R-wave detection algorithm works as intended, we used the Physionet MIT BIH Arrhythmia Database and the MIT BIH Atrial Fibrillation Database. The Arrhythmia Database contains 48 half-hour long recordings that are sampled at 360 Hz. The Atrial Fibrillation Database contains 25 ten-hour long recordings that are sampled at 250 Hz and have a total of 299 episodes of atrial fibrillation. Both databases come with annotation files that state the truth locations of R-waves and atrial fibrillation. The atrial fibrillation database also comes with some notes about the recordings in the database that might affect our data analysis. We made sure to take those scenarios into account when performing our algorithm on the atrial fibrillation database.

Using the two databases to test the algorithm, we used the corresponding annotation files for each record provided by Physionet to determine the actual location of the R-waves and compared them to the output of the R-wave detection algorithm, using the ANSI/AAMI EC57:1998 standard and the ANSI/AAMI EC38:1998 standard. This was accomplished using the WFDB Toolbox, which reads in information from Physionet. For our purposes, we read in the raw data from the Physionet database and the annotation files that list the exact locations of the R-waves and also contain information about the sampling frequency.

Some key functions from the WFDB Toolbox that we used are “rdann”, “rdsamp”, “wrann”, and “bxb.” The function “rdsamp” is used to read the ECG vector from a data file, read the sampling frequency from the corresponding header file, and determine whether to plot the signal or not. The “rdann” function is used to read the annotation file provided by Physionet, the “wrann” function is used to write to a file, and “bxb” is an ANSI/AAMI-compliant beat-by-beat comparator function which is used to compare the annotation files provided by Physionet and the output pulse train of our detection algorithm. For our purposes, we used “wrann” to write the output R-wave detection locations to a .test file, which we then used “bxb” to compare our annotation file with the one Physionet provided us.

6.3: R-Wave Detection Algorithm Design Validation

We wrote a comparator() function using WFDB toolbox functions that creates a bxb() report, which is shown in Figure 6.6. The function can be found in Appendix F.1. In the report, the QRS sensitivity and QRS positive predictivity are noted. QRS sensitivity is determined by how sensitive the detector is, and QRS positive predictivity is determined by how accurate the QRS detections are (i.e the detection is within 150 ms of the truth annotation). Additionally, there is also a table that shows the number of R-waves detected and number of R-waves missed by the algorithm. This is denoted by ‘N’ and ‘n’, which means that they are beats that were successfully detected, ‘Q’ which are unknown beats, and ‘O’, which denote missed beats. Other annotations include ‘V’, which is premature ventricular contraction (PVC), and ‘X’ which is to denote incorrect beats.

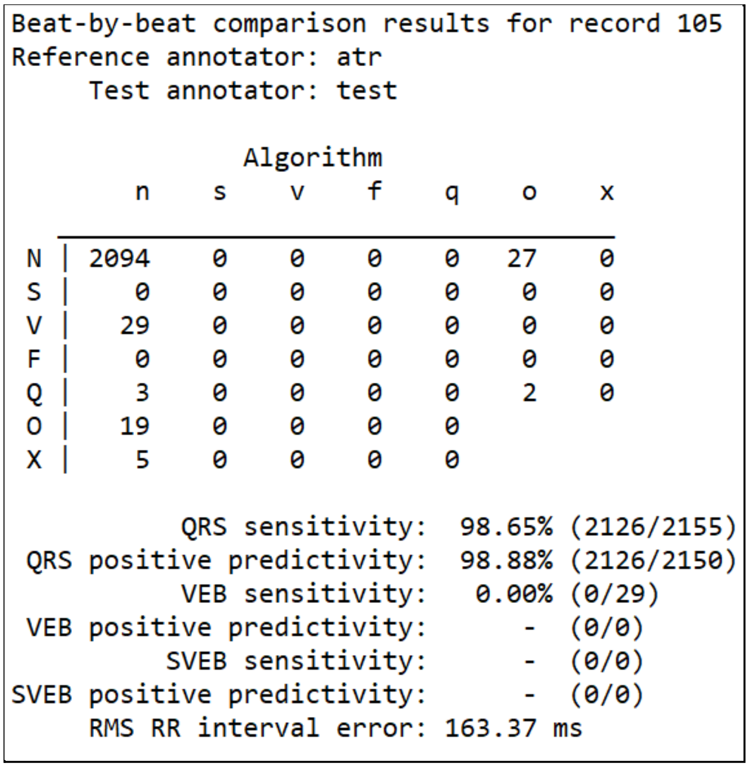

```
Beat-by-beat comparison results for record 105
Reference annotator: atr
     Test annotator: test

               Algorithm
        n    s    v    f    q    o    x
   ____________________________________
 N | 2094    0    0    0    0   27    0
 S |    0    0    0    0    0    0    0
 V |   29    0    0    0    0    0    0
 F |    0    0    0    0    0    0    0
 Q |    3    0    0    0    0    2    0
 O |   19    0    0    0    0
 X |    5    0    0    0    0

          QRS sensitivity:  98.65% (2126/2155)
 QRS positive predictivity:  98.88% (2126/2150)
          VEB sensitivity:   0.00% (0/29)
 VEB positive predictivity:       -  (0/0)
         SVEB sensitivity:       -  (0/0)
SVEB positive predictivity:       -  (0/0)
     RMS RR interval error: 163.37 ms
```

Figure 6.6: bxb Report Example from subject 105

We wanted to automate collecting all the QRS sensitivity and QRS positive predictivity from the individual reports created from each record. Thus, we wrote the bxbreport_table() function, which can be found in Appendix F.2. The function reads the bxb report that is inputted into the function, and then modifies a .csv file that tabulates each of the results. From there, we were able to use Microsoft Excel functions to perform statistical analysis, such as calculating the average and standard deviation, to understand the overall accuracy of our algorithm.

We started by comparing our results to Pan-Tompkins' results for the arrhythmia database as stated in their paper. Their subject-by-subject results are listed in Appendix D.1. All of their testing was done on Channel 1, as they realized that Channel 2 generally has a lower amplitude ECG signal and has poor SNR. Another observation is that the number of beats our detector found is less than what Pan-Tompkins found, and this could be due to Physionet making some modifications to the annotation files since Pan-Tompkins tested on their algorithm in 1985. The overall accuracy for their algorithm was 99.325%. Appendix D.2 and D.3 have the subject-by-subject results of our algorithm for the two databases, and Table 6-1 shows the accuracy of the QRS sensitivity and QRS positive predictivity.

Table 6-1: Accuracy of the R-Wave Detection Algorithm for Different Databases with a 5-15 Hz Bandpass Filter Cutoff and Second-Order Lowpass Filter

Database	QRS sensitivity (%)	QRS positive predictivity (%)
Arrhythmia	94.26 ± 17.61	99.78 ± 0.86
Atrial Fibrillation	83.40 ± 31.80	94.63 ± 13.58

There were three or four records in both databases that had a very low sensitivity percentage which is why our averages were affected. While they are full readings in themselves, they are outliers in our overall data analysis.

In an attempt to optimize and fix these outliers, our next step was to modify the orders and cutoff frequencies on the bandpass and lowpass filters and determine the effect they have on the performance results. Using that, we determined what the best set of parameters are to detect R-waves. The first modification we tested on was changing the higher cutoff frequency in the bandpass filter from 15 Hz to 12 Hz and changing the order of the lowpass filter for the moving average. As previously mentioned, the moving average is simply a poor lowpass filter, so decreasing the order of the filter deviates the stopband from reaching its ideal characteristics. We initially created a second-order lowpass filter, but to see the effect on the data, we changed it to a first-order. The subject-by-subject results that have the effect of the change on each record can be found in Appendix D.4 and D.5, and the average and standard deviations are displayed in Table 6-2.

Table 6-2: Accuracy of the R-Wave Detection Algorithm for Different Databases with a 5-12 Hz Bandpass Filter Cutoff and First-Order Lowpass Filter

Database	QRS sensitivity (%)	QRS positive predictivity (%)
Arrhythmia	95.44 ± 14.97	99.59 ± 1.63
Atrial Fibrillation	81.48 ± 29.69	94.87 ± 13.51

Some key takeaways we got after implementing the change is that the average QRS sensitivity for the arrhythmia database increased, but the average predictivity got worse. For the atrial fibrillation database, the average predictivity got a bit better but the average QRS sensitivity got worse. Comparing the values in the subject-by-subject data results, record 104 from the arrhythmia database initially had a QRS sensitivity of 27.63%, but after the modification to the bandpass and lowpass filters, it substantially improved to have a QRS sensitivity of 87.29%. Reducing the cutoff frequency in the bandpass filter from 15 to 12 Hz and changing the order of the lowpass filter to a first order greatly helped the detector take in more of the missed lower amplitude QRS signals, which is where the majority of the signals in this record are located.

While there were some improvements to the data after implementing a bandpass filter with a high cutoff at 12 Hz and first-order lowpass filter, some of the data that were previously fine did worse after the change. An example of this is record 07879 from the atrial fibrillation database, where in the original scenario, there was a QRS sensitivity of 99.17%, but after the modification had a QRS sensitivity of 67.53%. Other pitfalls of the modification is that for some records, while the other statistics were close to that for the second-order lowpass filter, the QRS positive predictivity would be affected, usually decreasing.

The second modification that we tested on was using the second channel of the ECG array. We used the same filter parameters as our first round of testing, which was a fourth-order bandpass filter with a passband of 5-15 Hz, and a second-order lowpass filter with a cutoff frequency of 5 Hz. Additionally, the ECG array that Physionet provides has two columns; one for Lead I, and one for Lead II. So far, all of our testing had been on Lead I and we wanted to see the effect that Lead II might have on the statistics.

Some key takeaways from this modification was that all of our outliers except one had a QRS sensitivity over 98% when using Lead II instead of Lead I, but there were other records that did not do well with the modification, some dropping from 95% or higher accuracy to less than 50%. The subject-by-subject results that have the effect of the change on each record can be found in Appendix D.6 and D.7, and the average and standard deviations are displayed in Table 6-3.

Table 6-3: Accuracy of the R-Wave Detection Algorithm for Different Databases by using Channel 2 instead of Channel 1

Database	QRS sensitivity (%)	QRS positive predictivity (%)
Arrhythmia	84.50 ± 28.29	97.29 ± 10.41
Atrial Fibrillation	87.024 ± 27.77	94.41 ± 13.65

The final modification we tested on was changing the higher cutoff frequency in the bandpass filter from 15 Hz to 12 Hz, changing the order of the lowpass filter for the moving average to a first-order, and changing the lowpass filter cutoff frequency to 6 Hz. The subject-by-subject results that have the effect of the change on each record can be found in Appendix D.8 and D.9, and the average and standard deviations are displayed in Table 6-4.

Table 6-4: Accuracy of the R-Wave Detection Algorithm for Different Databases with a 5-12 Hz Bandpass Filter Cutoff and First-Order Lowpass Filter with a 6 Hz Cutoff Frequency

Database	QRS sensitivity (%)	QRS positive predictivity (%)
Arrhythmia	95.50 ± 14.94	99.57 ± 1.67
Atrial Fibrillation	81.92 ± 29.56	94.88 ± 13.50

Our overall conclusion from this study is that while adjusting the cutoff frequencies and the order of the filters might have an effect on the accuracy of the R-wave detections, it is not enough to eliminate all of our outliers. As seen in the third modification, the QRS sensitivity and QRS positive predictivity are almost the same as the first modification where we had a lowpass cutoff frequency of 5 Hz instead of 6 Hz. The peak detection section will need to be further modified with more complex logic to accommodate R-wave peak amplitudes changing greatly over the course of minutes or hours.

6.4: Discussion

Our initial set of parameters seem to have worked well with the least number of outliers in both databases, since the QRS sensitivity and positive predictivity are quite similar for both databases. The overall performance of the algorithm is about the same for both databases, which makes our algorithm useful for accurately detecting R-waves locations when later detecting atrial fibrillation.

After the initial set of testing, we noticed a QRS sensitivity of 85% or higher for 64/71 of the traces we tested from both the Physionet arrhythmia and atrial fibrillation databases, and a QRS positive predictivity of 91% or higher for 69/71 traces from both databases. In the effort to optimize our algorithm, our goal was to then eliminate the seven data outliers without compromising on the accuracy of those that are producing high accuracy.

After testing with a first-order lowpass filter and a cutoff frequency of 5-12 Hz on the bandpass filter, we noticed a QRS sensitivity of 85% or higher for 61/71 of the traces we tested from both the Physionet arrhythmia and atrial fibrillation databases, and a QRS positive predictivity of 91% or higher for 70/71 traces from both databases. While we were able to remove one of the seven outliers that the first set of testing produced, our overall improvement was not much better.

In another attempt to remove the outliers, we used the filter parameters from our first round of testing, a fourth-order bandpass filter with a 5-15 Hz passband and a second-order lowpass with a cutoff frequency at 5 Hz, and tested it on the second channel from the ECG array for the all records, with specific focus on the ones that were not doing well when using the first channel. Six out of seven of the records performed significantly better, with a QRS sensitivity above 98% and QRS positive predictivity above 97%. However, there were records that previously did well using Channel 1 that did not perform as well when using Channel 2. This is expected however, because generally one channel has a lower amplitude ECG signal and has poor SNR. What was interesting was seeing some results were about the same regardless of the channel, which could simply mean that the SNR was about the same for both channels. The subject-by-subject results from this can be found in Appendix D.6 and D.7. The only record that has low QRS sensitivity and positive predictivity when using either channel is record 07162 in the atrial fibrillation database.

The final modification we did was change the highpass high cutoff frequency from 15 Hz to 12 Hz, lowpass cutoff frequency from 5 Hz to 6 Hz, and the lowpass filter order from a second to a first-order filter. After testing with this modification, we noticed a QRS sensitivity of 85% or higher for 62/71 of the traces we tested from both the Physionet arrhythmia and atrial fibrillation databases, and a QRS positive predictivity of 91% or higher for 70/71 traces from both databases. This modification was slightly better than the first modification we did, but it is overall almost the same.

Record 07162 was the only record that yielded a QRS sensitivity and positive predictivity of 33% or less for all the different modifications we tried. Zooming in and manually looking at the amplitudes of the signal, the peaks seem to be very erratic, some are at a very large amplitude and others are at a very low amplitude in a short period of time. Additionally, the R-waves appear to be inverted, as shown in Figure 6.7:

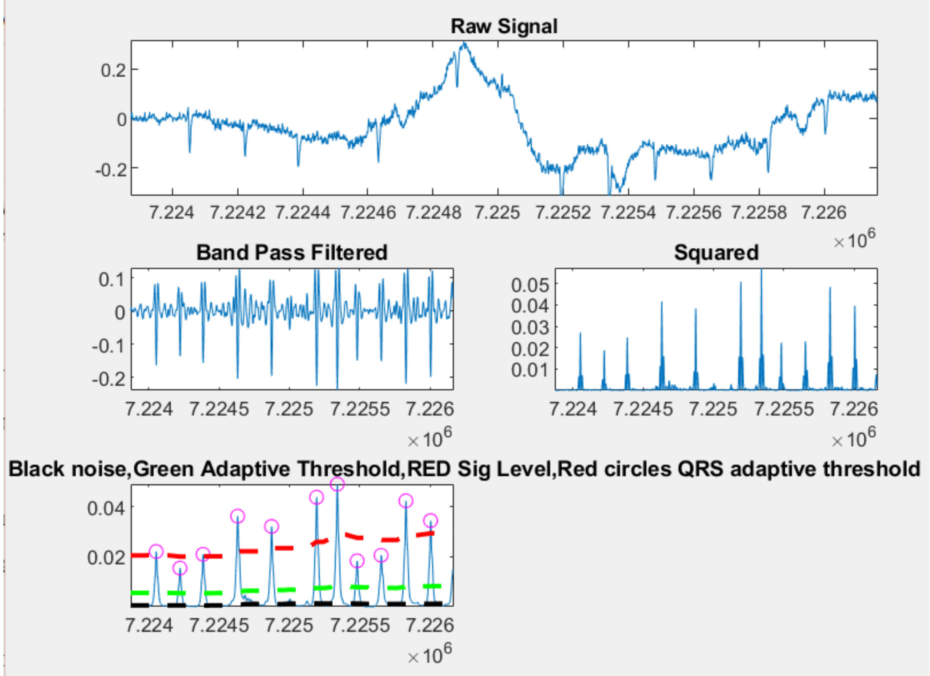

Figure 6.7: Record 07162 Raw Signal- Inverted R-waves in the raw signal for about 2000 samples

We would need to further optimize the R-wave detector, first by trying more combinations of cutoff frequencies and orders, and by implementing more complex logic for these kinds of situations. Another situation that we've noticed is that there are some really large peaks, maybe due to noise, that fall within the filter cutoff frequencies, but affect the thresholds that are set. For example, the 08219 record in the atrial fibrillation database has a higher amplitude in the first third of the data collected than the rest of the data, as shown in Figure 6.8.

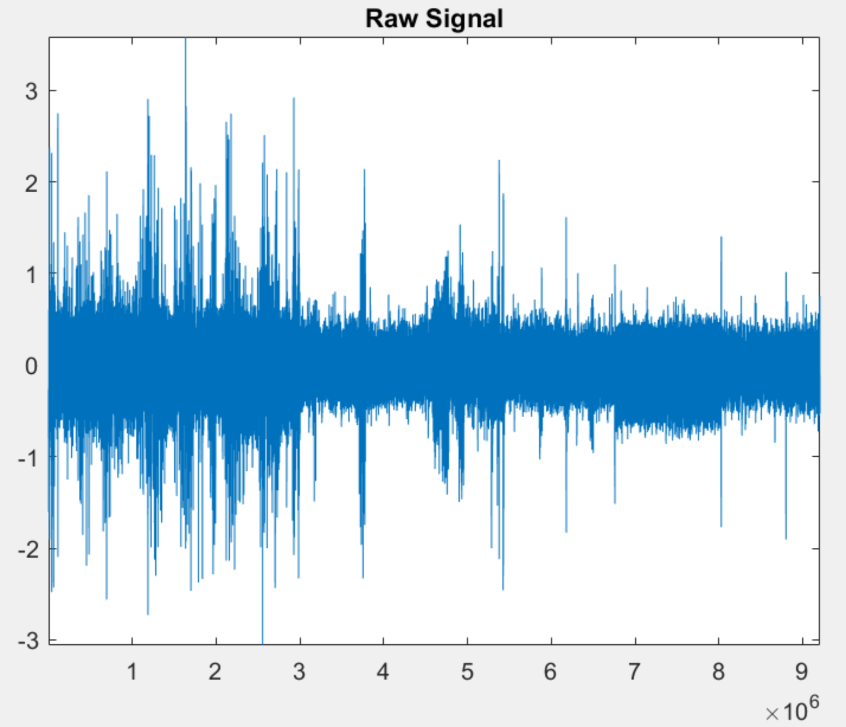

Figure 6.8: Record 08219 Raw Signal- The first 3x10^6 samples have a significantly higher amplitude than the rest of the 6x10^6 samples with the exception of some peaks

This is why, when changing the filter cutoff frequencies, the R-waves after one-third of the trace are difficult to catch by the detector. The thresholds may need to be better adjusted with more logic to accommodate special situations like these, since thresholds are determined primarily from the first two seconds of the recording. The rest of the outliers all have a similar pattern, with record 104 in the arrhythmia database being the exception, as described earlier.

A possible solution to fix the thresholds is to take the raw signal and split it into smaller intervals, such as an interval of 1000 samples, and then testing each interval individually to determine what the thresholds are being set to in each learning phase. Additionally, more R-waves would be detected from this method because the threshold from very high amplitude peaks are not being considered, so it might be more accurate. However, the implementation and testing of this would be needed for a more accurate conclusion.

A reason for the amplitude change that was stable after the change could be due to a lead moving or falling off, which could be skewing the trace. With that said, there are a few spikes later in the graph that reach the earlier trace amplitude, which could be due to noise, so it is also possible that the first one third of the trace was very noisy.

Overall, Physionet was an excellent resource to provide arrhythmia and atrial fibrillation recordings to test our algorithm. It has allowed us to test and compare the effect of different parameters to determine what works best and what could be improved. We were also able to learn a lot about the WFDB toolbox and how to use it, since that was a roadblock early in the project.

7: Atrial Fibrillation Algorithm

This section discusses the methods used to develop the atrial fibrillation detection algorithm. A brief analysis of different RR interval segment lengths, window characteristics, and threshold values was conducted. Plans for future work are outlined at the end of the section.

7.1: Design Process

The atrial fibrillation detection algorithm was based on the algorithm created by Lee et al. The first step in the development of the MATLAB algorithm was to read in the data downloaded from Physionet, specifically the MIT/BIH Atrial Fibrillation database. Physionet is a free database of physiological signals that have been reviewed by medical professionals to ensure the accuracy of all annotations. The MIT/BIH Atrial Fibrillation database contains 25 ECG recordings that are each 10 hours in length. ECG data and its corresponding annotations were read in using functions in the WFDB toolbox. This toolbox interfaces with the Physionet database and allows for easy manipulation of the data files. The WFDB toolbox was originally developed in the "C" programming language and using wrapper functions is compatible with MATLAB, the programming language we used for our algorithm.

The differences between successive R-wave locations were calculated and a vector of RR-intervals was created. Before any calculations were done, ectopic beats were removed from the vector. This is done by first calculating the RR-interval ratio between the current beat and the previous beat for all beats in the vector. The ratios are stored in a new vector. Next, the 1st, 25th and 99th percentile values of the ratio vector are found. The percentiles are then used as threshold values to indicate if a beat is ectopic using the logic from equations 2.49 - 2.51 in the Background chapter. If the beat is ectopic, it is removed from the vector along with the following beat.

The time varying coherence function was calculated for beat segments with a length of 128 RR intervals. The MATLAB function mscohere() was used to calculate the magnitude squared coherence for adjacent segments of the RR-interval vector. This function uses a Welch based spectral estimate. A hamming window with 50% overlap was used as part of this function initially. The magnitude squared coherence represents the first half of equation 2.52 in the

Background chapter . The two halves of the TVCF equation are complex conjugates, and therefore multiplying the two halves together is the same as squaring the results of one of the halves [41]. For our algorithm we decided to square the magnitude squared coherence function, instead of using the full TVCF equation from Lee et al., because of its simplicity.

The y-intercept of the TVCF for each beat segment was calculated by fitting a line to the data and used as an indicator of atrial fibrillation. Through testing of the algorithm, a y-intercept threshold value will be determined to aid in classifying segments as atrial fibrillation or normal sinus rhythm. This replaces the frequency variation parameter used by Lee et al.

Shannon entropy was also found for the same RR-interval segments as the TVCF equation. The Shannon entropy function created was modified from a function found on Github created by Noah Goldstein, Dan Song, and Dan Thompson [42]. The method of Shannon entropy calculation, explained in the Background chapter, was implemented in this function. Once these values were found, the segments were classified as normal sinus rhythm or containing atrial fibrillation using the Shannon entropy and the y-intercept threshold values of about 0.79 and 0.71, respectively. For segments with a Shannon entropy above 0.79 and a y-intercept below 0.71, the segment is classified as atrial fibrillation

The results of the algorithm will be tested using an episode-by-episode comparator function in the WFDB toolbox, which will compare the results to the annotation file. The function compares the two annotation files using the ANSI/AAMI EC38:2007 standard and reports back the accuracy of the detected values versus the truth values. The parameters for segment length and the threshold values will be varied to test their effect on the accuracy of the algorithm. The ideal values will be determined to create the highest accuracy.

7.2: Design Verification

The first part of verifying the design of the algorithm was to test specific parameters in order to accurately detect atrial fibrillation. These parameters include the RR-interval segment length, the size and amount of overlap in the hamming window, the slope threshold values, and the Shannon entropy threshold values.

7.2.1 Optimizing Segment Length

During the initial development of the atrial fibrillation algorithm, a segment length of 128 beats was used. This value was suggested by Lee et al., but when implemented, resulted in significantly noisier TVCF values than those achieved in the journal article(Figure 7.1).

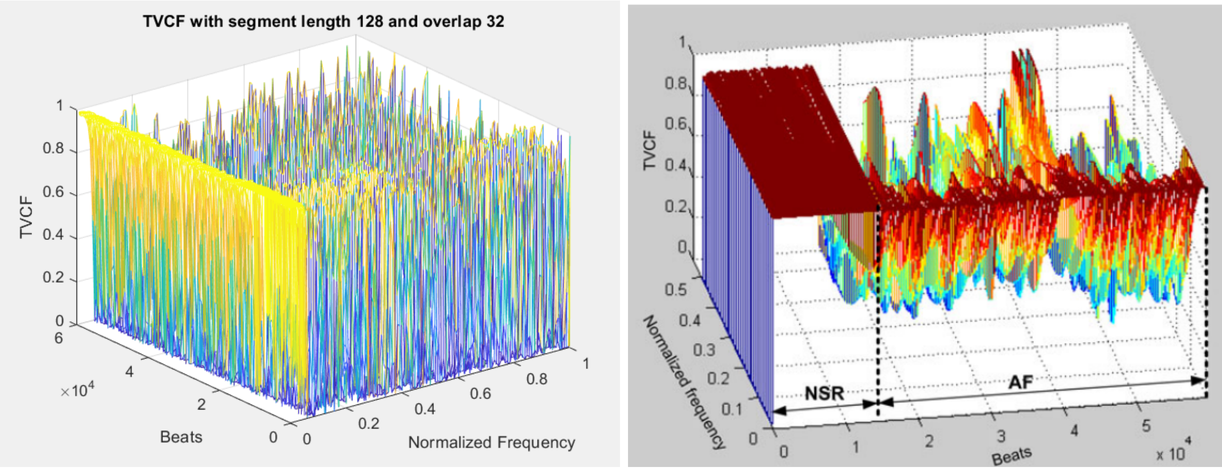

Figure 7.1: Plot of TVCF data for subject 08455 with RR interval length of 128. Our data left and Lee et al.[9] data right

In order to smooth out the data, different segment lengths were tested; the tested RR interval lengths were 128, 150, 192, and 256. The plots looked smoother with each segment increase but with each increase, the magnitude of the TVCF values decreased. This is not ideal because one of the indicators of normal sinus rhythm is the TVCF being near one across the frequency spectrum. The plots for segment lengths 192 and 256 are shown in Figure 7.2.

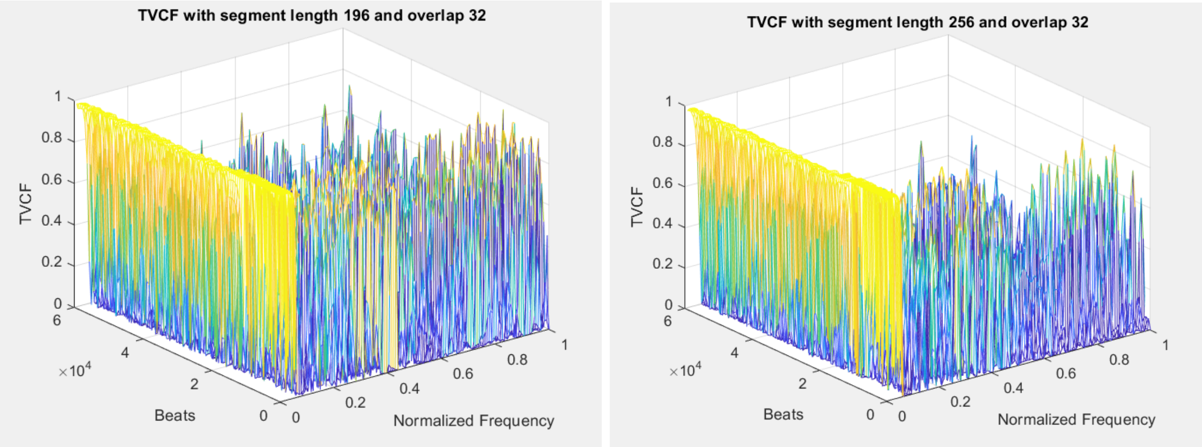

Figure 7.2: Plot of TVCF data for subject 08455. Segment length 196 left and segment length 256 right

Another concern with the increase in segment length is the loss of resolution. For example, within a segment, an individual might go in and out of atrial fibrillation, and this information would be missed by the algorithm. Before a decision can be made on the segment length, the window needs to also be tested to see the impact it has on the TVCF values.

7.2.2 Varying Window Size

We decided to vary the window size and type used when calculating the coherence in an attempt to reduce noise and create a clearer visual distinction between normal sinus rhythm and atrial fibrillation. The window used was changed from a hamming to a hanning window because in the time domain it reaches zero, and therefore eliminates all discontinuity [43]. The size of the window was reduced to a value of 15 instead of 64, the value used by Lee et al., and the amount of overlap was also reduced to 13 because the overlap must be smaller than the window size. The resulting TVCF values are plotted in Figure 7.3 below.

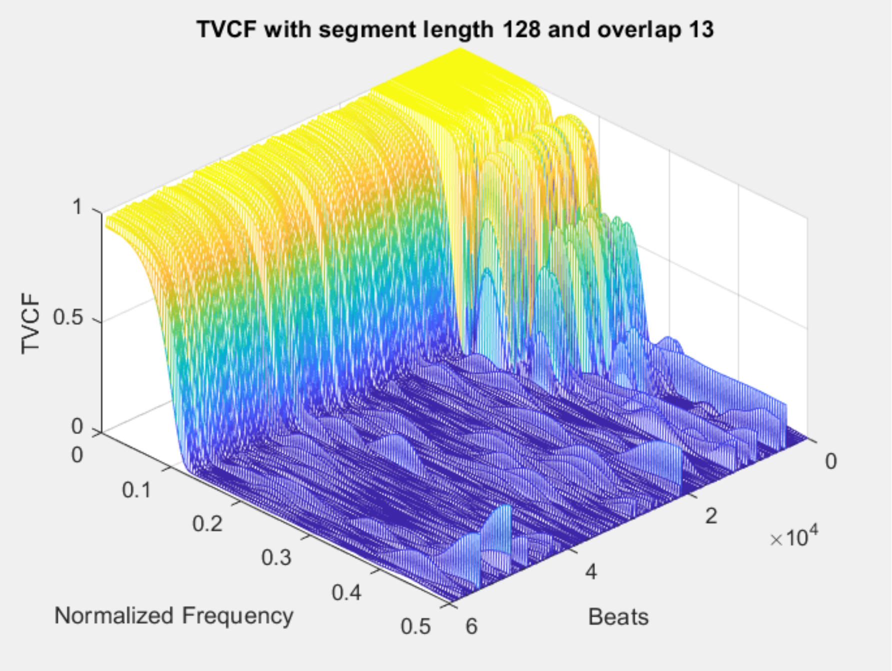

Figure 7.3: Plot of TVCF values for a segment length of 128, window size of 15, and an overlap of 13

The frequency resolution decreased when the window size was reduced. This was expected but the information lost may not be necessary for accurate classification; therefore, this loss of resolution may not affect the overall outcome of the classification algorithm.

7.2.3 Optimizing Window Overlap

During the calculation of the TVCF values from the RR-interval data the cross power spectral density is calculated. The amount of overlap in this window is automatically set to 50% of the window size and can contribute to the smoothness of the TVCF plot. By increasing the overlap the expected response was a reduction of noise. The overall impact on the TVCF values was minimal but the higher amount of overlap did result in a greater degree of smoothing. The overlap values tested were at 50%, 75%, and almost about 90% of the window size for both a 64-point and 15-point Fourier transform.

7.2.4 Classification Parameters

The two parameters we used for the classification of atrial fibrillation are the y-intercept of the TVCF and the Shannon entropy of the RR interval segments. The y-intercept values for subject 08455 are shown in Figure 7.4. For the first 120 segments, this subject is in normal sinus rhythm and for the remaining segments, the subject is in atrial fibrillation. Figure 7.4a is the y-intercept with a segment length of 128, using a hamming window with length 64 and overlap of 60. Figure 7.4b shows the y-intercepts with the 128 beat segment length but using a hanning window size of 15 and an overlap of 13. The visual distinction between atrial fibrillation and normal sinus rhythm is significantly more visually distinct using the parameters from Figure 7.4b.

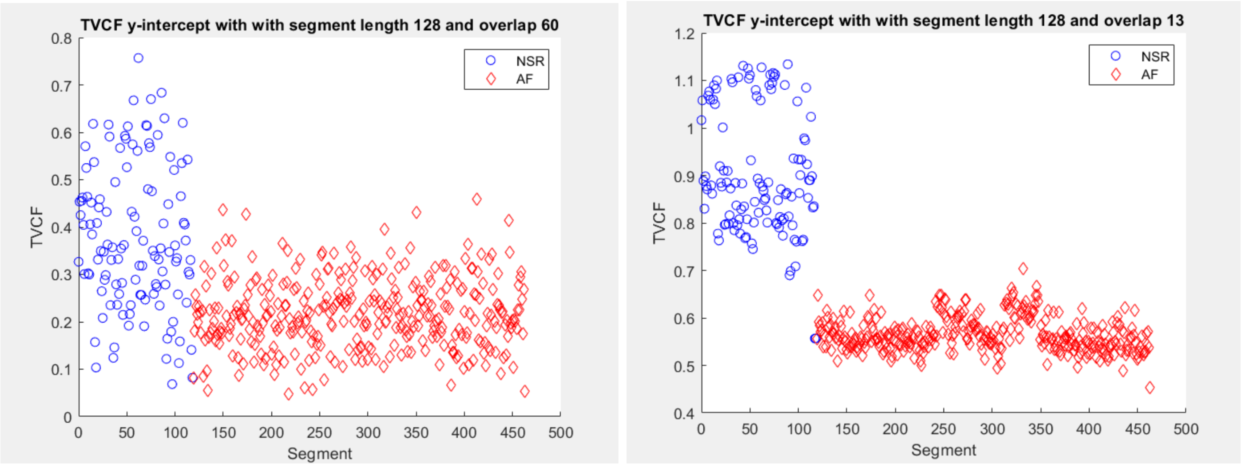

Figure 7.4a(left) and b(right): a)Y-intercept values of TVCF with segment length 128, window type hamming, window size 64, and overlap 60 b) Y-intercept values of TVCF with segment length 128, window type hanning, window size 15, and overlap 13

Shannon entropy for each segment was also calculated with the results plotted in Figure 7.5. The figure plots the results from subject 08455, where the transition from normal sinus rhythm to atrial fibrillation is around segment 120.

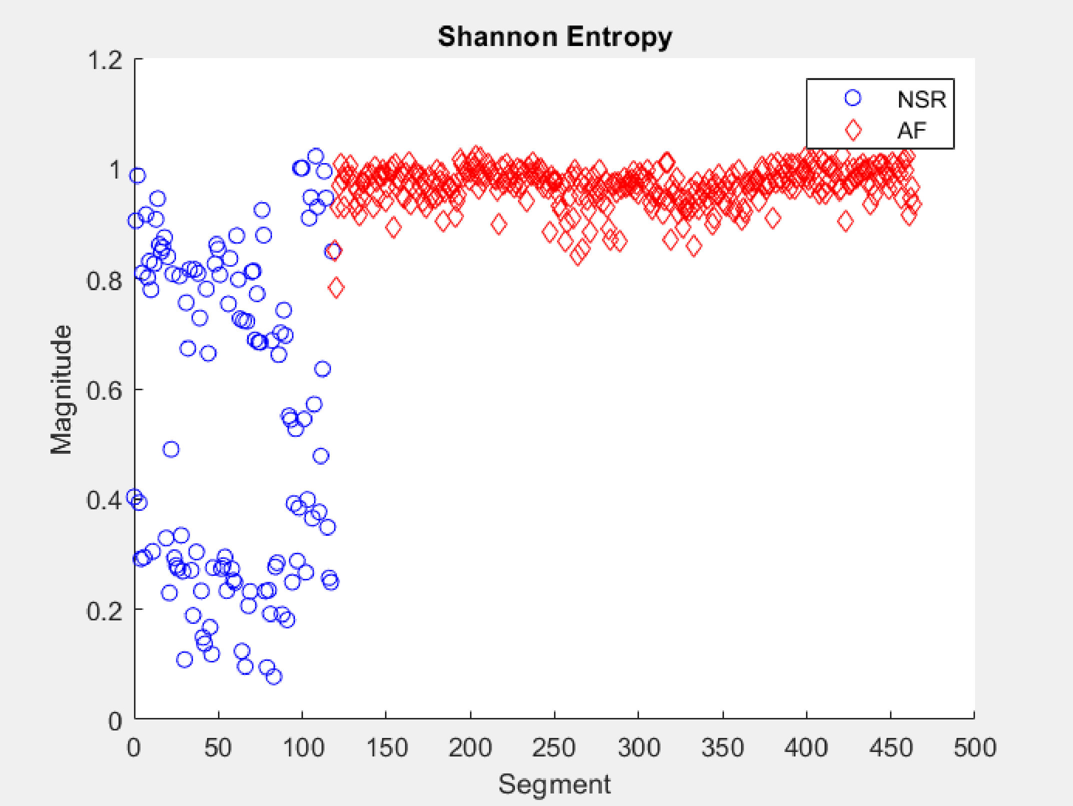

Figure 7.5: Shannon entropy segment length 128 subject 08455

7.3: Design Validation

For the classification portion of our algorithm, threshold values were set for y-intercept of the TVCF and Shannon entropy. The initial values selected were estimated from Figure 7.6 where NSR is normal sinus rhythm and AF is atrial fibrillation. The thresholds chosen were 0.79 for Shannon entropy, as suggested by Lee et al., and 0.7 for y-intercept. With further testing, these parameters will be shifted to produce the highest accuracy classification across all subjects in the MIT/BIH Atrial Fibrillation database.

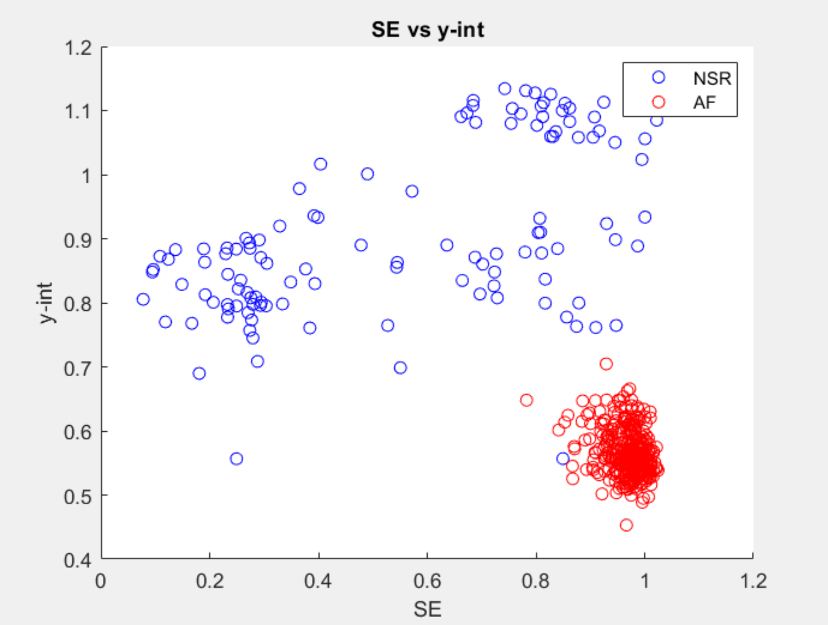

Figure 7.6: Shannon entropy vs y-intercept of TVCF

The logic associated with these thresholds is any value greater than 0.79 for Shannon entropy and less than 0.71 for the y-intercept is classified as atrial fibrillation. Any segment that does not meet both these requirements is classified as normal sinus rhythm.

7.4: Discussion

The atrial fibrillation algorithm is able to classify RR-interval segments as normal sinus rhythm or atrial fibrillation using the thresholds described above. The algorithm will utilize a RR-interval segment size of 128 and the TVCF function will use a hanning window of size 15 and an overlap of 13. This method works accurately for subject 08455 from the MIT/BIH Atrial Fibrillation database but still needs to be tested on the rest of the subjects. This portion of the algorithm will be thoroughly tested next term so that we can optimize the threshold values for Shannon entropy and y-intercept.

8. Discussion

Our project is just a start and there are a lot of future directions our project can go. On the hardware side, we can incorporate an LCD or a seven-segment display that can display the heart rate in real time while it is mounted on the body. For the R-wave algorithm, it can be further optimized by adjusting thresholds so that special cases such as record 08219, which was described earlier, can detect R-waves despite the amplitude shift in the data. There is also the case of record 07162 where changing filter parameters and trying both channels of the ECG array did not improve the QRS sensitivity and QRS positive predictivity, so we would need to further examine how to produce better results. There are also probably better ways to automate testing the data so that we don't have to manually change the .dat file that we want to analyze, but that is something that future iterations of the detector can add.

As a team, we were able to learn a lot from each other and our advisor about what ECG circuits need, how to reduce noise, and concepts such as PCB layout. We have also been learning how to understand and modify the embedded code for the MCU. For the algorithms, we learned how to use the WFDB toolbox for MATLAB and the methodology for the algorithms. We had also never heard of the bxb comparator for R-wave detection until our advisor recommended we try it, and it was interesting to see how accurate our algorithm really was, since we were initially relying on manual verification. Overall, Physionet was able to give us a visual understanding of what the signals will look like for normal sinus rhythm, arrhythmias, and atrial fibrillation, which will help when we collect our own data and analyze it. It also allowed us to test the limits of our algorithm so that we knew how to improve it.

Some challenges we faced included understanding how to install and use the functions in the WFDB toolbox. Additionally, while testing the records using our comparator() function, we realized that MATLAB would freeze often, which slowed down our testing a lot. We were able to bypass this hindrance by strategically exiting out of the MATLAB program once our test file was written to and we were still able to produce an accurate bxb report file.

If we had more time, the goals that we would like to be able to reach would be to change the peripheral nodes to one that could handle only two electrodes, making it easier to conceal. To accomplish this we would need to modify the circuit by changing a few components in front of the instrumentation amplifier. A stretch goal for the project is to process the data in real time.

This task is made difficult due to slight time delays between the different electrodes and the MCU. The scope of this project will likely include post processing that could take up to a minute to display results.

9. Summary

The primary focus of this project was to build a multi-lead wireless ECG monitor. The two components involved are the hardware, which is an ECG circuit with a Nordic microcontroller compatibility to collect the heart signals from a subject, and the software portion that is comprised of MATLAB algorithms to detect R-waves and detect atrial fibrillation. The R-wave detection algorithm and testing is complete and ready to be used to analyze data collected from the ECG circuit. The ECG circuit and atrial fibrillation algorithms are making significant progress and are expected to be completed by the end of C-term 2022. Due to a member of the team graduating early, the focus of this paper has been the team's progress and a close study of the R-wave detection algorithm and testing it.

Appendix

Appendix A: Gantt Chart A-Term

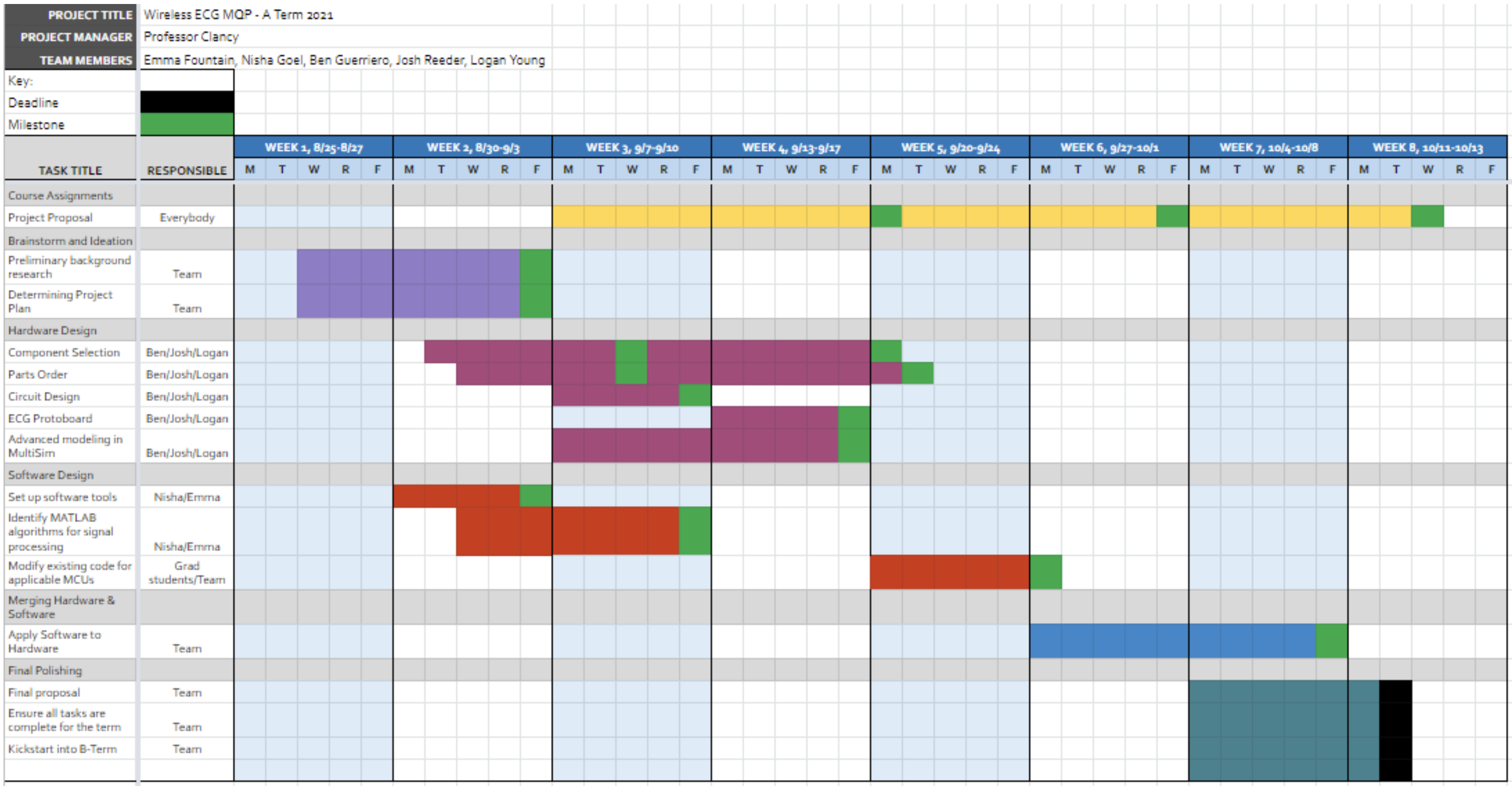

PROJECT TITLE Wireless ECG MQP - A Term 2021

PROJECT MANAGER Professor Clancy

TEAM MEMBERS Emma Fountain, Nisha Goel, Ben Guerriero, Josh Reeder, Logan Young

Key:

Deadline ⬛

Milestone 🟩

		WEEK 1, 8/25-8/27					WEEK 2, 8/30-9/3					WEEK 3, 9/7-9/10					WEEK 4, 9/13-9/17					WEEK 5, 9/20-9/24					WEEK 6, 9/27-10/1					WEEK 7, 10/4-10/8					WEEK 8, 10/11-10/13				
TASK TITLE	RESPONSIBLE	M	T	W	R	F	M	T	W	R	F	M	T	W	R	F	M	T	W	R	F	M	T	W	R	F	M	T	W	R	F	M	T	W	R	F	M	T	W	R	F
Course Assignments																																									
Project Proposal	Everybody											🟨	🟨	🟨	🟨	🟨	🟨	🟨	🟨	🟨	🟨	🟩	🟨	🟨	🟨	🟨	🟨	🟨	🟨	🟨	🟩	🟨	🟨	🟨	🟨	🟨	🟨	🟨	🟩		
Brainstorm and Ideation																																									
Preliminary background research	Team			🟪	🟪	🟪	🟪	🟪	🟪	🟪	🟩																														
Determining Project Plan	Team																																								
Hardware Design																																									
Component Selection	Ben/Josh/Logan							🟪	🟪	🟪	🟪	🟪	🟪	🟩	🟪	🟪	🟪	🟪	🟪	🟪	🟪	🟩																			
Parts Order	Ben/Josh/Logan								🟪	🟪	🟪	🟪	🟪	🟩	🟪	🟪	🟪	🟪	🟪	🟪	🟪	🟪	🟩																		
Circuit Design	Ben/Josh/Logan											🟪	🟪	🟪	🟪	🟩																									
ECG Protoboard	Ben/Josh/Logan																🟪	🟪	🟪	🟪	🟩																				
Advanced modeling in MultiSim	Ben/Josh/Logan											🟪	🟪	🟪	🟪	🟪	🟪	🟪	🟪	🟪	🟩																				
Software Design																																									
Set up software tools	Nisha/Emma						🟥	🟥	🟥	🟥	🟩																														
Identify MATLAB algorithms for signal processing	Nisha/Emma								🟥	🟥	🟥	🟥	🟥	🟥	🟥	🟩																									
Modify existing code for applicable MCUs	Grad students/Team																					🟥	🟥	🟥	🟥	🟥	🟩														
Merging Hardware & Software																																									
Apply Software to Hardware	Team																										🟦	🟦	🟦	🟦	🟦	🟦	🟦	🟦	🟦	🟩					
Final Polishing																																									
Final proposal	Team																															▩	▩	▩	▩	▩	▩	⬛			
Ensure all tasks are complete for the term	Team																																								
Kickstart into B-Term	Team																																								

Appendix B: Gantt Chart B-Term

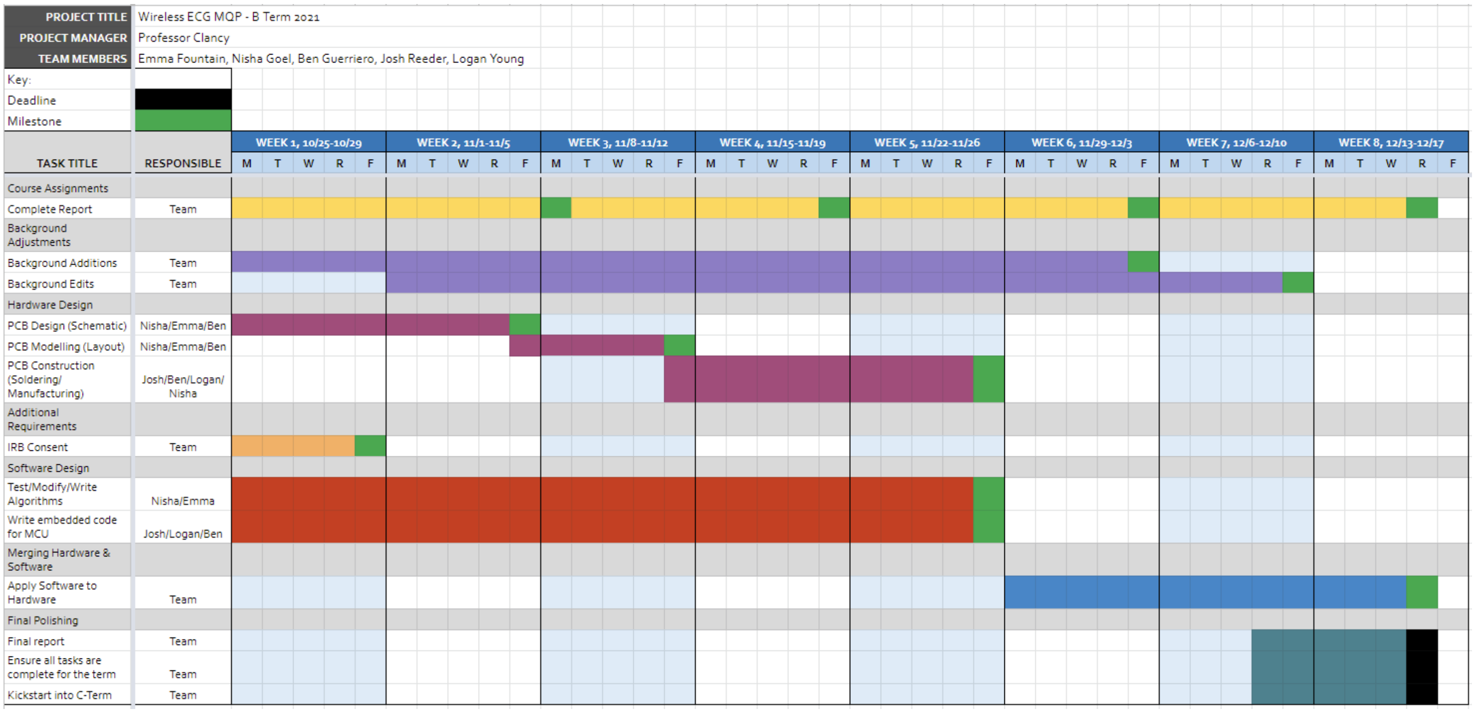

PROJECT TITLE	Wireless ECG MQP - B Term 2021
PROJECT MANAGER	Professor Clancy
TEAM MEMBERS	Emma Fountain, Nisha Goel, Ben Guerriero, Josh Reeder, Logan Young
Key:	
Deadline	⬛
Milestone	🟩

TASK TITLE	RESPONSIBLE	WEEK 1, 10/25-10/29					WEEK 2, 11/1-11/5					WEEK 3, 11/8-11/12					WEEK 4, 11/15-11/19					WEEK 5, 11/22-11/26					WEEK 6, 11/29-12/3					WEEK 7, 12/6-12/10					WEEK 8, 12/13-12/17				
		M	T	W	R	F	M	T	W	R	F	M	T	W	R	F	M	T	W	R	F	M	T	W	R	F	M	T	W	R	F	M	T	W	R	F	M	T	W	R	F
Course Assignments																																									
Complete Report	Team	🟨	🟨	🟨	🟨	🟨	🟨	🟨	🟨	🟨	🟨	🟩	🟨	🟨	🟨	🟨	🟨	🟨	🟨	🟨	🟩	🟨	🟨	🟨	🟨	🟨	🟨	🟨	🟨	🟨	🟩	🟨	🟨	🟨	🟨	🟨	🟨	🟨	🟨	🟩	
Background Adjustments																																									
Background Additions	Team	🟪	🟪	🟪	🟪	🟪	🟪	🟪	🟪	🟪	🟪	🟪	🟪	🟪	🟪	🟪	🟪	🟪	🟪	🟪	🟪	🟪	🟪	🟪	🟪	🟪	🟪	🟪	🟪	🟪	🟩										
Background Edits	Team						🟪	🟪	🟪	🟪	🟪	🟪	🟪	🟪	🟪	🟪	🟪	🟪	🟪	🟪	🟪	🟪	🟪	🟪	🟪	🟪	🟪	🟪	🟪	🟪	🟪	🟪	🟪	🟪	🟪	🟩					
Hardware Design																																									
PCB Design (Schematic)	Nisha/Emma/Ben	🟫	🟫	🟫	🟫	🟫	🟫	🟫	🟫	🟫	🟩																														
PCB Modelling (Layout)	Nisha/Emma/Ben										🟫	🟫	🟫	🟫	🟫	🟩																									
PCB Construction (Soldering/ Manufacturing)	Josh/Ben/Logan/ Nisha															🟫	🟫	🟫	🟫	🟫	🟫	🟫	🟫	🟫	🟫	🟩															
Additional Requirements																																									
IRB Consent	Team	🟧	🟧	🟧	🟧	🟩																																			
Software Design																																									
Test/Modify/Write Algorithms	Nisha/Emma	🟥	🟥	🟥	🟥	🟥	🟥	🟥	🟥	🟥	🟥	🟥	🟥	🟥	🟥	🟥	🟥	🟥	🟥	🟥	🟥	🟥	🟥	🟥	🟥	🟩															
Write embedded code for MCU	Josh/Logan/Ben	🟥	🟥	🟥	🟥	🟥	🟥	🟥	🟥	🟥	🟥	🟥	🟥	🟥	🟥	🟥	🟥	🟥	🟥	🟥	🟥	🟥	🟥	🟥	🟥	🟩															
Merging Hardware & Software																																									
Apply Software to Hardware	Team																										🟦	🟦	🟦	🟦	🟦	🟦	🟦	🟦	🟦	🟦	🟦	🟦	🟦	🟩	
Final Polishing																																									
Final report	Team																																	▨	▨	▨	▨	▨	▨	⬛	
Ensure all tasks are complete for the term	Team																																	▨	▨	▨	▨	▨	▨	⬛	
Kickstart into C-Term	Team																																	▨	▨	▨	▨	▨	▨	⬛	

Appendix C: IRB

Informed Consent Agreement for Participation in a Research Study

Investigators: Emma Fountain, Benjamin Guerriero, Joshua Reeder, Logan Young, Professor Edward A. Clancy

Contact Information: gr-ECG-MQP@wpi.edu (student team) or ted@wpi.edu (faculty advisor)

Title of Research Study: Developing a Multi-Lead Wireless Electrocardiogram (ECG)

Sponsor: None

Introduction: You are being asked to participate in a research study. Before you agree, however, you must be fully informed about the purpose of the study, the procedures to be followed, and any benefits, risks or discomfort that you may experience as a result of your participation. This form presents information about the study so that you may make a fully informed decision regarding your participation

Purpose of the study: This study will contribute to the development of a wireless ECG system (also known as an EKG system). This system will allow the user to monitor their heart rate and notify them if they are experiencing atrial fibrillation or other abnormal beating of their heart. This device will allow the user to monitor their heart rhythm and could possibly be utilized by medical professionals in the future. The goal of this study is to validate that the ECG system works to record, transmit, and process your heart data.

Procedures to be followed: This study will consist of one session of approximately 30 minutes duration. Testing will take place on WPI's campus in the Atwater Kent building. Upon arrival you will be asked to fill out a short questionnaire. You are not required to provide any information you are uncomfortable sharing. We will ask about your: sex, age, height, weight, and any diagnosed heart conditions.

We ask that participants wear a face mask and clothing that easily allows access to the upper chest and back. Women are encouraged to wear a sports bra or bathing suit top underneath a tank top (or T-shirt).. Before the electrodes are placed on the body, the skin at the application sites will be prepared using an alcohol wipe.

We will secure to your upper chest and back up to three of the wireless ECG systems that we are developing. Each will use three ECG electrodes. We may use ace bandage or other flexible wraps around your trunk and tape to hold the apparatus secure to your body. Each ECG device will be light-weight and small enough to be easily supported (e.g., smaller than the size of your fist).

You will be asked to sit in a chair and remain still during the recording, breathing normally and not speaking. The device(s) will record 15 minutes of data. Once data collection is complete the apparatus and electrodes will be removed.

Risks to study participants: There are no risks to participants. Some subjects experience discomfort when the electrodes are removed, as they can pull on body hair and the skin.

Benefits to research participants and others: There are no benefits to the participants or others.

Record keeping and confidentiality: For this study you will be assigned a subject ID number upon the signing of this document. This document will be the only record connecting your subject ID number to your name and will be stored privately. All electronic records will only refer to your data by your subject ID. Records of your participation in this study will be held confidential so far as permitted by law. However, the study investigators and, under certain circumstances, the Worcester Polytechnic Institute Institutional Review Board (WPI IRB) will be able to inspect and have access to confidential data that identify you by name. Any publication or presentation of the data will not identify you.

Compensation or treatment in the event of injury: WPI assumes no responsibility to pay for any injuries that you might receive as a result of participating in this research study. No funds have been set aside for payments or other forms of compensation (such as for lost wages, lost time, or discomfort). If you suffer a physical injury as a result of your participation in this study, you may choose to seek medical care in the same way as you would normally. If your insurance does not cover the cost, then you may be responsible for this cost. However, you do not give up any of your legal rights by signing this consent form.

Incidental findings: This study does not provide medical care. None of the investigators is a health care provider nor will your recorded ECG data be routinely reviewed by a healthcare provider. If you or the investigators note any possible abnormalities on your ECG, you should speak with your own health care provider about any concerns.

Data Reuse and Contribution of Your Data to a Public Data Archive: The data from this experiment will also be contributed to publicly available databases and/or reused by the study investigators in future research. The purpose of this data reuse is to share your data with other researchers (or reuse the data ourselves) to make further advances in medicine, science and teaching. Your data could be used for many different purposes. Most researchers will gain access to your data over the Internet. Before contributing your data, all information that identifies you as a subject in this experiment (including your name) will be coded. The only way to relate the code to your identifying information is by a “key” that the study investigators will maintain private. We will never reveal your identity, unless required to do so by law. The public database will not provide any direct access to your identity.

Cost/Payment: Healthy subjects will not be paid for their participation in this study. Subjects with a known diagnosis of atrial fibrillation will be paid $20 for completion of this study.

For more information about this research or about the rights of research participants, or in case of research-related injury, contact: MQP team, gr-ECG-MQP@wpi.edu; Edward (Ted) A. Clancy, Professor (WPI), Tel. 508-831-5778, Email: ted@wpi.edu; Ruth McKeogh, IRB Manager, Tel. 508 831- 6699, Email: irb@wpi.edu; and Gabriel Johnson, Human Protection Administrator, Tel. 508-831-4989, Email: gjohnson@wpi.edu

Your participation in this research is voluntary. Your refusal to participate will not result in any penalty to you or any loss of benefits to which you may otherwise be entitled. You may decide to stop participating in the research at any time without penalty or loss of other benefits. The project investigators retain the right to cancel or postpone the experimental procedures at any time they see fit.

By signing below, you acknowledge that you have been informed about and consent to be a participant in the study described above. Make sure that your questions are answered to your satisfaction before signing. You are entitled to retain a copy of this consent agreement.

____________________________ Date: ____________________

Study Participant Signature

____

Study Participant Name (Please print)

_____________________________________ Date: ____________________

Signature of Person who explained this study

Appendix D: R-Wave Detection Algorithm Results

D.1: Pan-Tompkins Results for the Arrhythmia Database [25]

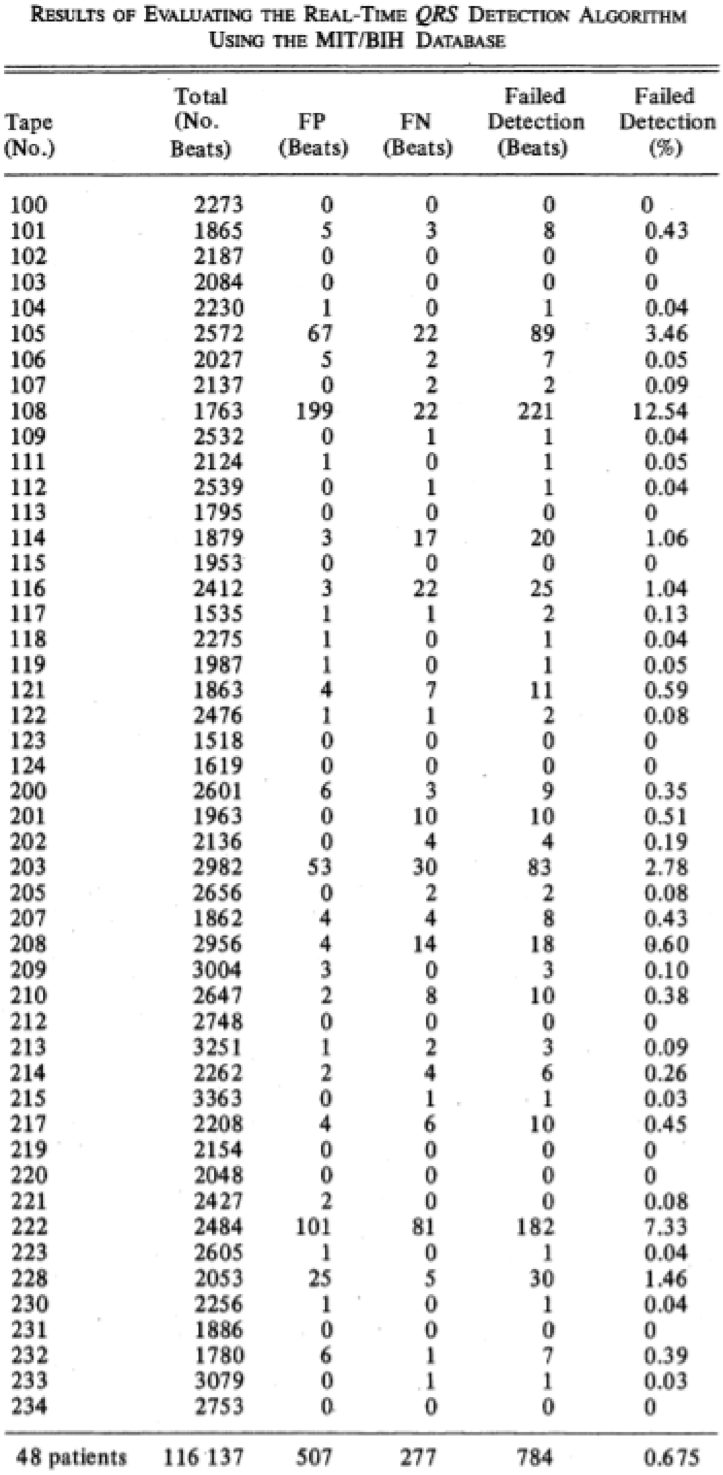

RESULTS OF EVALUATING THE REAL-TIME *QRS* DETECTION ALGORITHM USING THE MIT/BIH DATABASE

Tape (No.)	Total (No. Beats)	FP (Beats)	FN (Beats)	Failed Detection (Beats)	Failed Detection (%)
100	2273	0	0	0	0
101	1865	5	3	8	0.43
102	2187	0	0	0	0
103	2084	0	0	0	0
104	2230	1	0	1	0.04
105	2572	67	22	89	3.46
106	2027	5	2	7	0.05
107	2137	0	2	2	0.09
108	1763	199	22	221	12.54
109	2532	0	1	1	0.04
111	2124	1	0	1	0.05
112	2539	0	1	1	0.04
113	1795	0	0	0	0
114	1879	3	17	20	1.06
115	1953	0	0	0	0
116	2412	3	22	25	1.04
117	1535	1	1	2	0.13
118	2275	1	0	1	0.04
119	1987	1	0	1	0.05
121	1863	4	7	11	0.59
122	2476	1	1	2	0.08
123	1518	0	0	0	0
124	1619	0	0	0	0
200	2601	6	3	9	0.35
201	1963	0	10	10	0.51
202	2136	0	4	4	0.19
203	2982	53	30	83	2.78
205	2656	0	2	2	0.08
207	1862	4	4	8	0.43
208	2956	4	14	18	0.60
209	3004	3	0	3	0.10
210	2647	2	8	10	0.38
212	2748	0	0	0	0
213	3251	1	2	3	0.09
214	2262	2	4	6	0.26
215	3363	0	1	1	0.03
217	2208	4	6	10	0.45
219	2154	0	0	0	0
220	2048	0	0	0	0
221	2427	2	0	0	0.08
222	2484	101	81	182	7.33
223	2605	1	0	1	0.04
228	2053	25	5	30	1.46
230	2256	1	0	1	0.04
231	1886	0	0	0	0
232	1780	6	1	7	0.39
233	3079	0	1	1	0.03
234	2753	0	0	0	0
48 patients	116 137	507	277	784	0.675

D.2: Arrhythmia Database

Filter Parameters:

```
[b, a] = butter(2, [5 15]*2/fs, 'bandpass');  % 5-15 Hz 4th-order Bandpass Filter
[b,a] = butter(2,5*2/fs,'low');  % 2nd-order Lowpass Filter with 5 Hz cutoff freq
```

Record Number	QRS sensitivity (%)	QRS positive predictivity (%)
100	100	100
101	100	99.87
102	85.28	100
103	99.65	100
104	27.63	100
105	98.65	98.88
106	99.29	99.94
107	97.53	100
108	99.19	94.65
109	99.76	100
111	97.75	99.88
112	100	100
113	99.93	100
114	44.95	97.43
115	100	100
116	98.51	99.9
117	100	100
118	100	100
119	100	100
121	99.87	100
122	100	100
123	100	100

124	98.76	100
200	99.82	100
201	95.92	100
202	99.2	100
203	86.58	99.63
205	99.77	100
207	99.75	99.87
208	99.1	99.88
209	100	99.92
210	96.05	99.86
212	100	100
213	99.74	100
214	100	100
215	99.82	100
217	98.64	99.95
219	99.66	100
220	100	100
221	99.65	100
222	90.74	100
223	99.45	100
228	14.21	100
230	100	100
231	100	100
232	99.93	100
233	99.65	100
234	99.91	100

D.3: Atrial Fibrillation Database

Filter Parameters:

```
[b, a] = butter(2, [5 15]*2/fs, 'bandpass');  % 5-15 Hz 4th-order Bandpass Filter
[b,a] = butter(2,5*2/fs,'low');  % 2nd-order Lowpass Filter with 5 Hz cutoff freq
```

Record Number	QRS sensitivity (%)	QRS positive predictivity (%)
08455	99.23	99.72
08434	99.8	97.63
08405	98.86	97.08
08378	98.63	98.24
08219	18.72	97.86
08215	99.71	97.78
07910	99.98	96.75
07879	99.17	97.15
07859	88.2	97.04
07162	31.42	33.05
06995	99.89	97.35
06453	99.89	99.9
06426	92.52	97.62
05261	99.44	97.74
05121	94.18	97.69
05091	93.39	96.78
04936	99.8	97.28
04908	99.9	97.75
04746	6.62	98.9
04126	89.08	96.66
04048	99.68	99.68
04043	99.66	97.72

04015	9.52	88.88

D.4: Arrhythmia Database- Changed Parameters

Filter Parameters:

```
[b, a] = butter(2, [5 12]*2/fs, 'bandpass');  %changed the higher freq from 15 to 12
[b,a] = butter(1,5*2/fs,'low');  % changed from 2nd to 1st order LPF
```

Record Number	QRS sensitivity (%)	QRS positive predictivity (%)
100	100	100
101	100	99.87
102	93.03	100
103	99.65	100
104	87.29	100
105	98.38	98.42
106	99.17	100
107	97.48	100
108	98.99	91.51
109	99.76	100
111	95.5	99.88
112	100	100
113	99.93	100
114	40.59	92.34
115	100	100
116	98.22	99.85
117	100	100
118	100	100
119	100	100
121	99.87	100

122	100	100
123	100	100
124	98.9	100
200	99.72	100
201	97.17	99.8
202	99.2	100
203	84.89	99.67
205	99.64	100
207	99.69	99.87
208	99.22	99.83
209	100	99.84
210	96.55	99.95
212	100	100
213	99.7	100
214	100	100
215	99.36	100
217	97.45	99.94
219	99.66	100
220	100	100
221	99.75	100
222	89.41	99.63
223	99.27	100
228	14.09	100
230	100	100
231	100	100
232	99.93	99.93

233	99.65	100
234	99.96	100

D.5: Atrial Fibrillation Database- Changed Parameters

Filter Parameters:

```
[b, a] = butter(2, [5 12]*2/fs, 'bandpass');  %changed the higher freq from 15 to 12
[b,a] = butter(1,5*2/fs,'low');  % changed from 2nd to 1st order LPF
```

Record Number	QRS sensitivity (%)	QRS positive predictivity (%)
08455	99.19	99.66
08434	99.79	97.64
08405	98.7	97.07
08378	97.4	98.21
08219	20.16	96.99
08215	99.7	97.78
07910	99.97	96.73
07879	67.53	97.1
07859	82.04	97.04
07162	30.93	33.13
06995	98.22	97.09
06453	99.87	99.91
06426	91.81	97.65
05261	99.38	97.66
05121	94.2	97.68
05091	93.46	96.78
04936	99.79	97.29
04908	97.99	97.71
04746	27.25	99.69

04126	68.84	95.49
04048	99.57	99.69
04043	99.54	97.67
04015	8.66	96.32

D.6: Arrhythmia Database- Channel 2

Using the Original Filter Parameters, but testing Channel 2 instead of Channel 1:

```
[b, a] = butter(2, [5 15]*2/fs, 'bandpass');  % 5-15 Hz 4th-order Bandpass Filter
[b,a] = butter(2,5*2/fs,'low');  % 2nd-order Lowpass Filter with 5 Hz cutoff freq
```

Record Number	QRS sensitivity (%)	QRS positive predictivity (%)
100	99.84	100
101	0.13	50
102	99.84	99.95
103	59.4	93.45
104	98.49	99.56
105	79.26	94.16
106	17.33	96.39
107	97.53	100
108	96.96	98.02
109	99.29	100
111	100	100
112	97.44	99.76
113	99.93	100
114	99.88	100
115	76.18	99.36
116	99.45	100
117	100	100

118	99.95	100
119	99.82	99.94
121	99.81	100
122	99.76	100
123	100	100
124	94.37	100
200	1.66	46.75
201	94.81	100
202	99.79	100
203	87.59	97.53
205	43.93	99.38
207	99.62	99.94
208	46.53	98.52
209	30.81	98.35
210	90.65	99.6
212	65.25	100
213	99.85	100
214	96.27	99.83
215	99.71	100
217	98.1	99.78
219	99.83	100
220	100	100
221	15.69	100
222	99.67	100
223	97.91	100
228	99.82	99.82

230	100	100
231	76.37	100
232	99.73	99.73
233	98.01	100
234	99.52	100

D.7: Atrial Fibrillation Database- Channel 2

Using the Original Filter Parameters, but testing Channel 2 instead of Channel 1:

```
[b, a] = butter(2, [5 15]*2/fs, 'bandpass');  % 5-15 Hz 4th-order Bandpass Filter
[b,a] = butter(2,5*2/fs,'low');  % 2nd-order Lowpass Filter with 5 Hz cutoff freq
```

Record Number	QRS sensitivity (%)	QRS positive predictivity (%)
08455	99.16	99.78
08434	99.62	97.78
08405	99.47	97.26
08378	98.07	98.19
08219	99.65	97.6
08215	99.79	97.78
07910	99.8	96.41
07879	99.88	97.52
07859	24.37	97.92
07162	33.8	33.17
06995	5.15	85.06
06453	99.55	99.93
06426	98.91	97.97
05261	99.13	97.54
05121	99.45	97.77
05091	99.79	97.46

04936	99.76	97.2
04908	99.09	97.45
04746	99.99	97.66
04126	59.7	95.27
04048	99.25	99.6
04043	89.94	97.51
04015	98.23	97.56

D.8: Arrhythmia Database- Lowpass Cutoff Frequency Changed

Using the Original Filter Parameters, but testing Channel 2 instead of Channel 1:

```
[b, a] = butter(2, [5 12]*2/fs, 'bandpass');  % changed from 5-15 Hz to 5-12 Hz
4th-order Bandpass Filter
[b,a] = butter(1,6*2/fs,'low');  % changed to 1st-order Lowpass Filter with 6 Hz
cutoff freq
```

Record Number	QRS sensitivity (%)	QRS positive predictivity (%)
100	100	100
101	100	99.87
102	91.76	100
103	99.65	100
104	89.66	100
105	98.65	98.29
106	99.17	99.94
107	97.48	100
108	99.05	91.45
109	99.76	100
111	95.5	99.88
112	100	100
113	99.93	100

114	40.71	92.1
115	100	100
116	98.22	99.85
117	100	100
118	100	100
119	100	99.94
121	99.87	100
122	100	100
123	100	100
124	98.76	100
200	99.72	100
201	97.24	99.26
202	99.2	100
203	85.93	99.67
205	99.68	100
207	99.69	99.87
208	99.22	99.83
209	100	99.84
210	96.55	99.95
212	100	100
213	99.7	100
214	100	100
215	99.43	100
217	97.56	99.94
219	99.66	100
220	100	100

221	99.7	100
222	89.74	99.63
223	99.32	100
228	13.98	100
230	100	100
231	100	100
232	99.93	99.93
233	99.65	100
234	99.96	100

D.9: Atrial Fibrillation Database- Lowpass Cutoff Frequency Changed

Using the Original Filter Parameters, but testing Channel 2 instead of Channel 1:

```
[b, a] = butter(2, [5 15]*2/fs, 'bandpass');  % 5-15 Hz 4th-order Bandpass Filter
[b,a] = butter(2,5*2/fs,'low');  % 2nd-order Lowpass Filter with 5 Hz cutoff freq
```

Record Number	QRS sensitivity (%)	QRS positive predictivity (%)
08455	99.2	99.66
08434	99.79	97.64
08405	98.71	97.07
08378	96.65	98.2
08219	20.36	96.92
08215	99.7	97.78
07910	99.97	96.73
07879	68.08	97.12
07859	84.54	97.12
07162	31.03	33.17
06995	98.32	97.08

06453	99.87	99.9
06426	91.67	97.66
05261	99.38	97.66
05121	94.2	97.69
05091	92.93	96.91
04936	99.73	97.29
04908	99.21	97.74
04746	27.28	99.7
04126	75.68	95.83
04048	99.58	99.7
04043	99.55	97.62
04015	8.68	96.14

Appendix E: R-Wave Detection Algorithm [40]

```
function [qrs_i_raw]=R_Wave_Detector(ecg,fs,gr)
%% function [qrs_i_raw]=R_Wave_Detector(ecg,fs, gr)
%% Inputs
% ecg : raw ecg vector signal 1d signal
% fs : sampling frequency e.g. 200Hz, 400Hz and etc
% gr : flag to plot or not plot (set it 1 to have a plot or set it zero not
% to see any plots
%% Output
% qrs_i_raw : index of R waves
%% References:
%[1] Sedghamiz. H, "Matlab Implementation of Pan Tompkins ECG QRS detector.",2014.
%https://www.researchgate.net/publication/313673153_Matlab_Implementation_of_Pan_To
mpkins_ECG_QRS_detector
%[2] PAN.J, TOMPKINS. W.J,"A Real-Time QRS Detection Algorithm" IEEE
% TRANSACTIONS ON BIOMEDICAL ENGINEERING, VOL. BME-32, NO. 3, MARCH 1985.
%%  ================= Read In Data ==================== %%
[ecg,fs,gr] = rdsamp('100.dat'); %Make sure to modify this prior to each run
%% ================= BioSigKit ==================== %%
ecg = ecg(:,1); % choose ecg column from dataset
if ~isvector(ecg)
  error('ecg must be a row or column vector');
end
if nargin < 3
    gr = 1;   % on default the function always plots
end
%% ======================= Initialize =============================== %
delay = 0;
skip = 0;                                   % becomes one when a T wave is detected
m_selected_RR = 0;
mean_RR = 0;
ser_back = 0;
%%  bandpass filter for Noise cancelation of other sampling frequencies(Filtering)
[b, a] = butter(2, [5 15]*2/fs, 'bandpass');
[Hnew, f] = freqz(b, a, [], fs);
ecg_bp = filtfilt(b, a, ecg);
ecg_bp = ecg_bp/max(abs(ecg_bp));
if gr
 plot(ecg);axis tight;title('Raw Signal'); zoom on;
end
%% ========== Squaring nonlinearly enhance the dominant peaks ========== %%
 ecg_s = ecg_bp.^2;
%% ============  Moving average ================== %%
%Implement a lowpass filter to calculate moving average
[b,a] = butter(2,5*2/fs,'low');
ecg_m = filtfilt(b,a,ecg_s);
ecg_m = ecg_m/ max(abs(ecg_m));
delay = delay + round(0.150*fs)/2;
%% ===================== Fiducial Marks ============================== %%
% Note : From a physiological point of view no RR wave can occur in less
% than 200 msec distance
[pks,locs] = findpeaks(ecg_m,'MINPEAKDISTANCE',round(0.2*fs));
%% =================== Initialize Some Other Parameters =============== %%
LLp = length(pks);
% ---------------- Stores QRS wrt Sig and Filtered Sig ------------------%
qrs_amp = zeros(1,LLp);         % amplitude of R
qrs_i = zeros(1,LLp);           % index
qrs_i_raw = zeros(1,LLp);       % amplitude of R raw
qrs_amp_raw= zeros(1,LLp);      % Index of raw signal
% ------------------- Noise Buffers ---------------------------------%
noise_c = zeros(1,LLp);
noise_i = zeros(1,LLp);
% ------------------- Buffers for Signal and Noise ----------------- %
SIGL_buf = zeros(1,LLp);
NOISE_buf = zeros(1,LLp);
SIGL_buf1 = zeros(1,LLp);
NOISE_buf1 = zeros(1,LLp);
THRS_buf1 = zeros(1,LLp);
THRS_buf = zeros(1,LLp);
%% initialize the training phase (2 seconds of the signal) to determine the THR_SIG
and THR_NOISE
THR_SIG = max(ecg_m(1:2*fs))*1/3;                       % 0.25 of the max amplitude
THR_NOISE = mean(ecg_m(1:2*fs))*1/2;% 0.5 of the mean signal is considered as noise
SIG_LEV= THR_SIG;
NOISE_LEV = THR_NOISE;
%% Initialize bandpass filter threshold(2 seconds of the bandpass signal)
THR_SIG1 = max(ecg_bp(1:2*fs))*1/3;                     % 0.25 of the max amplitude
THR_NOISE1 = mean(ecg_bp(1:2*fs))*1/2;
SIG_LEV1 = THR_SIG1;                            % Signal level in Bandpassed filter
NOISE_LEV1 = THR_NOISE1;                         % Noise level in Bandpassed filter
%% ============ Thresholding and decision rule ============= %%
Beat_C = 0;                                                             % Raw Beats
Beat_C1 = 0;                                                       % Filtered Beats
Noise_Count = 0;                                                    % Noise Counter
for i = 1 : LLp
   %% ===== locate the corresponding peak in the filtered signal === %%
    if locs(i)-round(0.150*fs)>= 1 && locs(i)<= length(ecg_bp)
          [y_i,x_i] = max(ecg_bp(locs(i)-round(0.150*fs):locs(i)));
       else
          if i == 1
            [y_i,x_i] = max(ecg_bp(1:locs(i)));
            ser_back = 1;
          elseif locs(i)>= length(ecg_bp)
```

```
            [y_i,x_i] = max(ecg_bp(locs(i)-round(0.150*fs):end));
          end
    end
 %% == calculate the mean last 8 R waves to ensure that QRS is not ==== %%
       if m_selected_RR
           test_m = m_selected_RR;              %if the regular RR available use it
       elseif mean_RR && m_selected_RR == 0
           test_m = mean_RR;
       else
           test_m = 0;
       end
    if test_m
          if (locs(i) - qrs_i(Beat_C)) >= round(1.66*test_m)      % it shows a QRS
is missed
              [pks_temp,locs_temp] = max(ecg_m(qrs_i(Beat_C)+
round(0.200*fs):locs(i)-round(0.200*fs))); % search back and locate the max in this
interval
              locs_temp = qrs_i(Beat_C)+ round(0.200*fs) + locs_temp -1; % location
              if pks_temp > THR_NOISE
               Beat_C = Beat_C + 1;
               qrs_amp(Beat_C) = pks_temp;
               qrs_i(Beat_C) = locs_temp;
              % ------------- Locate in Filtered Sig ------------- %
               if locs_temp <= length(ecg_bp)
                  [y_i_t,x_i_t] = max(ecg_bp(locs_temp-round(0.150*fs):locs_temp));
               else
                  [y_i_t,x_i_t] = max(ecg_bp(locs_temp-round(0.150*fs):end));
               end
              % ----------- Band pass Sig Threshold ------------------%
               if y_i_t > THR_NOISE1
                  Beat_C1 = Beat_C1 + 1;
                  qrs_i_raw(Beat_C1) = locs_temp-round(0.150*fs)+ (x_i_t - 1); %
save index of bandpass
                  qrs_amp_raw(Beat_C1) = y_i_t;        % save amplitude of bandpass
                  SIG_LEV1 = 0.25*y_i_t + 0.75*SIG_LEV1;      % when found with the
second thres
               end
               not_nois = 1;
               SIG_LEV = 0.25*pks_temp + 0.75*SIG_LEV ;    % when found with the
second threshold
             end
          else
              not_nois = 0;
          end
    end
    %% ===================  find noise and QRS peaks ================== %%
    if pks(i) >= THR_SIG
```

```
      % ------ if No QRS in 360ms of the previous QRS See if T wave ------%
       if Beat_C >= 3
          if (locs(i)-qrs_i(Beat_C)) <= round(0.3600*fs)
              Slope1 = mean(diff(ecg_m(locs(i)-round(0.075*fs):locs(i))));    %
mean slope of the waveform at that position
              Slope2 =
mean(diff(ecg_m(qrs_i(Beat_C)-round(0.075*fs):qrs_i(Beat_C)))); % mean slope of
previous R wave
              if abs(Slope1) <= abs(0.5*(Slope2))   % slope less then 0.5 of
previous R
                 Noise_Count = Noise_Count + 1;
                 noise_c(Noise_Count) = pks(i);
                 noise_i(Noise_Count) = locs(i);
                 skip = 1;                                  % T wave identification
                 % ----- adjust noise levels ------ %
                 NOISE_LEV1 = 0.125*y_i + 0.875*NOISE_LEV1;
                 NOISE_LEV = 0.125*pks(i) + 0.875*NOISE_LEV;
              else
                 skip = 0;
              end

           end
        end
        %---------- skip is 1 when a T wave is detected -------------- %
        if skip == 0
          Beat_C = Beat_C + 1;
          qrs_amp(Beat_C) = pks(i);
          qrs_i(Beat_C) = locs(i);
        %--------------- bandpass filter check threshold --------------- %
          if y_i >= THR_SIG1
              Beat_C1 = Beat_C1 + 1;
              if ser_back
                 qrs_i_raw(Beat_C1) = x_i;                 % save index of bandpass
              else
                 qrs_i_raw(Beat_C1)= locs(i)-round(0.150*fs)+ (x_i - 1);   % save
index of bandpass
              end
              qrs_amp_raw(Beat_C1) =  y_i;             % save amplitude of bandpass
              SIG_LEV1 = 0.125*y_i + 0.875*SIG_LEV1;        % adjust threshold for
bandpass filtered sig
          end
         SIG_LEV = 0.125*pks(i) + 0.875*SIG_LEV ;             % adjust Signal level
        end
    elseif (THR_NOISE <= pks(i)) && (pks(i) < THR_SIG)
         NOISE_LEV1 = 0.125*y_i + 0.875*NOISE_LEV1;   % adjust Noise level in
filtered sig
         NOISE_LEV = 0.125*pks(i) + 0.875*NOISE_LEV;    % adjust Noise level in MVI
    elseif pks(i) < THR_NOISE
        Noise_Count = Noise_Count + 1;
        noise_c(Noise_Count) = pks(i);
        noise_i(Noise_Count) = locs(i);
        NOISE_LEV1 = 0.125*y_i + 0.875*NOISE_LEV1; % noise level in filtered signal
        NOISE_LEV = 0.125*pks(i) + 0.875*NOISE_LEV;     % adjust Noise level in MVI
    end
    %% ================== adjust the threshold with SNR ============= %%
    if NOISE_LEV ~= 0 || SIG_LEV ~= 0
        THR_SIG = NOISE_LEV + 0.25*(abs(SIG_LEV - NOISE_LEV));
        THR_NOISE = 0.5*(THR_SIG);
    end
    %------ adjust the threshold with SNR for bandpassed signal -------- %
    if NOISE_LEV1 ~= 0 || SIG_LEV1 ~= 0
        THR_SIG1 = NOISE_LEV1 + 0.25*(abs(SIG_LEV1 - NOISE_LEV1));
        THR_NOISE1 = 0.5*(THR_SIG1);
    end
%--------- take a track of thresholds of smoothed signal -------------%
SIGL_buf(i) = SIG_LEV;
NOISE_buf(i) = NOISE_LEV;
THRS_buf(i) = THR_SIG;
%-------- take a track of thresholds of filtered signal ----------- %
SIGL_buf1(i) = SIG_LEV1;
NOISE_buf1(i) = NOISE_LEV1;
THRS_buf1(i) = THR_SIG1;
% ----------------------- reset parameters -------------------------- %
skip = 0;
not_nois = 0;
ser_back = 0;
end
%% ======================= Adjust Lengths ============================ %%
qrs_i_raw = qrs_i_raw(1:Beat_C1);
qrs_amp_raw = qrs_amp_raw(1:Beat_C1);
qrs_i = qrs_i(1:Beat_C);
qrs_amp = qrs_amp(1:Beat_C);
%% ================== overlay on the signals ========================= %%
 if gr
   figure;
   plot(ecg-mean(ecg));
   title('Detected R-Waves on ECG signal'); axis tight; zoom on;
   line(repmat(qrs_i_raw,[2 1]),...
       repmat([min(ecg-mean(ecg))/2; max(ecg-mean(ecg))/2],size(qrs_i_raw)),...
       'LineWidth',2.5,'LineStyle','-.','Color','r');
 end
%% Optional Functionality: Compares output of this function to an annotation file
% comparator(qrs_i_raw);
end
```

Appendix F: Miscellaneous Functions Written For Testing

F.1: comparator() Function

```
function []=comparator(qrs_i_raw)
%% Input
% qrs_i_raw : one of the RWave_Detection() function outputs; the R-wave
% pulse train returned by the function
%% Output
% a bxb report is created as a .txt file
%% Be sure to modify the record number for each run
%read in the R-wave locations from Physionet annotation file
[sig_ann, ann_type,  subtype, chan, num, comments] = rdann('100', 'atr');

%write a .test file that has the locations of the R-waves as determined by the
RWave_Detection() function
wrann('100', 'test', qrs_i_raw, 'N', zeros(length(qrs_i_raw),1),
ones(length(qrs_i_raw),1), zeros(length(qrs_i_raw),1), []);

clear; clc;
bxb('100','atr','test','100_bxbReport.txt');
end
```

F.2: bxbreport_table() Function

```
function [CM, Sense, PosPr] = bxbreport_table(Rfile)
%% bxbrdrpt: Read report generated by Physionet bxb().
%% Inputs
% Rfile: (string) Full name of the report file (including any needed
%        path information and filename extension).
%% Outputs
% CM: Confusion matrix.  A 7x7 (double) confusion matrix, as printed by bxb().
%     Columns are labeled n, s, v, f, q, o and x (truth). Columns are
%     same order, but label test results.  Lower right 2x2 submatrix
%     not used, so set to zero values.
% Sense: QRS sensitiviy, as listed in the report file.
% PosPr: QRS positive predictivity, as listed in the report file.
% a test.csv file with all the values from all the report files compiled
%% Be sure to modify the record number for each run in the first two lines
Rfile = '100_bxbReport.txt';
record_nums = 100;

fid = fopen(Rfile, 'rt');  % Open report file.
if fid<0, error(['bxbrdrpt: Cannot open ' Rfile]); end

for i=1:7  % Read unused header lines.
  tline = fgetl(fid); if tline == -1, error(['bxbrdrpt: Bogus header in ' Rfile]);
end
end

%% Read 7 lines of tabular result data into confusion matrix CM.
%   Number of entries per line differ.  So, customize read for each line.
Label = 'NSVFQOX';       % Row labels, from bxb report table.
Entry = [7 7 7 7 7 5 5]; % Expected columns per row.
CM = zeros(7,7);         % Pre-allocate and initialize confusion matrix.
for row = 1:7  % Loop over each row in report file confusion matrix.
  tline = fgetl(fid);  % Read full line.
  if tline == -1, error(['bxbrdrpt: Bogus row' Label(row) ' in ' Rfile]); end
  for col = 1:Entry(row)  % Build format.  Skip first two strings.
    format = '%*s %*s'; for i=1:Entry(row), format = [format ' %d']; end
%#ok<AGROW>
  end
  Avec = sscanf(tline, format, [1 Entry(row)]); % Read confuse matrix entries.
  CM(row, 1:Entry(row)) = Avec; % Insert into confusion matrix.
end

% Read QRS sensitivity and positive predictivity.
%   Empty line.
tline = fgetl(fid);
if tline == -1, error(['bxbrdrpt: Bogus empty line after CM in ' Rfile]); end
```

```
%   QRS sensitivity.
tline = fgetl(fid);
if tline == -1, error(['bxbrdprt: Bogus QRS sensitivity line in ' Rfile]); end
Sense = sscanf(tline, '%*s %*s %f', [1 1]);
%   QRS positive predictivity.
tline = fgetl(fid);
if tline == -1, error(['bxbrdprt: Bogus QRS positive predictivity line in '
Rfile]); end
PosPr = sscanf(tline, '%*s %*s %*s %f', [1 1]);

% Close the file.
fclose(fid);

%% Tabulate all results into a csv
data = {'Record Number' 'QRS sensitivity' 'QRS positive predictivity'};
data1= {record_nums Sense PosPr};
Data = [data;data1];
if isfile('test.csv')
    read_arr = readmatrix('test.csv');
    [m,n] = size(read_arr);
    if m >= 1
        writecell(data1, 'test.csv','WriteMode','append')
    end     % File exists.
else
     writecell(Data, 'test.csv'); % File does not exist.
end
```

References

[1] "Ch. 1 Introduction - Anatomy and Physiology | OpenStax." https://openstax.org/books/anatomy-and-physiology/pages/1-introduction (accessed Dec. 14, 2021).

[2] Nyq, *Diagram of the human heart*. [Online]. Available: https://commons.wikimedia.org/wiki/File:Diagram_of_the_human_heart.svg

[3] *Anatomy and Pysiology*, vol. 2, 3 vols. 2013. Accessed: Oct. 13, 2021. [Online]. Available: https://textbookequity.org/Textbooks/anatomy+phys+vol2a.pdf

[4] Madhero88, *English: Electrical conduction system of the heart*. Accessed: Sep. 28, 2021. [Online]. Available: https://commons.wikimedia.org/wiki/File:Conductionsystemoftheheart.png

[5] S. Toinga, C. Carabali, and L. Ortega, "Development of a didactic platform for teaching the Einthoven's Triangle," in *2017 IEEE Second Ecuador Technical Chapters Meeting (ETCM)*, Oct. 2017, pp. 1–6. doi: 10.1109/ETCM.2017.8247542.

[6] J. Aspuru *et al.*, "Segmentation of the ECG Signal by Means of a Linear Regression Algorithm," *Sensors*, vol. 19, no. 4, p. 775, Feb. 2019, doi: 10.3390/s19040775.

[7] R. V. Andreao, B. Dorizzi, and J. Boudy, "ECG signal analysis through hidden Markov models," *IEEE Trans. Biomed. Eng.*, vol. 53, no. 8, pp. 1541–1549, Aug. 2006, doi: 10.1109/TBME.2006.877103.

[8] D. Nabil and F. Bereksi Reguig, "Ectopic beats detection and correction methods: A review," *Biomed. Signal Process. Control*, vol. 18, pp. 228–244, Apr. 2015, doi: 10.1016/j.bspc.2015.01.008.

[9] J. Lee, Y. Nam, D. D. McManus, and K. H. Chon, "Time-Varying Coherence Function for Atrial Fibrillation Detection," *IEEE Trans. Biomed. Eng.*, vol. 60, no. 10, pp. 2783–2793, Oct. 2013, doi: 10.1109/TBME.2013.2264721.

[10] D. S. Desai and S. Hajouli, "Arrhythmias," in *StatPearls*, Treasure Island (FL): StatPearls Publishing, 2021. Accessed: Dec. 10, 2021. [Online]. Available: http://www.ncbi.nlm.nih.gov/books/NBK558923/

[11] Springhouse, *ECG Interpretation: A 2-in-1 Reference for Nurses*. Philadelphia, UNITED STATES: Wolters Kluwer Health, 2004. Accessed: Oct. 04, 2021. [Online]. Available: http://ebookcentral.proquest.com/lib/wpi/detail.action?docID=2032544

[12] L. Sörnmo and P. Laguna, "Chapter 6 - The Electrocardiogram—A Brief Background," in *Bioelectrical Signal Processing in Cardiac and Neurological Applications*, L. Sörnmo and P. Laguna, Eds. Burlington: Academic Press, 2005, pp. 411–452. doi: 10.1016/B978-012437552-9/50006-4.

[13] Jmarchn, *English: Precordial electrodes necessary for a 12-lead ECG*. Accessed: Oct. 05, 2021. [Online]. Available: https://commons.wikimedia.org/wiki/File:Precordial_Leads_2.svg

[14] M. Cadogan, "ECG Lead positioning," *Life in the Fast Lane • LITFL*, May 20, 2021. https://litfl.com/ecg-lead-positioning/ (accessed Sep. 12, 2021).

[15] Jmarchn, *English: ECG electrodes*. Accessed: Oct. 05, 2021. [Online]. Available: https://commons.wikimedia.org/wiki/File:Limb_leads_2_ENG.svg

[16] Npatchett, *English: Derivation of the limb leads*. 2015. Accessed: Oct. 05, 2021. [Online]. Available: https://commons.wikimedia.org/wiki/File:Limb_leads_of_EKG.png

[17] "Holter Monitor."

https://www.hopkinsmedicine.org/health/treatment-tests-and-therapies/holter-monitor (accessed Oct. 12, 2021).

[18] L. G. Tereshchenko and M. E. Josephson, “Frequency Content and Characteristics of Ventricular Conduction,” *J. Electrocardiol.*, vol. 48, no. 6, pp. 933–937, 2015, doi: 10.1016/j.jelectrocard.2015.08.034.

[19] W. J. Tompkins and M. L. Ahlstrom, “Digital Filters for Real Time ECG,” *IEEE Xplore*. https://ieeexplore.ieee.org/abstract/document/4122146/citations#citations (accessed Dec. 06, 2021).

[20] R. P. Sallen and E. L. Key, “A Practical Method of Designing RC Active Filters,” *IEEE Xplore*.

[21] Electrical4u, “Summing Amplifier or Op Amp Adder,” Oct. 28, 2020. https://www.electrical4u.com/summing-amplifier/ (accessed Dec. 15, 2021).

[22] B. Le, T. W. Rondeau, J. H. Reed, and C. W. Bostian, “Analog-to-digital converters,” *IEEE Signal Process. Mag.*, vol. 22, no. 6, pp. 69–77, Nov. 2005, doi: 10.1109/MSP.2005.1550190.

[23] F. Shaffer, R. McCraty, and C. L. Zerr, “A healthy heart is not a metronome: an integrative review of the heart’s anatomy and heart rate variability,” *Front. Psychol.*, vol. 5, p. 1040, 2014, doi: 10.3389/fpsyg.2014.01040.

[24] D. Chabot, M. Bayer, and A. de Roos, “Instantaneous heart rates and other techniques introducing errors in the calculation of heart rate,” *Can. J. Zool.*, vol. 69, pp. 1117–1120, Apr. 1991, doi: 10.1139/z91-156.

[25] J. Pan and W. J. Tompkins, “A Real-Time QRS Detection Algorithm,” *IEEE Trans. Biomed. Eng.*, vol. BME-32, no. 3, pp. 230–236, Mar. 1985, doi: 10.1109/TBME.1985.325532.

[26] “Heart Rate Variability | Circulation.” https://www.ahajournals.org/doi/full/10.1161/01.cir.93.5.1043 (accessed Oct. 05, 2021).

[27] S. Dash, K. H. Chon, S. Lu, and E. A. Raeder, “Automatic Real Time Detection of Atrial Fibrillation,” *Ann. Biomed. Eng.*, vol. 37, no. 9, pp. 1701–1709, Sep. 2009, doi: 10.1007/s10439-009-9740-z.

[28] D. Cantillon MD and R. Amuthan MD, “Atrial Fibrillation,” *Cleveland Clinic Center for Continuing Education*, Aug. 2018. https://www.clevelandclinicmeded.com/medicalpubs/diseasemanagement/cardiology/atrial-fibrillation/#fig03

[29] W. B. Kannel, P. A. Wolf, E. J. Benjamin, and D. Levy, “Prevalence, incidence, prognosis, and predisposing conditions for atrial fibrillation: population-based estimates 11Reprints are not available.,” *Am. J. Cardiol.*, vol. 82, no. 7, Supplement 1, pp. 2N-9N, Oct. 1998, doi: 10.1016/S0002-9149(98)00583-9.

[30] K. Tateno and L. Glass, “Automatic detection of atrial fibrillation using the coefficient of variation and density histograms of RR and ARR intervals,” *Biol. Eng.*, vol. 39, p. 8, 2001.

[31] R. Peck, C. Olsen, and J. L. Devore, *Introduction to statistics and data analysis*, 3rd ed. Australia ; Belmont, CA: Thomson Brooks/Cole, 2008.

[32] J. Lee, D. McManus, and K. Chon, “Atrial Fibrillation detection using time-varying coherence function and Shannon Entropy,” in *2011 Annual International Conference of the IEEE Engineering in Medicine and Biology Society*, Boston, MA, Aug. 2011, pp. 4685–4688. doi: 10.1109/IEMBS.2011.6091160.

[33] International Electrotechnical Committee, “Medical electrical equipment - Part 2-25:

Particular requirements for the basic safety and essential performance of electrocardiographs." https://webstore.iec.ch/publication/2636 (accessed Sep. 22, 2021).

[34] "IEEE 802.15.1-2002 - IEEE Standard for Telecommunications and Information Exchange Between Systems - LAN/MAN - Specific Requirements - Part 15: Wireless Medium Access Control (MAC) and Physical Layer (PHY) Specifications for Wireless Personal Area Networks (WPANs)." https://standards.ieee.org/standard/802_15_1-2002.html (accessed Sep. 22, 2021).

[35] Analog Devices, "AD624 Datasheet." Accessed: Oct. 07, 2021. [Online]. Available: https://www.analog.com/media/en/technical-documentation/data-sheets/AD624.pdf

[36] Analog Devices, "AD8227 Datasheet." Accessed: Nov. 30, 2021. [Online]. Available: https://www.analog.com/media/en/technical-documentation/data-sheets/AD8227.pdf

[37] Linear Technology, "LT1167 Datasheet." [Online]. Available: https://www.analog.com/media/en/technical-documentation/data-sheets/1167fc.pdf

[38] Texas Instruments, "LM324-n Datasheet." Accessed: Dec. 01, 2021. [Online]. Available: https://www.ti.com/lit/ds/symlink/lm324-n.pdf?ts=1638353644532&ref_url=https%253A%252F%252Fwww.google.com%252F

[39] H.-Y. Hsieh, C.-H. Luo, and C.-C. Tai, "Wireless potential difference electrocardiogram constituted by two electrode-pairs wearing comfort," *J. Instrum.*, vol. 15, no. 08, pp. P08011–P08011, Aug. 2020, doi: 10.1088/1748-0221/15/08/P08011.

[40] "Complete Pan Tompkins Implementation ECG QRS detector - File Exchange - MATLAB Central." https://www.mathworks.com/matlabcentral/fileexchange/45840-complete-pan-tompkins-implementation-ecg-qrs-detector (accessed Oct. 11, 2021).

[41] A. Papoulis, *Probability, RandomVariables, and Stochastic Process*, Second. McGraw-Hill Book Company, 1984.

[42] N. Goldstein, D. Song, and D. Thompson, *Atrial-Fibrillation-Detection-from-BIH-MIT-Database*. 2015. Accessed: Dec. 16, 2021. [Online]. Available: https://github.com/danthompson41/Atrial-Fibrillation-Detection-from-BIH-MIT-Database

[43] S. Braun, "WINDOWS," in *Encyclopedia of Vibration*, S. Braun, Ed. Oxford: Elsevier, 2001, pp. 1587–1595. doi: 10.1006/rwvb.2001.0052.

[37] Conover, M. B. (2002). *Understanding Electrocardiography*. Elsevier Health Sciences. Pp. 4-7

[38] Babusiak, B., Borik, S., & Smondrk, M. (2020). Two-Electrode ECG for Ambulatory Monitoring with Minimal Hardware Complexity. *Sensors*, *20*(8), 2386. https://doi.org/10.3390/s20082386

[39] Texas Instruments, "TPS73615MDBVREP Datasheet." Accessed: Dec. 10, 2021. [Online]. Available: https://www.ti.com/lit/ds/symlink/tps73615-ep.pdf?HQS=dis-mous-null-mousermode-dsf-pf-null-wwe&ts=1639185179581&ref_url=https%253A%252F%252Fwww.mouser.com%252F

[40] Texas Instruments, "LP38841T-1.5/NOPB Datasheet." Accessed: Dec. 10, 2021. Available: https://www.ti.com/lit/ds/symlink/lp38841.pdf?HQS=dis-mous-null-mousermode-dsf-pf-null-wwe&ts=1639165339792